PNNL-34265, Rev. 0
RPT-DFTP-036, Rev. 0

Fiscal Year 2023 Filtration of Hanford Tank 241-AP-105 Supernatant at 16 °C

June 2023

JR Allred
C Alvarez
EC Buck
CA Burns
RC Daniel
JGH Geeting
AM Westesen
RA Peterson

U.S. DEPARTMENT OF ENERGY

Prepared for the U.S. Department of Energy
under Contract DE-AC05-76RL01830

PACIFIC NORTHWEST NATIONAL LABORATORY
operated by
BATTELLE
for the
UNITED STATES DEPARTMENT OF ENERGY
under Contract DE-AC05-76RL01830

Printed in the United States of America

Available to DOE and DOE contractors from the
Office of Scientific and Technical Information,
P.O. Box 62, Oak Ridge, TN 37831-0062;
ph: (865) 576-8401
fax: (865) 576-5728
email: reports@adonis.osti.gov

Available to the public from the National Technical Information Service
5301 Shawnee Rd., Alexandria, VA 22312
ph: (800) 553-NTIS (6847)
email: orders@ntis.gov <https://www.ntis.gov/about>
Online ordering: http://www.ntis.gov

PNNL-34265, Rev. 0
RPT-DFTP-036, Rev. 0

Fiscal Year 2023 Filtration of Hanford Tank 241-AP-105 Supernatant at 16 °C

June 2023

JR Allred
C Alvarez
EC Buck
CA Burns
RC Daniel
JGH Geeting
AM Westesen
RA Peterson

Prepared for
the U.S. Department of Energy
under Contract DE-AC05-76RL01830

Pacific Northwest National Laboratory
Richland, Washington 99354

Summary

Approximately 9 liters of supernatant from Hanford waste tank 241-AP-105 was delivered by Washington River Protection Solutions to the Radiochemical Processing Laboratory (RPL) at Pacific Northwest National Laboratory. The as-received AP-105 waste was diluted with process water (Columbia River water) from approximately 8.7 M sodium (nominal tank concentration) and partitioned into a batch of 7 M sodium and a batch of 5.5 M sodium. Dilution increased the combined volume of the two batches to approximately 7.8 liters of 7 M Na feed and 4.4 liters of 5.5 M Na feed.

These two batches of 241-AP-105 supernatant were chilled to 16 °C for 1 week prior to testing. Filtration testing was then conducted using a backpulse dead-end filter (BDEF) system equipped with a feed vessel and a Mott inline filter Model 6610 (Media Grade 5) in the hot cells of the RPL. This was done to assess the performance of the anticipated future feed to the Tank Side Cesium Removal (TSCR) system. Similar to samples from tanks 241-AP-101 and 241-AP-107, no visible solids were observed in the as-received or diluted samples.

The feed was filtered through the BDEF system at a targeted flux of 0.065 gpm/ft^2 to match the prototypic operation of the TSCR system. During filtration of the 5.5 M sodium batch, the differential pressure required to effect filtration at 0.065 gpm/ft^2 increased steadily over the filtration campaign. Once the bottoms of the bottles were added to the slurry, reservoir pressure rise increased and required two backpulses as the transmembrane pressure (TMP) reached 2 psid (the TSCR action limit). In contrast, the 7 M sodium batch did not require a backpulse for the feed volume tested. This indicates that the higher dilution of the feed resulted in more solids precipitating and these solids do settle over time. The prototypic filter cleaning process effectively restored filter performance.

Solids concentrated from the backpulse solutions displayed sodium nitrate, sodium carbonate, calcium sulfate, iron oxide, steel particles, titanium oxide particles, and aluminum oxides. Electron diffraction was used to determine the types of phases that were present in the solids. The possible identifications of gibbsite, natrite, nitrite, gypsum, anatase, allophane, and cancrinite were made during this investigation. Most of the phases found were only weakly crystalline, possibly owing to their rapid precipitation during the process water treatment. The identifications of the phases therefore are tentative.

Acknowledgments

The authors gratefully acknowledge the help of hot cell technicians Victor Aguilar and Robert Cox in conducting this work. We thank Renee Russell for conducting the technical review of this report. We also thank Matt Wilburn for technical editing of this report and David MacPherson for the quality reviews of the calculation packages and this report.

Microscopy work was performed at the Radiochemical Processing Laboratory Quiet-Suite at Pacific Northwest National Laboratory.

Acronyms and Abbreviations

AEA	alpha energy analysis
BDEF	backpulse dead-end filter (system)
CWF	clean water flux
EDS	X-ray energy dispersive spectroscopy
HAADF	high-angle annular dark-field
ICP-MS	inductively coupled plasma mass spectrometry
ICP-OES	inductively coupled plasma optical emission spectroscopy
IX	ion exchange
LAW	low-activity waste
MFC	mass flow controller
PNNL	Pacific Northwest National Laboratory
QA	quality assurance
R&D	research and development
RPL	Radiochemical Processing Laboratory
SAED	selected area electron diffraction
SEM	scanning electron microscopy
STEM	scanning transmission electron microscopy
TEM	transmission electron microscopy
TMP	transmembrane pressure
TRU	transuranic
TSCR	Tank Side Cesium Removal
WRPS	Washington River Protection Solutions
WTP	Waste Treatment and Immobilization Plant
WWFTP	WRPS Waste Form Testing Program

Contents

Figures

Tables

1.0 Introduction

The U.S. Department of Energy's Hanford Site houses 56 million gallons of high-level radioactive waste generated from plutonium production from 1944 to 1988 (Gerber 1992). The supernatant waste, currently stored in underground tanks, is intended to be vitrified following filtration and ^{137}Cs removal at the Hanford Waste Treatment and Immobilization Plant (WTP) Pretreatment Facility. Because the Pretreatment Facility will not be operational for several years, ^{137}Cs will be removed from low-activity waste (LAW) vitrification feeds using the Tank Side Cesium Removal (TSCR) system in a technology demonstration that will filter and then remove cesium from tank waste supernate to support transferring the TSCR-processed waste directly to the WTP LAW Melter Facility. The TSCR system is skid-mounted and employs two key technologies: (1) dead-end filtration for solids removal, which is necessary to protect the functionality of the ion exchange (IX) columns, and (2) IX for cesium removal.

A small-scale test platform was established in 2017 to demonstrate these processes in the Pacific Northwest National Laboratory (PNNL) 325 Building, also known as the Radiochemical Processing Laboratory (RPL).

Hanford waste tank 241-AP-105 (herein AP-105) is anticipated to be a future feed to TSCR, and was previously filtered at ambient hot-cell temperature in fiscal year (FY) 2020. The purpose of this filtration testing was to (a) demonstrate dead-end filtration testing of AP-105 feed at a previously untested temperature (16 °C) to obtain TSCR prototypic flux rates and identify issues that may impact filtration, and (b) provide feed to IX (also part of the test platform).

The presence of solids has been observed in previous filtration experiments using supernatant waste from Hanford tanks AP-101, AP-105, and AP-107 (Geeting et al. 2018a,b, 2019; Allred et al. 2020, 2021, 2022). Formation of solids in these tests was suspected to be due to tank mixing, dilution with process water, and reducing the feed temperature to 16 °C.

Therefore, the objective of the current work was to perform filtration under prototypic conditions using Mott Grade 5 sintered metal at the targeted flux of 0.065 gpm/ft^2 planned for TSCR, and at the lower (more challenging) TSCR operation temperature expected during the colder season. Filter resistance as a function of time was measured and the filter was backpulsed at the end of filtration testing. Backpulse solutions were collected, and the solids were concentrated and assessed by microscopy methods.

2.0 Quality Assurance

All research and development (R&D) work at PNNL is performed in accordance with PNNL's Laboratory-Level Quality Management Program, which is based on a graded application of NQA-1-2000, *Quality Assurance Requirements for Nuclear Facility Applications* (ASME 2000), to R&D activities. To ensure that all client quality assurance (QA) expectations were addressed, the QA controls of PNNL's Washington River Protection Solutions (WRPS) Waste Form Testing Program (WWFTP) QA program were also implemented for this work. The WWFTP QA program implements the requirements of NQA-1-2008, *Quality Assurance Requirements for Nuclear Facility Applications* (ASME 2008), and NQA-1a-2009*, Addenda to ASME NQA-1-2008* (ASME 2009).

The work described in this report was assigned the technology level "Applied Research". All staff members contributing to the work received proper technical and QA training prior to performing quality-affecting work.

3.0 Test Conditions

In October 2022, WRPS collected 36 supernatant samples (~250 mL each) from tank AP-105 in two batches (approximately 20 feet[1] below the liquid surface level) and provided them to PNNL for filtration testing. At the RPL, the as-received AP-105 waste was diluted with process water (Columbia River water) from approximately 8.7 M sodium (nominal tank concentration) and partitioned into a batch of 7 M sodium and a batch of 5.5 M sodium. Dilution increased the combined volume of the two batches to approximately 7.8 liters of 7 M Na feed and 4.4 liters of 5.5 M Na feed, respectively. No visible solids were observed in the as-received or diluted samples. The bottles of diluted AP-105 tank waste were chilled (16 °C setpoint) for approximately 1 week prior to testing. Filtration testing of the tank waste using a Mott Model 6610 (Media Grade 5) line filter with porous end cap began on December 4, 2022. This is a sintered 316L stainless steel filter with a 0.317-in. porous diameter, 1.463-in. porous length, and 1.51-in.^{2} filter area.

3.1 BDEF Filtration

3.1.1 Backpulse Dead-End Filter (BDEF) System Description

The filtration system is the same system that was used in FY22 (Allred et al. 2022), again using the trough heat exchanger to keep all the feed at the setpoint temperature until it was added to the BDEF system. The feed bottles were stored in the trough heat exchanger with a cover until the feed was transferred to the BDEF system.

Once the feed was added to the BDEF, the existing heat exchanger kept the feed at the setpoint temperature in the reservoir and in the BDEF recirculation loop. The filter housing clamshell heat exchanger kept the feed at the setpoint temperature as it exited the recirculation loop until it was filtered. After filtration, the temperature was no longer controlled. A piping and instrumentation diagram is provided in Appendix A. A photograph of the BDEF system installed in the RPL Shielded Analytical Laboratory hot cell is shown in Figure 3.1.

---

[1] Per RPP-PLAN-65241, *Tank 241-AP 105 Large Volume Sample Collection to Support Platform Testing, Phase 1, FY23*, and RPP-PLAN-65242, *Tank 241-AP 105 Large Volume Sample Collection to Support Platform Testing, Phase 2, FY23*.

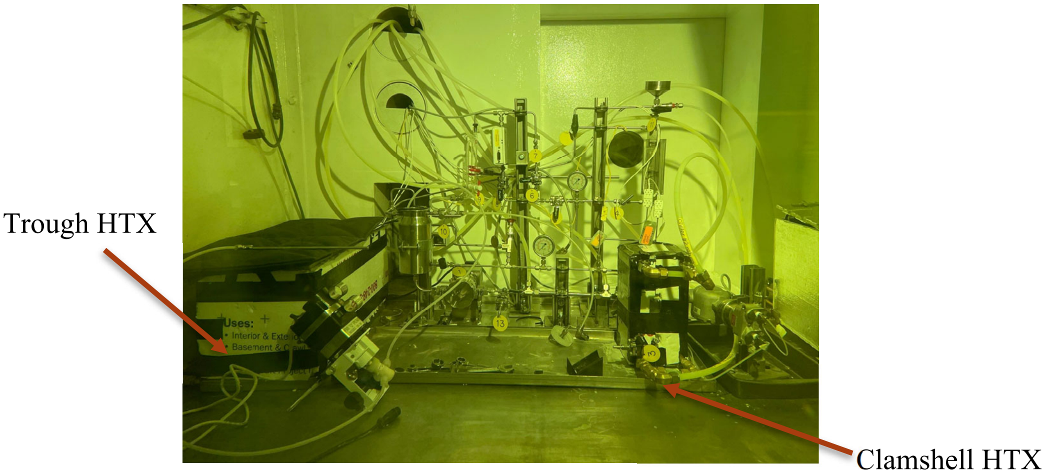

Figure 3.1. BDEF system installed in hot cell. HTX = heat exchanger.

The BDEF system is composed of a slurry recirculation loop, a filter assembly, and a permeate system. The main recirculation loop consists of a 1-liter stainless steel container (Eagle, EPV1A), a low-shear quaternary diaphragm pump (Quattro Flow QF150), a heat exchanger, and a throttle valve. The pump speed is controlled by a variable frequency drive that is located outside the hot cell. The slurry flow rate and pressure are controlled by adjusting the pump variable frequency drive (pump speed control) and throttle valve. The recirculation loop provides mixed, pressurized feed to the filter assembly. During the testing described in this report, the slurry temperature was controlled at a 16 °C setpoint.

The filter assembly receives pressurized slurry from the slurry recirculation loop. The filter assembly is composed of a filter, a Rosemount differential pressure transducer, and a flush valve (V3 in Appendix A). The flush valve is actuated during backpulse operations used to clear solids off the filter and out of the system.

The permeate system receives permeate produced by the filter assembly. The permeate flow rate is controlled with a mass flow controller (MFC), which can control feed in the range of 0.15 to 0.33 liter/hour. (These rates equate to allowable filter areas of 1.5 to 3.3 in.^{2} assuming flux of 0.065 gpm/ft^2.) The MFC measures flow rate and density of the permeate, and a glass flowmeter is provided as a secondary flow rate measurement device. The permeate system can also perform a backpulse function. Pressurized air can be introduced (V12) into the backpulse chamber and used to force permeate (or other fluids) backward through the filter and out of the system through V3.

The Mott 6610 filter used in testing is cylindrical, with dimensions of 0.317-in. diameter × 1.5-in. length and a filtration area of 1.51 in.^{2}. The filter element is fabricated from a seamless sintered stainless-steel tube that is a closed/dead-end porous tube (with a porous end cap); the open end is welded to a pipe-reducing bushing. At 0.065 gpm/ft^2, the rate of filter processing is 3.7 liters of feed per 24-hour day. Figure 3.2 shows a schematic of the filter assembly and a photo of the filter.

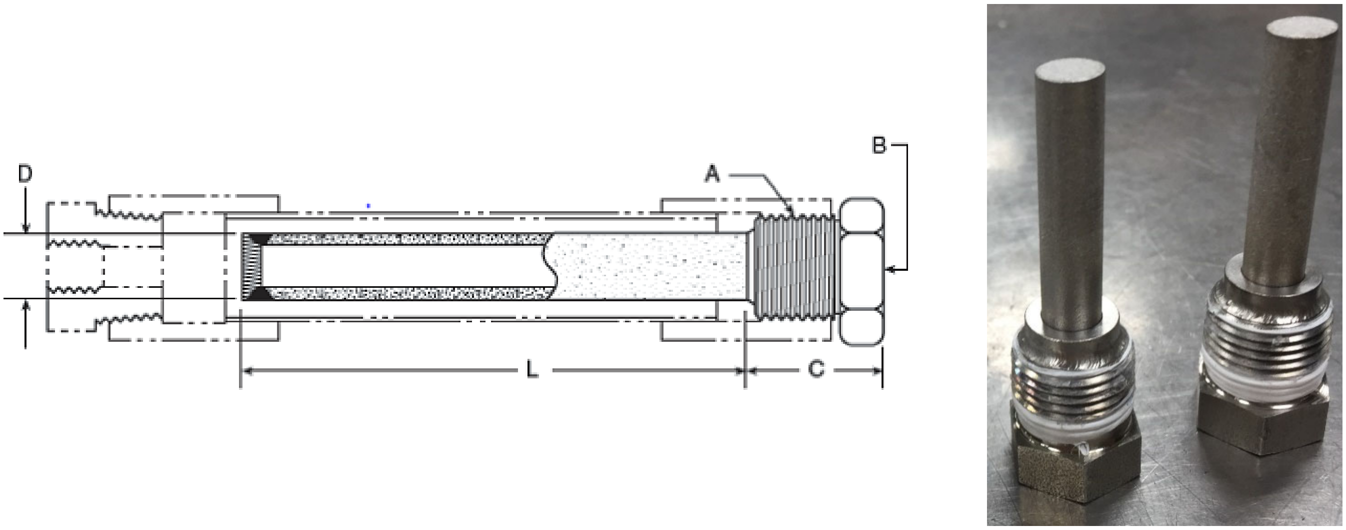

(a) (b)

Figure 3.2. (a) Filter housing schematic (note that the 6610 series filter was welded to a 3/8-in. pipe fitting, making the configuration similar to the 6480 series illustrated here); (b) photo of modified filters with filter housings removed. (Mott 6480 line filter schematic from https://mottcorp.com.)

3.1.2 System Operation during Testing

The steps used to test the AP-105 waste samples are outlined below.

1. Diluted AP-105 batch 1 feed from 8.72 M to 5.5 M sodium using process water. Diluted AP-105 batch 2 feed from 8.72 M to 7.0 M sodium using process water. These dilutions were performed approximately 1 month prior to filtration.

2. Chilled feed to 16 ± 2.2 °C for 1 week prior to the start of filtration.

3. Clean water flux (CWF) measurement: The CWF measurement served as a system leak test and provided a baseline measurement of the filter resistance and was conducted at nominal test conditions of 0.065 gpm/ft^2 and run for approximately 10 minutes.

4. Filtration of the 5.5 M Na feed: Filtration was performed using a Mott Grade 5 sintered metal filter at a targeted flux of 0.065 gpm/ft^2. The targeted flux is based on the scaled flux used during AVANTech testing[1] (0.306 gpm through 4.7 ft^2 of Mott sintered metal filter [0.065 gpm/ft^2]). Filtration was performed at a targeted temperature of 16 °C. Filter resistance as a function of time was measured and the filter was backflushed ("backpulsed") if the differential pressure increased to 2 psi across the filter. Backflush solutions were collected, and the solids found were concentrated then analyzed.

5. Filter cleaning after the 5.5 M feed: The filter was cleaned using a prototypic TSCR protocol by soaking in 0.1 M NaOH for 2 hours.

---

[1] TSCR Dead End Filter Scoping Test Summary, presentation by AVANTech, Inc. on November 13, 2018, in Richland, Washington.

6. Filtration of the 7 M Na feed: Filtration was performed using a Mott Grade 5 sintered metal filter at a targeted flux of 0.065 gpm/ft^2. Filtration was performed at a targeted temperature of 16 °C. Filter resistance as a function of time was measured and the filter was backflushed ("backpulsed") if the differential pressure increased to 2 psi across the filter. Backflush solutions were collected, and the solids found were concentrated then analyzed.

7. Filter cleaning after the 7 M feed: The filter was cleaned using a prototypic TSCR protocol by soaking in 0.1 M NaOH for 2 hours.

8. Filtered permeate from testing was collected and retained for use as feed for subsequent IX testing (outside the scope of this test plan). After filtration, the permeate bottles were placed back into the cooling trough.

9. CWF: After cleaning, the BDEF was rinsed and another CWF test was executed on the filter.

10. The BDEF system was laid-up for storage.

Table 3.1 provides a mass balance for the batch 1 BDEF testing. A total of 5193.1 g of AP-105 supernatant was added to the BDEF system during testing, and a total of 5143.5 g was removed. The missing mass (~50 g) is due to evaporation and material that wets the inside of the BDEF system. It is not recoverable, and only represents less than 0.6% of the initial feed.

Table 3.1. Mass balance – batch 1 (5.5M Na) BDEF.

Description	In (g)	Out (g)
Decanted supernate filtration	5193.1	
Product to IX		4883.0
Permeate samples		20.9
Backpulse samples		229.2
Drained from BDEF		10.4
Total	5193.1	5143.5

Table 3.2 provides a mass balance for the batch 2 BDEF testing. A total of 9596.5 g of AP-105 supernatant was added to the BDEF system during testing, and a total of 9520.8 g was removed. The missing mass (~76 g) is due to evaporation and material that wets the inside of the BDEF system. It is not recoverable, and only represents less than 0.8% of the initial feed.

Table 3.2. Mass balance – batch 2 (7.0 M Na) BDEF.

Description	In (g)	Out (g)
Decanted supernate filtration	9596.5	
Product to IX		9397.8
Permeate samples		24.4487
Backpulse samples		64.3
Drained from BDEF		34.3
Total	9596.5	9520.8

3.2 Dilution

Dilution of the feed material received from tank AP-105 was based on the previous characterization performed in FY20 (Allred et al. 2020). The density was 1.414 g/mL and the sodium concentration was 8.72 M. For batch 1, the target end point Na concentration was 5.5 M. For batch 2, the target end point Na concentration was 7.0 M. Dilution was performed using raw (unprocessed) water from the Colombia River. The volumetric basis for dilution was estimated by

$$C_1V_1 = C_2V_2$$

$$V_2 = \frac{C_1V_1}{C_2}$$

Where C_1 is the sodium concentration of the undiluted tank waste, V_1 is the undiluted tank waste volume, C_2 is the target final sodium concentration, and V_2 is the diluted tank waste volume. From this a dilution factor is derived. The dilution factor is defined as

$$DF = \frac{V_2}{V_1}$$

where V_1 is the initial solution volume and V_2 is the final solution volume.

For batch 1, the contents of three AP-105 sample jars were combined and diluted with the process water at a mass ratio of nominally 1000:414 (undiluted tank waste: raw water) to achieve a volume dilution factor of 1.585. The same process was performed for batch 2 but using a mass ratio of nominally 1000:174 to achieve a volume dilution factor of 1.246.

3.3 Feed Temperature Control

Figure 3.3 provides the temperature profile of the AP-105 feed as it awaited introduction into the BDEF system for filtration. The feed was chilled and held at the 16 °C setpoint temperature for approximately 1 week before the start of filtration testing, beginning on 11/28/2022, and continued to be chilled throughout the filtration process. A 100-ohm platinum resistance temperature detector probe, labeled TE-104, measured the temperature in a feed bottle held in the trough heat exchanger and averaged 16.0 °C throughout the chilling duration. TE-104 was placed in feed bottles using a lid with a feedthrough, allowing TE-104 to be submerged without risk of spill.

A series of temperature deviations that exceeded the 16 °C ± 2.2 °C threshold were reported by TE-104 starting at 12/3/22 2154. While the exact cause of the sharp changes in temperature are unknown, as no manual changes were applied to the feed bottles in the trough or the chiller settings configuration during this period, the temperature returned to the normal ranges at 0444 on 12/04/22 – approximately 9.5 hours before filtration began.

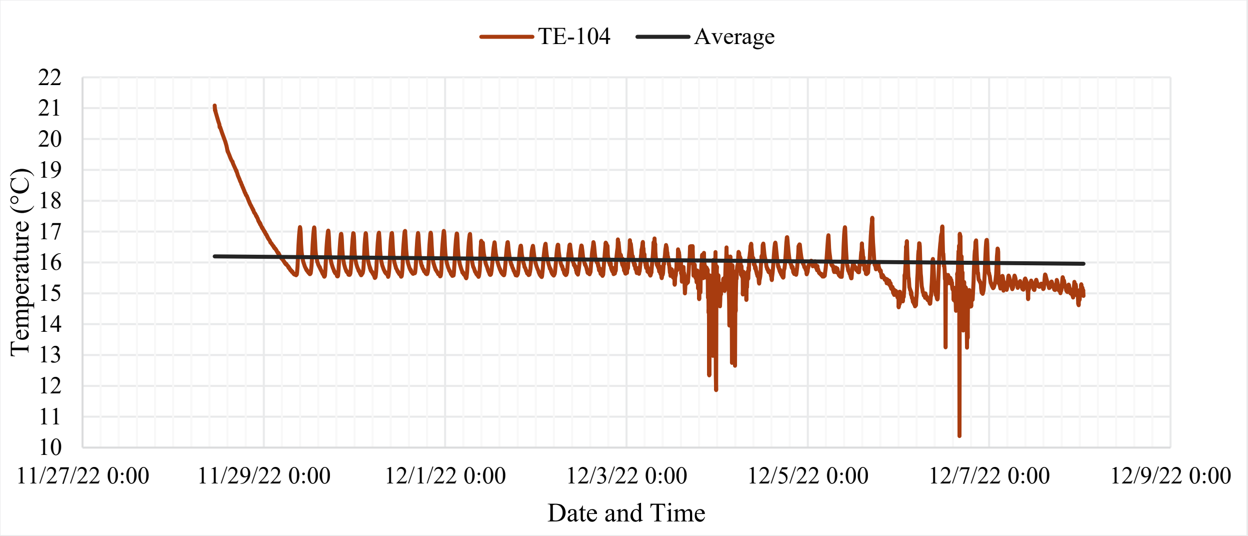

Figure 3.3. AP-105 temperature in the trough heat exchanger.

An impulse drop in 5-minute average temperature of approximately 6.2 °C was reported by TE-104 at 1608 on 12/06/2022. The temperature was promptly returned to the normal operating range over the following 5-minute period. Due to the extreme change in reported temperature over a single time increment followed by the immediate reversal of the change, it is likely that the minimum temperature reported was not reflective of the actual temperature of the feed bottle solution in the trough. The average temperature of the feed while cooling prior to testing was 16.2 °C and the average during filtration testing was 16.0 °C.

The filtration test temperatures of batch 1 and batch 2 AP-105 slurry feed in the BDEF recirculation loop (TE-101) are shown in Figure 3.4 and Figure 3.5, respectively. Where the small rise in temperature of the TE-101 is indicative of the feed additions to the slurry reservoir via transfer pump from the feed cooling trough. The higher spikes with TE-101 in Figure 3.4 denote backpulse times where the recirculation is stopped and the reservoir isolated. An offset in ambient cell temperature readings is seen between TE-102 and TE-103. TE-103 was found to be 1.6 °C higher when compared to TE-102, the TE-102 signal was also found to be much noisier for some undetermined reason. Temperature profiles of the AP-105 stream immediately before (TE-102) and after (TE-103) the filter – both contained within the clamshell heat exchanger – are overlayed in Figure 3.4 and Figure 3.5 for the individual batches.

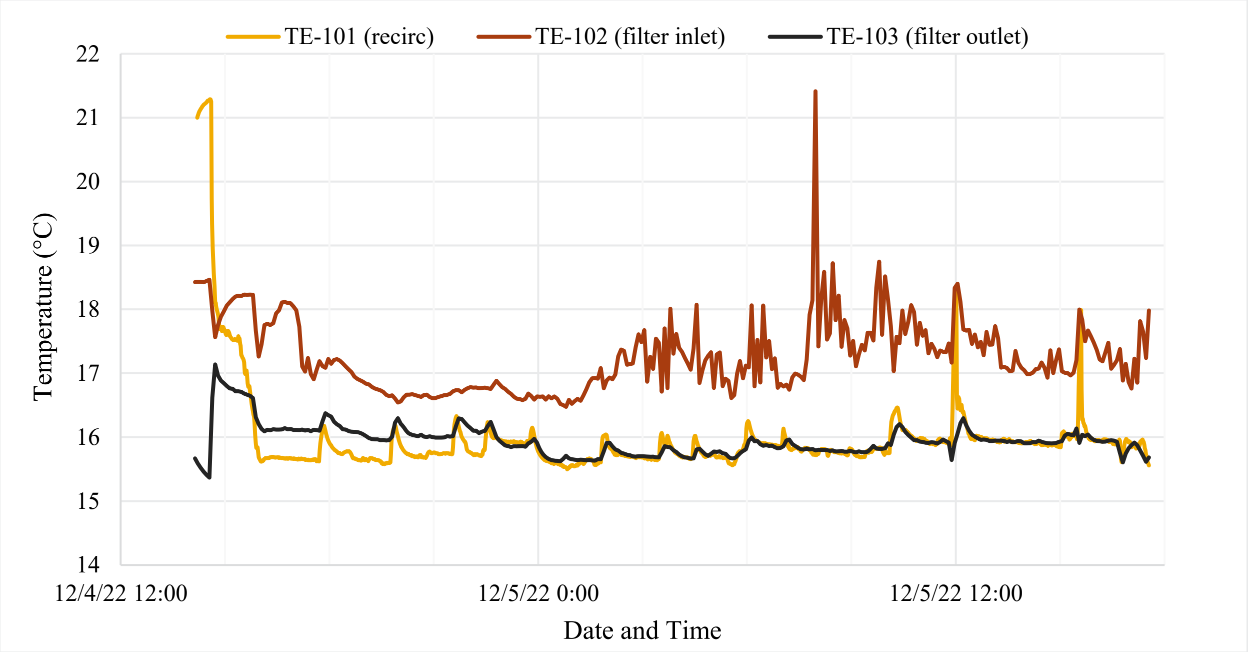

Figure 3.4. AP-105 temperature in the BDEF recirculation loop and clamshell for batch 1.

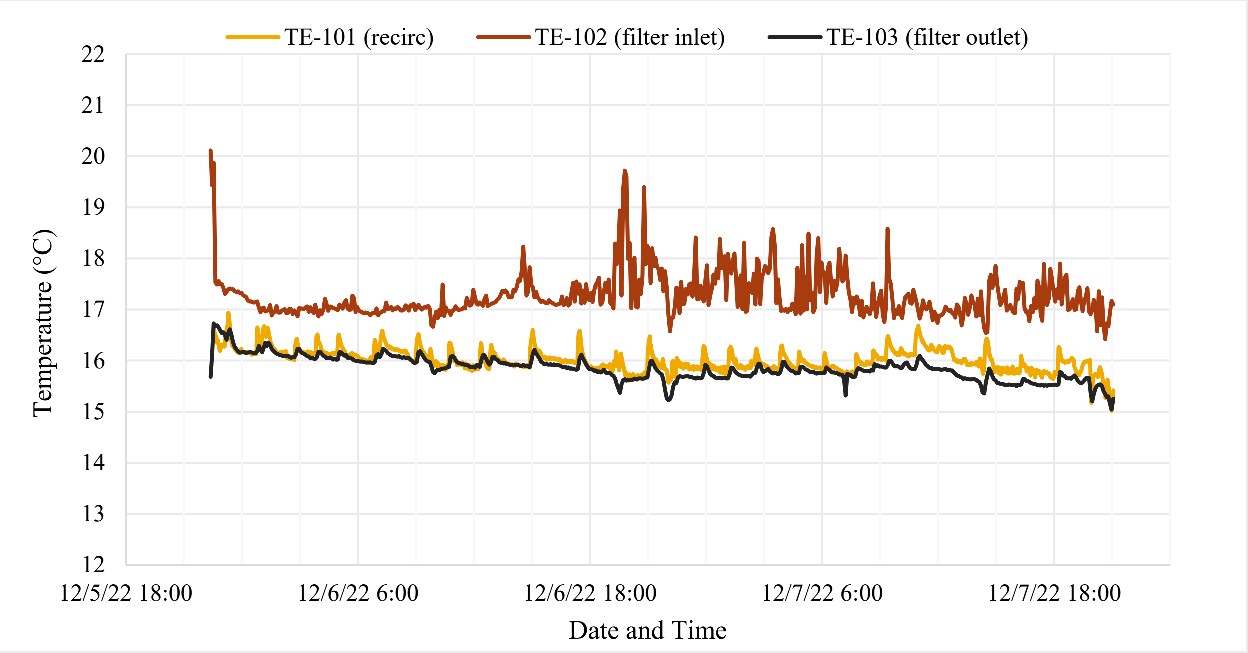

Figure 3.5. AP-105 temperature in the BDEF recirculation loop and clamshell for batch 2.

3.4 Sample Analysis

Three permeate samples from each batch were collected (TI-136-P1, TI-136-P2, TI-136-P3 for batch 1 and TI-136-P4, TI-136-P5, TI-136-P6 for batch 2) after approximately 1/3, 2/3, and 3/3 of the AP-105 feed had been filtered for each batch. These samples were submitted for total alpha analysis to determine the transuranic (TRU) content of the filtered permeate.

Backpulse concentrates from each batch were retained and kept separate. Upon completion of filtration testing, the solids from these batches were concentrated as shown in Figure 3.6. To concentrate solids from each batch, solution collected was centrifuged at 2500 rpm for 10 minutes. The bulk amount of the supernatant was decanted and the solids from the centrifuge tubes were suspended and combined. Once removed from the hot cell, these solutions were rinsed to reduce dose to microscopy staff. Figure 3.7 shows the solids that were collected from the backpulsed solution after the solutions were centrifuged and decanted.

Batch 1 samples were rinsed with a 1.0 M NaOH/4.6M $NaNO_3$ solution. Batch 2 samples were rinsed with a 1.1 M NaOH/5.9M $NaNO_3$ solution. After rinsing, each sample was centrifuged at 3000 rpm for 5 minutes. This process was performed two times. TI-136-XXM Solids-1 samples were left to air dry for approximately 2 weeks, while TI-136-XXM Solids-2 samples were left in approximately 1 mL of the rinse solutions as noted in Table 3.3. Figure 3.8 shows the solids after the rinsing process and air drying. Very few solids were collected and there was only sufficient sample available to conduct scanning electron microscopy (SEM) analysis. The SEM results are reported in Section 4.6.

Table 3.3. Backpulsed solids sample descriptions.

Sample ID	Sample Description
TI-136-5.5M Solids-1	Concentrated AP-105 solids from batch 1 left to dry
TI-136-5.5M Solids-2	Concentrated AP-105 solids from batch 1 left in liquid state
TI-136-7.0M Solids-1	Concentrated AP-105 solids from batch 2 left to dry
TI-136-7.0M Solids-2	Concentrated AP-105 solids from batch 2 left in liquid state

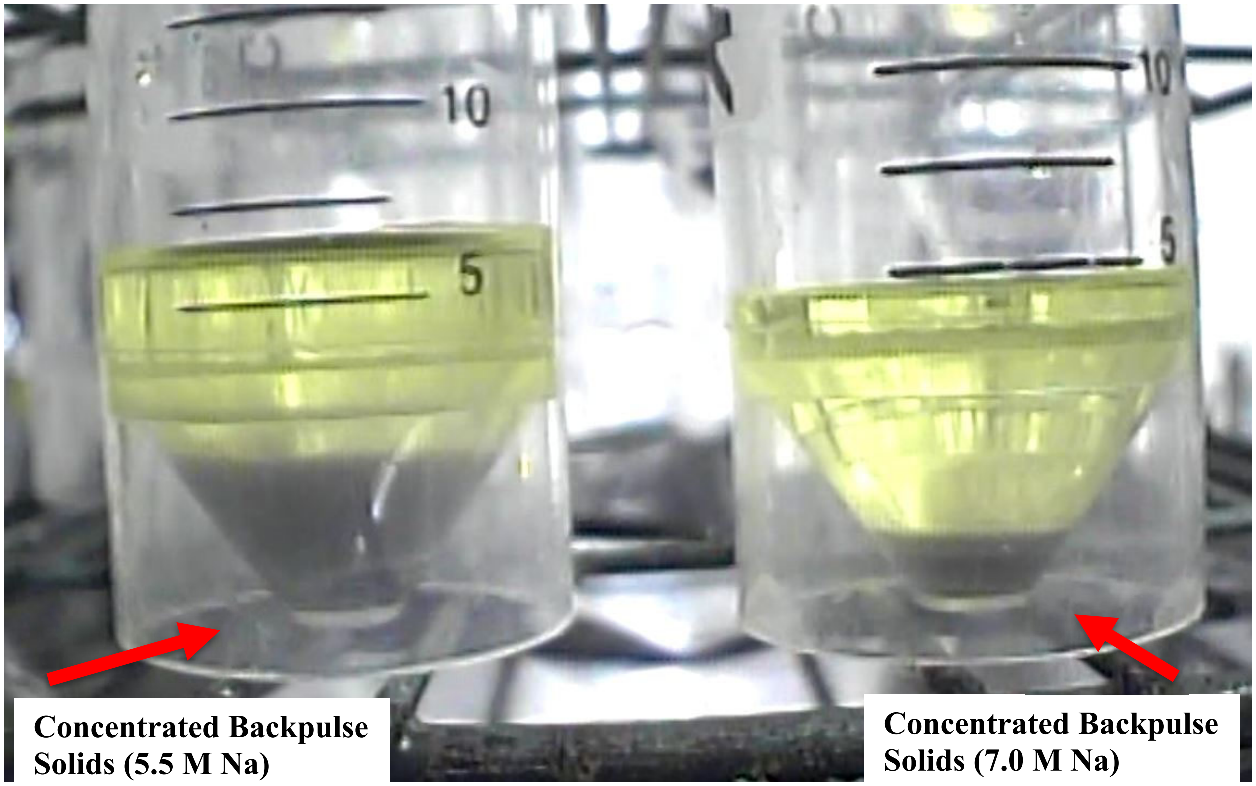

Figure 3.6. Concentrated solids after centrifuging in hot cell.

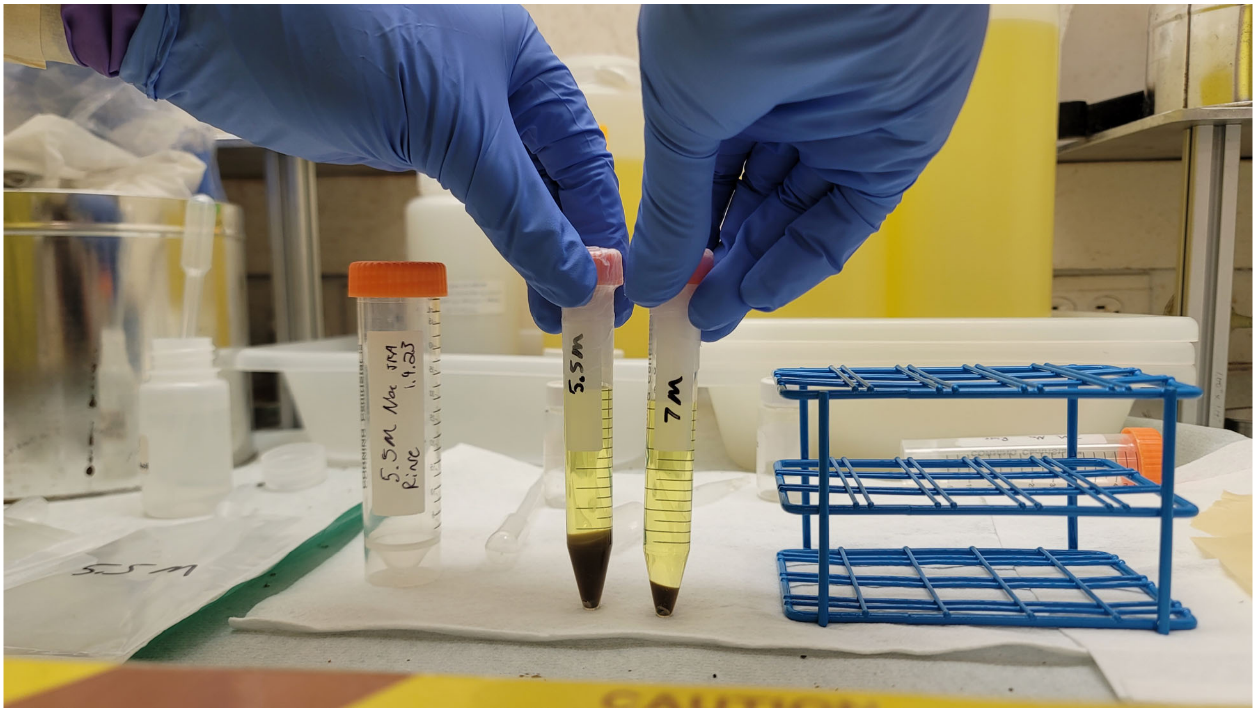

Figure 3.7. Concentrated solids in fumehood after centrifuging.

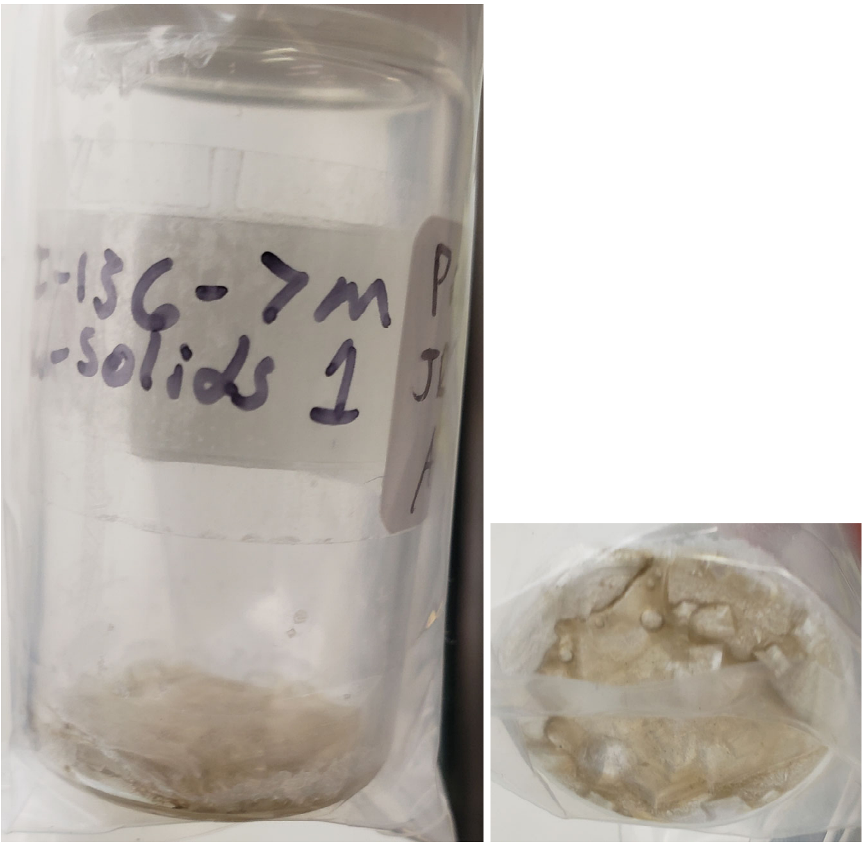

Figure 3.8. Concentrated solids after rinse and air drying.

4.0 Results

4.1 Dilution Process Results

A sample of each batch of diluted AP-105 solution was checked for density to assess the dilution. Density was measured using a 10-mL Class A volumetric flask and an analytical balance. For batch 1, density was measured to be 1.265 g/mL at an ambient cell temperature of 25.7 °C. Batch 2 density was measured to be 1.317 g/mL at 25.7 °C. The Na concentration was not measured after dilution but was measured after filtration (which should not affect Na concentration) and will be included in the IX report for FY23 (RPT-DFTP-037, *Cesium Removal from 5.5 and 7.0 M Na AP-105 Using Crystalline Silicotitanate*; currently being drafted).

The density of the raw Colombia River water used for dilution was measured to be 0.9942 g/mL at 15.6 °C.

4.2 Clean Water Flux

The objective of the CWF was to assess the state of the system at the start of testing to ensure a uniform basis for comparing different filtration trials, and in particular to ensure that the system is "clean" at the start of testing. Figure 4.1 shows the initial CWF at 16 °C using 0.01 M NaOH with the Media Grade 5 stainless steel BDEF filter. The CWF tests were conducted at ambient cell temperature at a nominal 2.57 mL/min (0.065 gpm/ft^2) permeate flow rate. The transmembrane pressure (TMP) averaged 0.116 psid in the initial CWF with an average filter resistance of 1.65×10^{10} m^{-1}. Resistance, R [m^{-1}], is calculated via Darcy's law:

$$Q = \frac{PA_t}{\mu R}$$

where Q is the volumetric flow rate [m^3/s], P is the TMP [Pa], A_t is the total filter area [m^2] [9.74×10^{-4} m^2], and μ is the filtrate dynamic viscosity [Pa·s] (assumed to be 1.11 cP at 16 °C). Rearranging so that:

$$R(t) = \frac{P(t)A_t}{\mu Q(t)}$$

Prior CWF results on the BDEF system with this filter ranged from 0.015 to 0.2 psid TMP (Allred et al. 2022). These values all are likely within the accuracy of the CWF measurement and represent a relatively clean filter. Estimates of the resistance for the Mott 6610 series Grade 5 are on the order of 2×10^{10} m^{-1}. The average TMP of 0.124 psid (shown in Figure 4.1) during the CWF indicates a lack of fouling on the filter (due to residual solids in the system). As such, these results indicate an overall clean system at the start of testing.

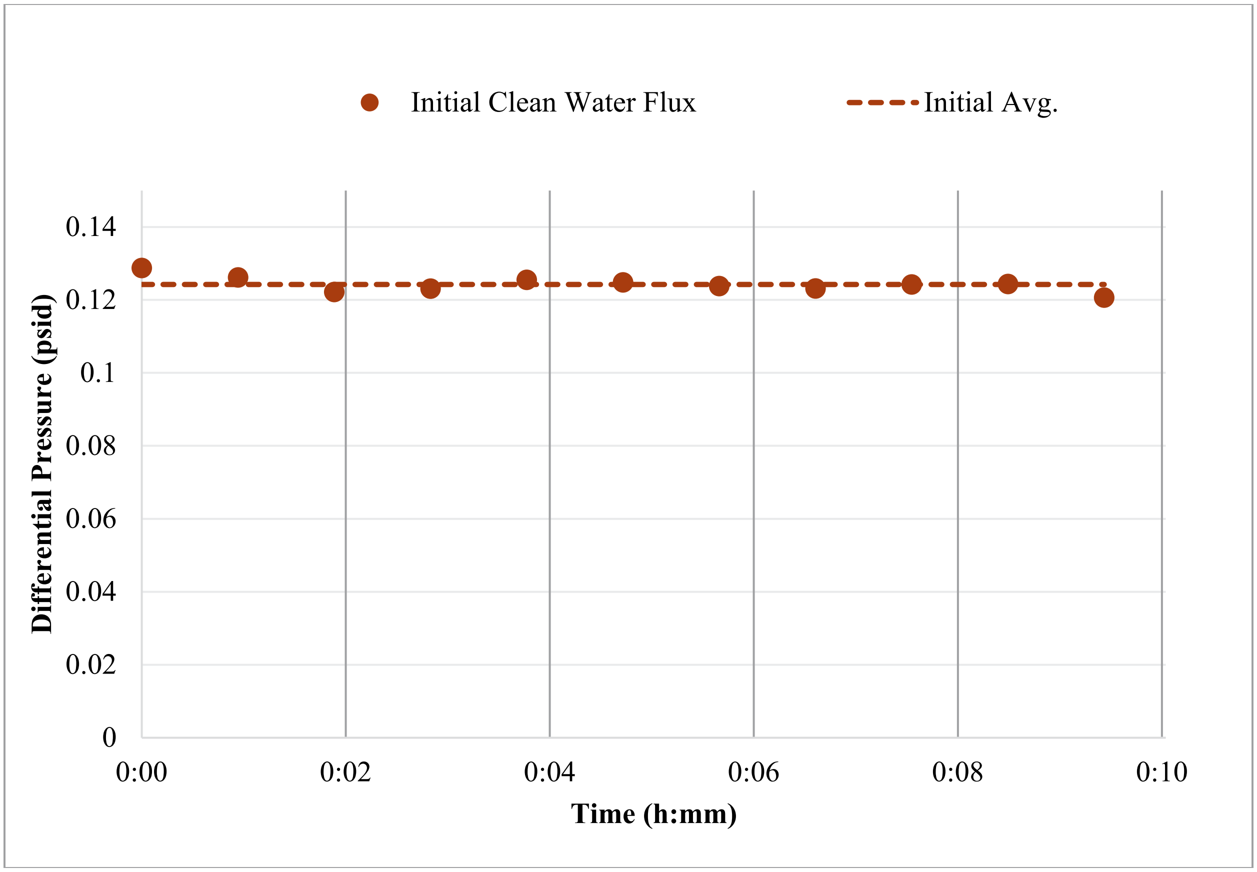

Figure 4.1. CWF measurements for Media Grade 5 BDEF at 2.57 mL/min (0.065 gpm/ft^2) permeate rate (nominal) before testing. (Dashed line is average pressure over the 10-minute period.)

4.3 Waste Filtering

4.3.1 Batch 1 (5.5 M Na)

Each BDEF feed bottle was positioned in the trough heat exchanger to maintain feed temperature control (16 ± 1 °C). Feed was then transferred into the BDEF reservoir via metering pump until approximately 2 inches of AP-105 solution remained in the feed bottle. The remaining “bottoms” from each feed bottle were consolidated and fed into the system toward the end of the filtration process. The filtration rate was controlled via an MFC set at 2.57 mL/min (0.065 gpm/ft^2). The actual flow rate averaged 2.56 mL/min. Slurry recirculation line pressure was kept between 20 and 25 psi, with adjustments made for any deviations. Three backpulses were performed during the filtration process: two during filtration when the 2-psid TMP limit (the threshold to indicate that a backpulse was needed) was reached and one after the feed was exhausted.

Table 4.1 provides a timeline for the filtration testing, indicating feed bottle change, permeate bottle change, process liquid flow, and sampling sequences. Note that the filtration of feed bottle “bottoms” began after 2.87 m^3/m^2 of feed had been filtered.

Table 4.1. Batch 1 system timeline.

Date	Time	Volume Filtered (m^3/m^2)	Event
4-Dec	14:12	0.0	Filtration Started with BDEF-AP5-1
	17:41	0.29	Filtering from feed bottle BDEF-AP5-2
	22:23	1.03	IX-AP5-1 full, permeate switched to recycle
	22:24	1.03	IX-AP5-2 in place, permeate switched for collection
	22:26	1.04	Filtering from feed bottle BDEF-AP5-3
5-Dec	0:45	1.40	V10 switched to reservoir. TI-136-P1 sample taken directly from dewatering line
	0:46	1.40	Dewatering line replaced back to IX-AP5-2
	3:32	1.84	Filtering from feed bottle BDEF-AP5-4
	4:53	2.05	IX-AP5-2 full, permeate switched to recycle
	4:55	2.06	IX-AP5-3 in place, permeate switched for collection
	9:56	2.85	TI-136-P2 sample taken from IX-AP5-3
	10:05	2.87	Filtering from combined BDEF-AP5-3 and BDEF-AP-4 bottoms from BDEF-AP5-3 feed bottle
	11:32	3.10	IX-AP5-3 full, permeate switched to recycle
	11:33	3.10	IX-AP5-4 in place, permeate switched for collection
	11:48	3.14	V5 closed to prepare for backpulse
	11:57	3.14	Backpulse performed and collected into TI-136-S1 via V3
	12:02	3.15	Continue dewatering into IX-AP5-4
	15:28	3.68	Backpulse performed and collected into TI-136-S2 via V3
	15:37	3.68	Filtration of remaining feed in slurry reservoir resumed
	16:41	3.85	V5 closed to refill backpulse chamber
	16:45	3.85	V5 opened to resume filtration. Bubbles in reservoir. Pump reduced to 1200 rpm to reduce entrained air.
	17:13	3.92	Pump reduced to 900 rpm
	17:23	3.95	Pump reduced to 800 rpm
	17:27	3.96	Pump reduced to 600 rpm
	17:33	3.97	End of Batch 1 filtration

Testing was started on the afternoon of December 4. TMP remained steady at ~0.2 psid until 1.2 m^3/m^2 filtered as seen in Figure 4.2. TMP then steadily increased to 0.432 psid with 2.87 m^3/m^2 filtered, after which TMP increase rapidly until the 2 psid TMP limit was reached at 3.14 m^3/m^2 filtered. After the completion of the first backpulse, the TMP began at 0.23 psid. From there, it increased to 1.05 psid then decreased quickly to 0.55 psid at 3.44 m^3/m^2 filtered; this is assumed to be due to solids soughing/shifting on the filter as no operator actions had taken place at that time. Another TMP decrease (from 1.52 to 1.02 psid) occurred at 3.62 m^3/m^2 filtered, again with no operator input. TMP reached 2 psid again at 3.68 m^3/m^2 filtered and a backpulse was performed. After the second backpulse, TMP was recovered to 0.3 psid. TMP increased to 0.85 psid at 3.85 m^3/m^2 when the backpulse chamber was filled in preparation for the final backpulse as the feed in the system was being exhausted. From that point the final ~100 mL was filtered, and the pump speed lowered until the minimum operable liquid level was reached. The test was ended and the final backpulse performed.

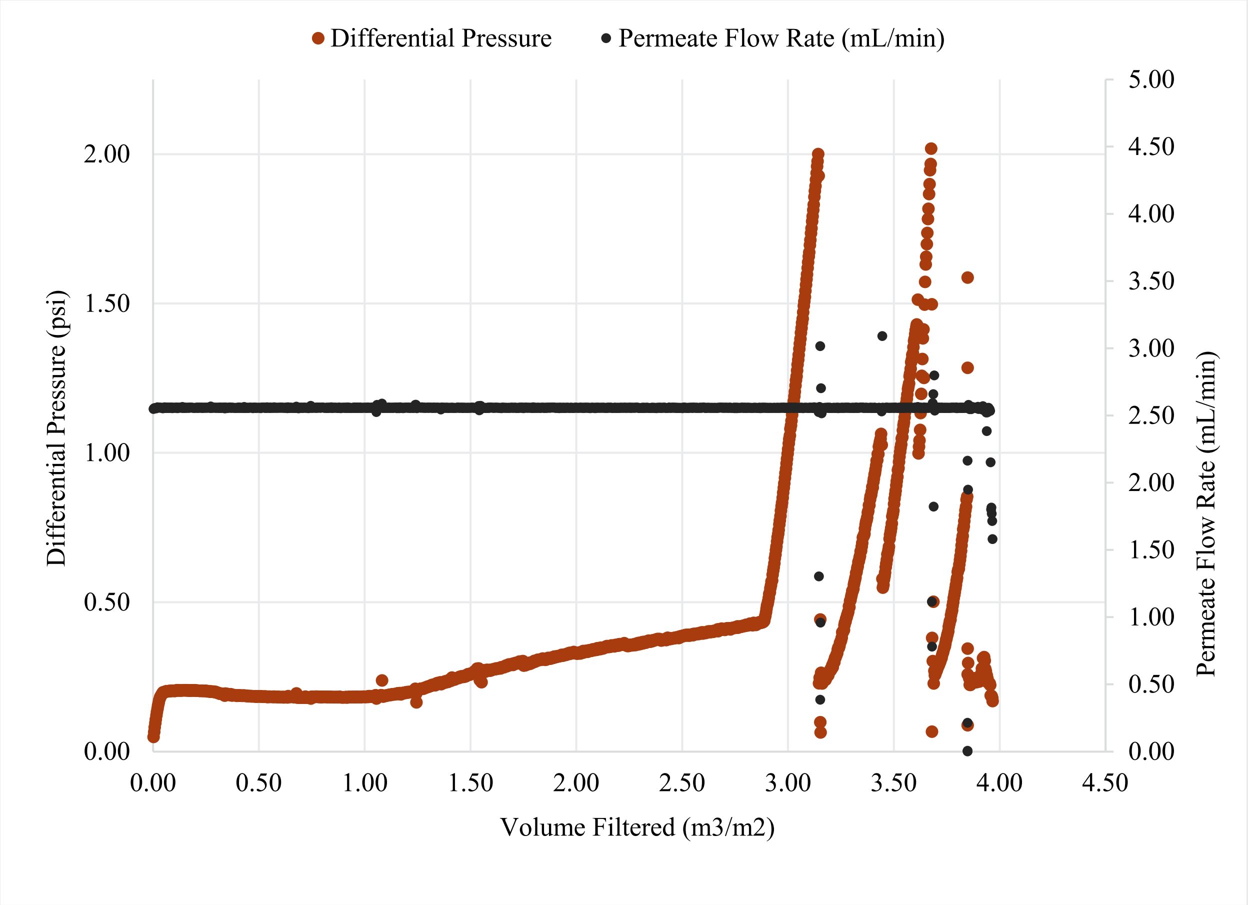

Figure 4.2. Filter differential pressure and MFC flow rate during batch 1 filtering operations.

As stated before, Darcy's law relates the flow rate through a porous media to the pressure drop causing that flow:

$$Q(t) = \frac{\Delta P}{(\mu * R(t))}$$

where Q is the filter volumetric flow rate, ΔP is the TMP, μ is the fluid viscosity, and R_{tot} is the total filtration resistance.

Rearranging produces:

$$R(t) = \frac{\Delta P}{(\mu * Q(t))}$$

Figure 4.3 shows total filter resistance as a function of volume filtered over the 2 days of batch 1 testing.

To assess the nature of the fouling occurring, multiple fouling mechanism functions were fit to the data using curve fit methodology developed in Hermia (1982) and applied in the FY20 AP-105 filtration testing detailed in RPT-DFTP-021 (Allred et al. 2020). The filtration laws developed by Hermia (1982) are for constant pressure dead-end filtration but can be readily recast into constant flux formulas as documented by Hlavacek and Bouchet (1993). For the present analysis, Hermia's laws are recast into scaled resistance form, such that

$$R^n = R_o^n \left(1 + \mathrm{sign}(n)\, \sigma v\right)$$

Here, the exponent n defines the blocking regime, R scaled resistance, $v = V/A$ is the specific volume filtered, and σ is the regime dependent blocking parameter. In the present analysis, R_o is a reference resistance corresponding to the start of a given filtration period (either after start-up or backflushing), and v is the specific volume filtered relative to that same reference point. The fouling mechanism is characterized by the value of n. Hermia (1982) defined four blocking regimes:

- cake filtration blocking ($n = 1$)
- intermediate blocking ($n = 0$)
- standard blocking ($n = -0.5$)
- pore / complete blocking ($n = -1$)

For the current data, a best-fit value of n is assessed for specific filtration periods using Microsoft Excel's built in solver to minimize the root mean square error (RMSE) defined by:

$$\mathrm{RMSE} = \sqrt{\sum_i \left(R_i^{(\mathrm{p})} - R_i^{(\mathrm{m})}\right)^2}$$

where $R_i^{(\mathrm{p})}$ and $R_i^{(\mathrm{m})}$ are the predicted and measured resistances for an individual measurement i in the filtration period. To avoid the need to regress a best fit value of σ, it is estimated as

$$\sigma = \frac{\mathrm{sign}(n)}{v_f}\left[\left(\frac{R_f}{R_o}\right)^n - 1\right]$$

where R_f and v_f are the final resistance and specific volume filtered of the period. Table 4.2 details the blocking parameters and regime exponent n determined by this analysis.

Table 4.2. Batch 1 filtration regime exponent n and blocking parameter σ.

Period	**Regime Exponent n**	**Blocking Parameter σ, 1/m**
Initial Fouling	1.90	2.00
Backflush 1	0.39	3.07
Backflush 2A	0.14	0.78
Backflush 2B	1.00	10.04
Backflush 2C	1.04	17.81
Backflush 3	-0.07	0.56

The Table 4.2 results show evaluation of four filtration periods: the initial period of filtration and the periods leading up to the first, second, and third filter backflushes. The second backflush period evidences spontaneous decreases in filter resistance which we attribute to solids “sluffing” off the filter surface due to either gravity, vibration, or some combination thereof. For this reason, the second backflush period is broken into three subperiods (A, B, and C).

The Table 4.2 results indicate the fouling behavior in the initial period, with a regime exponent approximately equal to 2, is anomalous, at least with respect to Hermia’s standard exponents. In this period, fouling slows with time, and may be the result of feed variability or complex hydrodynamics within the filter annulus. The remaining periods have relatively standard regime exponents. Filtration periods prior to backflushing (Backflush 1, Backflush 2A, and Backflush 3) exhibit filter resistance increases best characterized by intermediate fouling ($n \sim 0$). Interestingly, the periods following solids “sluffing” (Backflush 2B and 2C) exhibit cake filtration fouling behavior rather than the intermediate regime following backflush operation, suggesting that solids cakes form or reform readily after disruptions that occur by means other than backflushing and chemical cleaning. Regardless, Batch 1 filtration is characterized in all cases by flow exponents greater than zero ($n > 0$), suggesting that deposition is largely occurring on the on the surface of the filter membrane rather than within its porous substructure. This, in turn, suggests that Batch 1 solids are sufficiently large (from a hydrodynamic or chemical interaction basis) not to permeate into the depths of the filter itself.

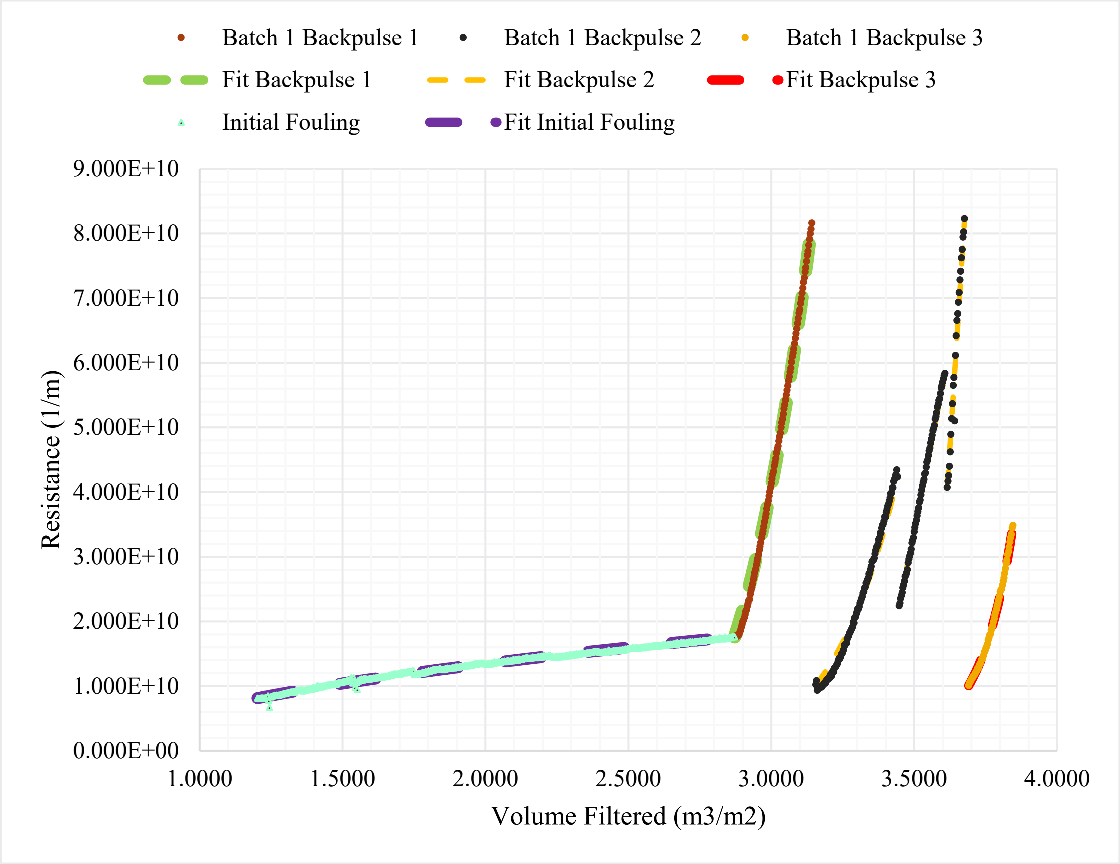

Figure 4.3. Fit to batch 1 experimental data using classical fouling mechanisms.

Table 4.3. Batch 1 test parameters prior to backpulsing.

Test Event	Filtration Resistance (1/m)	Volume Filtered since Last Backpulse (m^3/m^2)	Transmembrane Pressure (psid)
Backpulse 1	7.96×10^{10}	3.14	2.00
Backpulse 2	6.26×10^{10}	0.53	2.02
Backpulse 3[(a)]	1.12×10^{10}	0.29	0.17

(a) Feed exhausted, TMP target not reached.

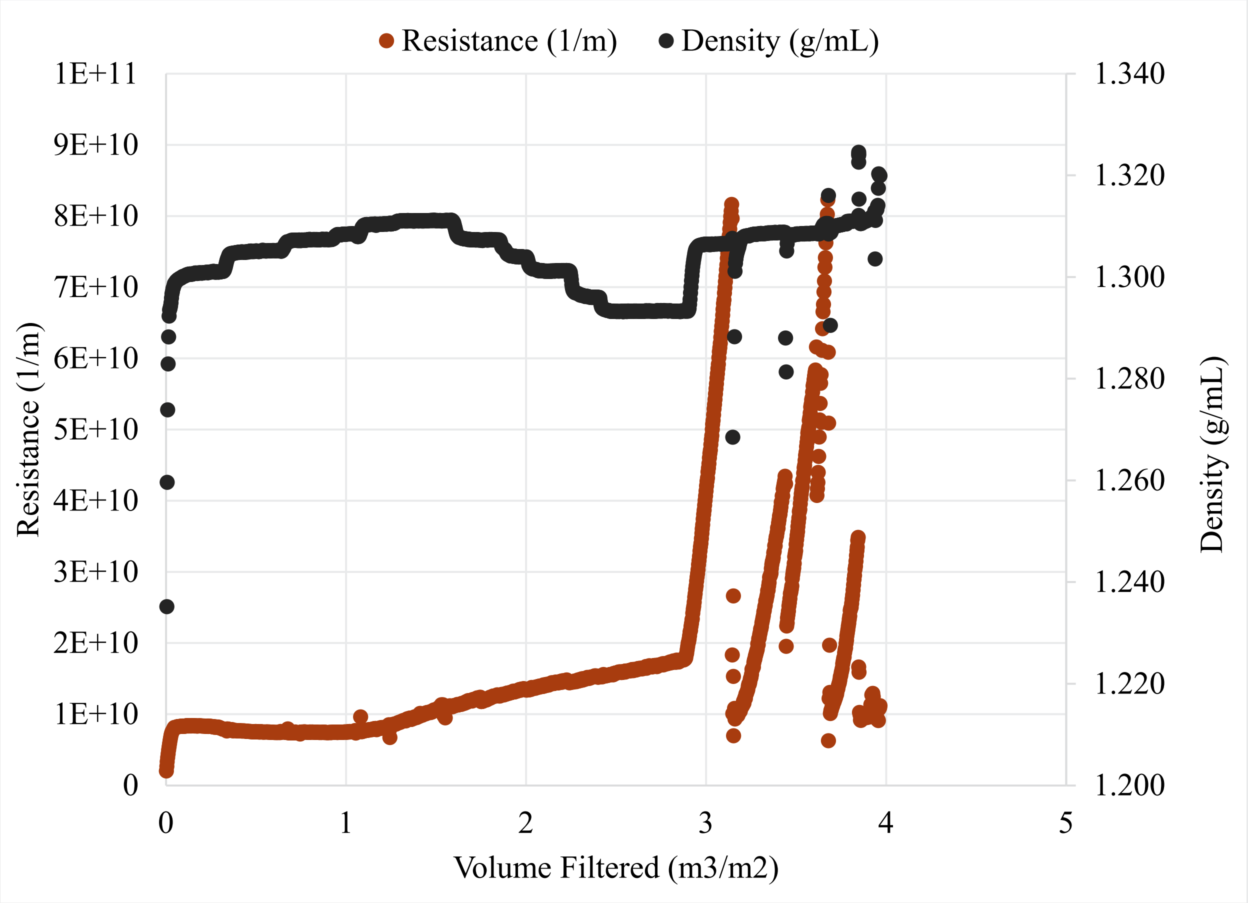

Figure 4.4. AP-105 batch 1 density during filtration process.

The density of the diluted AP-105 solution ranged between approximately 1.29 and 1.31 g/mL per the MFC as shown in Figure 4.4. A large increase in density at approximately 2.87 m^3/m^2 corresponds with the beginning of adding the 5.5 M Na AP-105 bottoms to the slurry reservoir, which eventually peaked at 1.31 g/mL. The consolidated bottoms of each feed bottle had a higher density than the previous volume that was filtered.

Post filtration analysis of the product bottles prior to IX included the measurement of product density. Density measurement was performed in a 10-mL volumetric flask at 24.4 °C. These values are reported in Table 4.4 and show little variation in density between bottles. Average bottle density was found to be 1.2629 g/mL with a standard deviation of 0.0076 g/mL.

Table 4.4. Batch 1 post filtration density measurements of product bottles.

Bottle ID	Density (g/mL)
IX-AP5-1	1.2715
IX-AP5-2	1.2642
IX-AP5-3	1.2507
IX-AP5-4	1.2653

4.3.2 Batch 2 (7.0 M Na)

Feed bottle temperature control and feed transfers were performed the same as in batch 1. The measured flow rate averaged 2.55 mL/min. Slurry recirculation line pressure was kept between 20 and 25 psi, with adjustments made for any deviations. Only one backpulse was performed during the filtration process of this batch, which occurred once the feed was exhausted.

Table 4.5 provides a timeline for the filtration testing, indicating feed bottle change, permeate bottle change, process liquid flow, and sampling sequences. Note that the filtration of feed bottle "bottoms" began after 5.10 m^3/m^2 of feed had been filtered. At 6.85 m^3/m^2 volume filtered, the last of the bottoms were poured in the slurry reservoir. This resulted in a slurry recirculation pressure spike, and valve V1 needed to be opened more to reduce pressure. Prior to this, TMP was 1.57 psid; after V1 was adjusted and the system regained equilibrium, TMP had decreased to ~0.3 psid. This is assumed to be due to solids soughing/shifting on the filter during backpressure adjustment.

Table 4.5. Batch 2 system timeline.

Date	Time	Volume Filtered (m^3/m^2)	Event
5-Dec	22:33	0.00	Begin filtering BDEF-AP5-5, collecting permeate in IX-AP5-5
6-Dec	1:02	0.39	Filtering from BDEF-AP5-6
	5:18	1.06	IX-AP5-5 full, permeate switched to recycle
	5:19	1.07	IX-AP5-6 in place, permeate switched for collection
	7:06	1.35	Filtering from BDEF-AP5-7
	12:07	2.14	IX-AP5-6 full, permeate switched to recycle
	12:09	2.14	IX-AP5-7 in place, permeate switched for collection
	12:47	2.24	Filtering from BDEF-AP5-8
	15:04	2.60	Switched V10 to reservoir, sampled IX-AP5-07 to TI-136-P4
	15:14	2.63	Resumed dewatering into IX-AP5-07
	18:35	3.15	IX-AP5-7 full, permeate switched to recycle
	18:38	3.16	IX-AP5-8 in place, permeate switched for collection
	19:30	3.30	Filtering from BDEF-AP5-9
	22:33	3.78	Filtering from BDEF-AP5-10
7-Dec	1:06	4.18	IX-AP5-8 full, permeate switched to recycle
	1:07	4.18	IX-AP5-9 in place, permeate switched for collection
	2:30	4.40	Filtering from BDEF-AP5-11
	2:22	4.38	Transferring TE-104 from BDEF-AP5-11 into product bottle IX-AP5-1
	7:07	5.13	Glass flow meter slipped down clamp. Closed V5 to stop filtration and reseat flow meter. ~20 mL spill in secondary containment pan.
	7:15	5.13	Filtering of BDEF-AP5-11 resumed
	7:44	5.21	Poured BDEF-AP5-10 bottoms into slurry reservoir for filtering
	8:28	5.32	IX-AP5-9 full, permeate switched to recycle

8:30	5.33	IX-AP5-10 in place, permeate switched for collection
9:17	5.19	BDEF-AP5-bottoms pumped into slurry reservoir
10:11	5.59	TI-136-P5 sample (~5 mL) pipetted from IX-AP5-9
14:34	6.28	IX-AP5-10 full, permeate switched to recycle
14:40	6.30	IX-AP5-11 in place, permeate switched for collection
18:11	6.85	Bottoms of BDEF-AP5-5 swirled and poured into slurry reservoir for filtering
19:50	7.11	V5 closed to fill backpulse chamber
19:55	7.11	V5 reopened
21:02	7.29	V5 closed. End of batch 2 Filtration

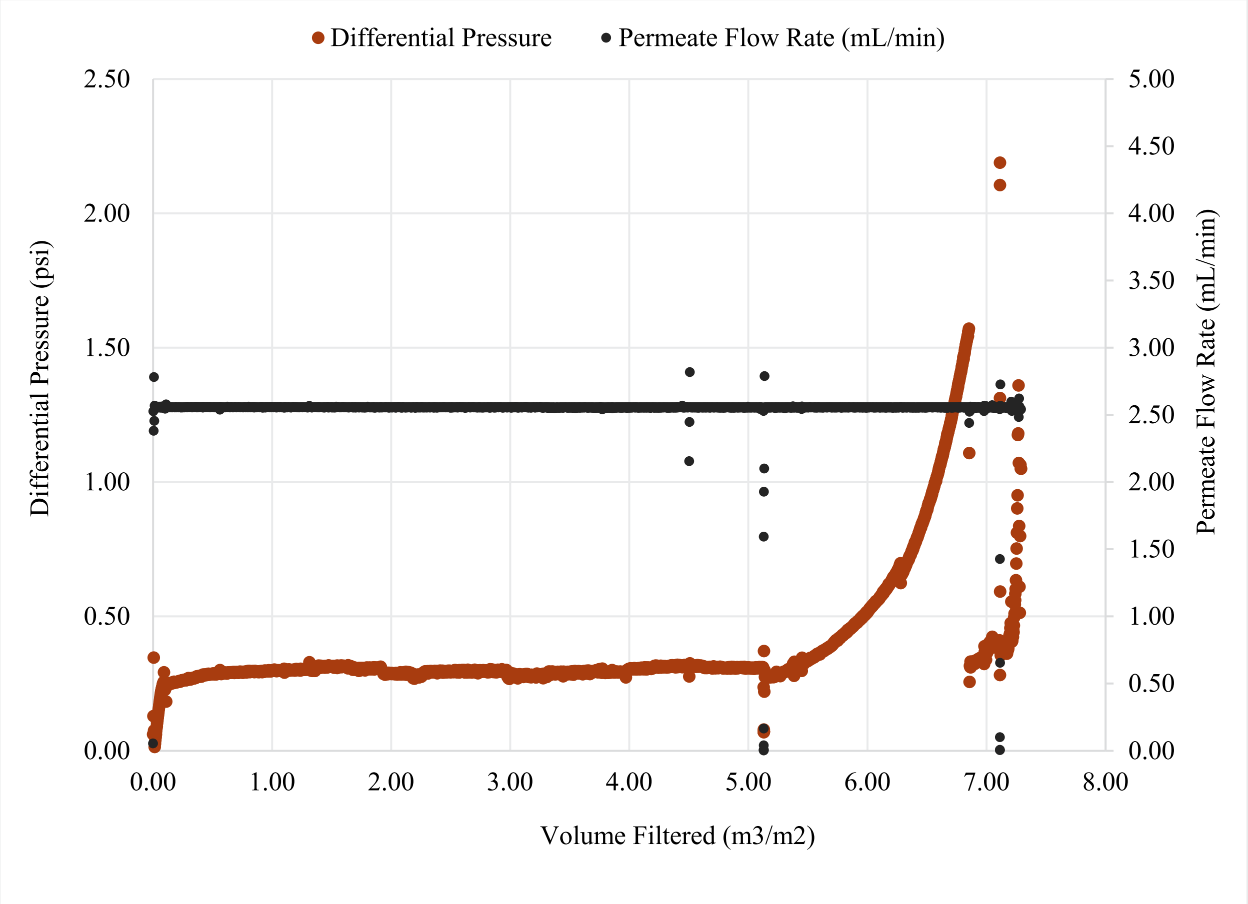

Figure 4.5. Filter differential pressure and MFC flow rate during batch 2 filtering operations.

For batch 2, no initial fouling regime was seen like that seen in batch 1. Fouling only began after filtration of feed bottle “bottoms” began at 5.10 m^3/m^2 volume filtered. The same blocking regime analysis employed for Batch 1 was applied to Batch 2 fouling dynamics. The results are shown in Table 4.6. Here, the standard blocking fouling mechanism fit well with the experimental data shown in Figure 4.6. Standard blocking, per Hermia (1982), indicates deposition of solids within the porous substructure of the filter. This, along with the lack of initial fouling, suggest solids for Batch 2 are sufficiently “small” as to penetrate the filter and result in depth fouling not observed in Batch 1. The batch 2 test parameters prior to backpulse are detailed in Table 4.7, highlighting that the TSCR action limit was not reached with 7.28 m^3/m^2 volume filtered.

Table 4.6. Batch 2 filtration regime exponent n and blocking parameter σ.

Period	**Regime Exponent n**	**Blocking Parameter σ, 1/m**
Backflush 1	-0.63	0.39

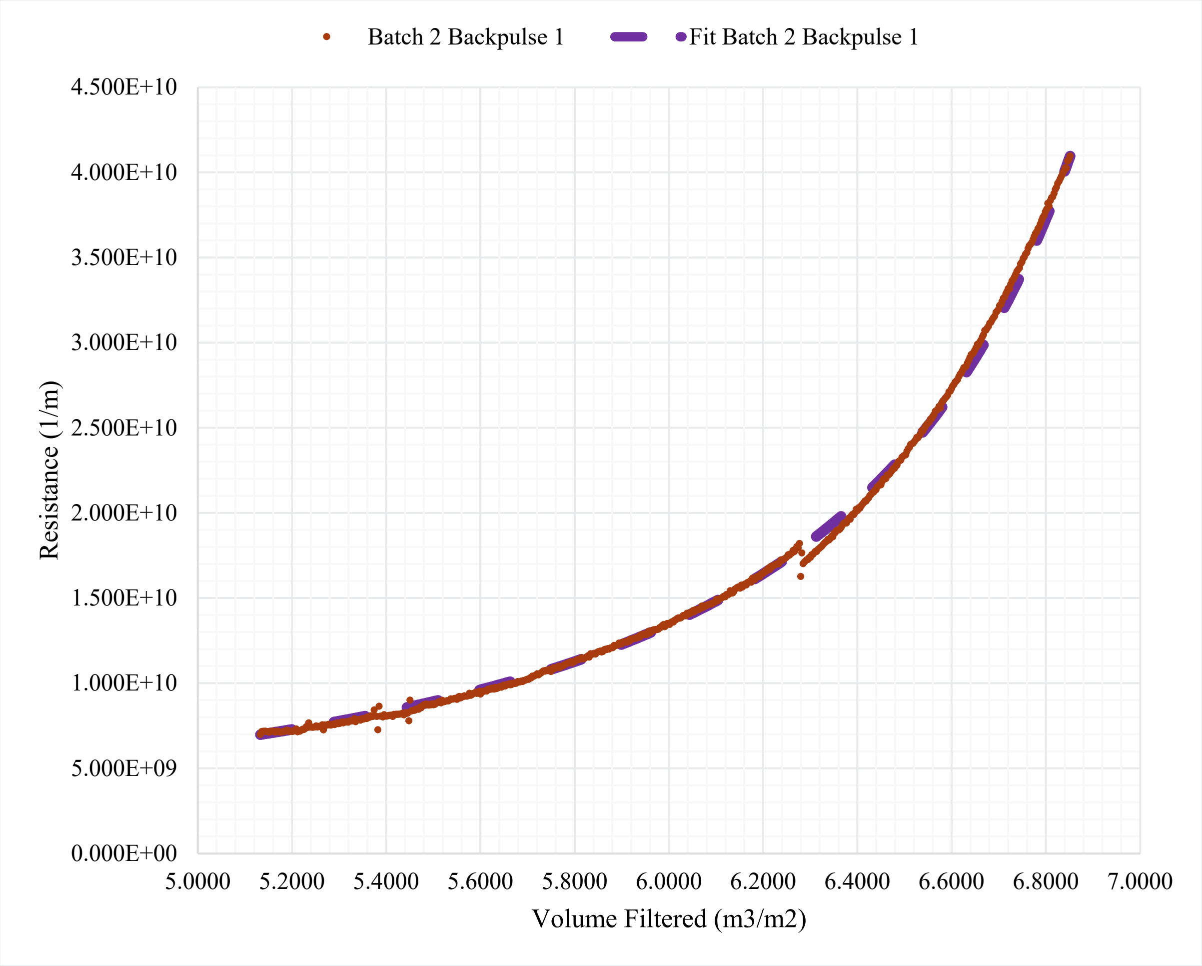

Figure 4.6. Fit to batch 2 experimental data using classical fouling mechanisms.

Table 4.7. Batch 2 test parameters prior to backpulsing.

Test Event	Filtration Resistance (1/m)	Volume Filtered Since Last Backpulse (m^3/m^2)	Transmembrane Pressure (psid)
Backpulse 1[(a)]	2.75×10^{10}	7.28	1.06

(a) Feed exhausted, TMP target not reached.

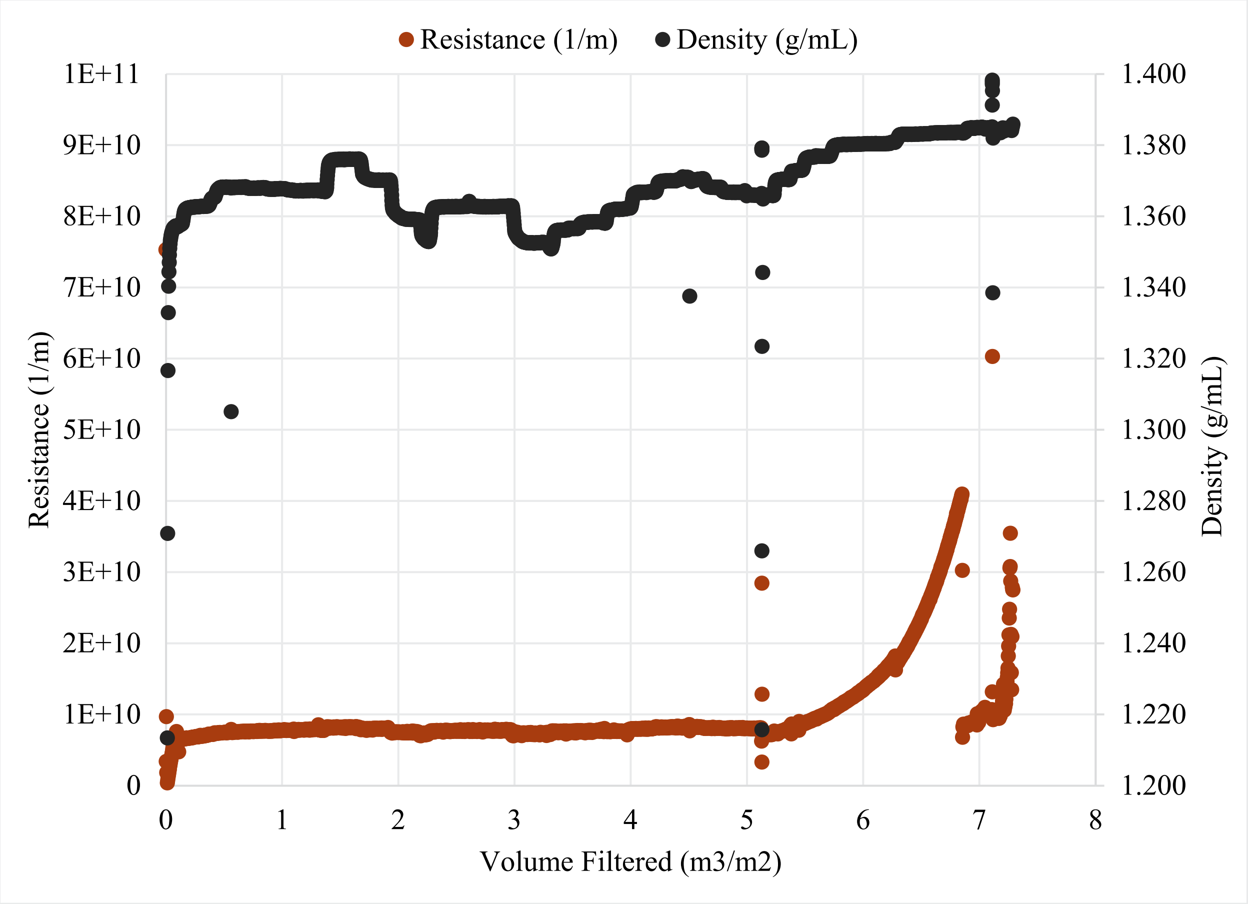

Figure 4.7. AP-105 batch 2 density during filtration process.

The density of the diluted AP-105 in batch 2 nominally ranged from 1.354 to 1.386 g/mL per the MFC as shown in Figure 4.7. Filtration of the bottle bottoms at 5.10 m^3/m^2 volume filtered again shows an elevated density value, increasing from 1.366 to 1.386 g/mL as more bottle bottoms were added to the slurry reservoir.

Post filtration analysis of the product bottles prior to IX included the measurement of product density. Density measurement was performed in a 10-mL volumetric flask at 24.6 °C. These values are reported in Table 4.8 and show little variation in density between bottles. Average bottle density was found to be 1.3122 g/mL with a standard deviation of 0.0086 g/mL.

Table 4.8. Batch 2 post filtration density measurements of product bottles.

Bottle ID	Density (g/mL)
IX-AP5-5	1.2973
IX-AP5-6	1.3160
IX-AP5-7	1.3043
IX-AP5-8	1.3083
IX-AP5-9	1.3155
IX-AP5-10	1.3215
IX-AP5-11	1.3223

4.4 Final CWF

At the conclusion of AP-105 filtration, a second filter cleaning was performed, and the CWF was measured again. Figure 4.8 compares this final CWF with the intermediate and initial CWFs. The filter differential pressure of the final CWF was averaged to be 0.104 psid. This sits between the initial and intermediate CWF average TMP, which was 0.085 psid. This indicates each filter cleaning dissolved nearly all of the solids that were deposited on the filter during each batch.

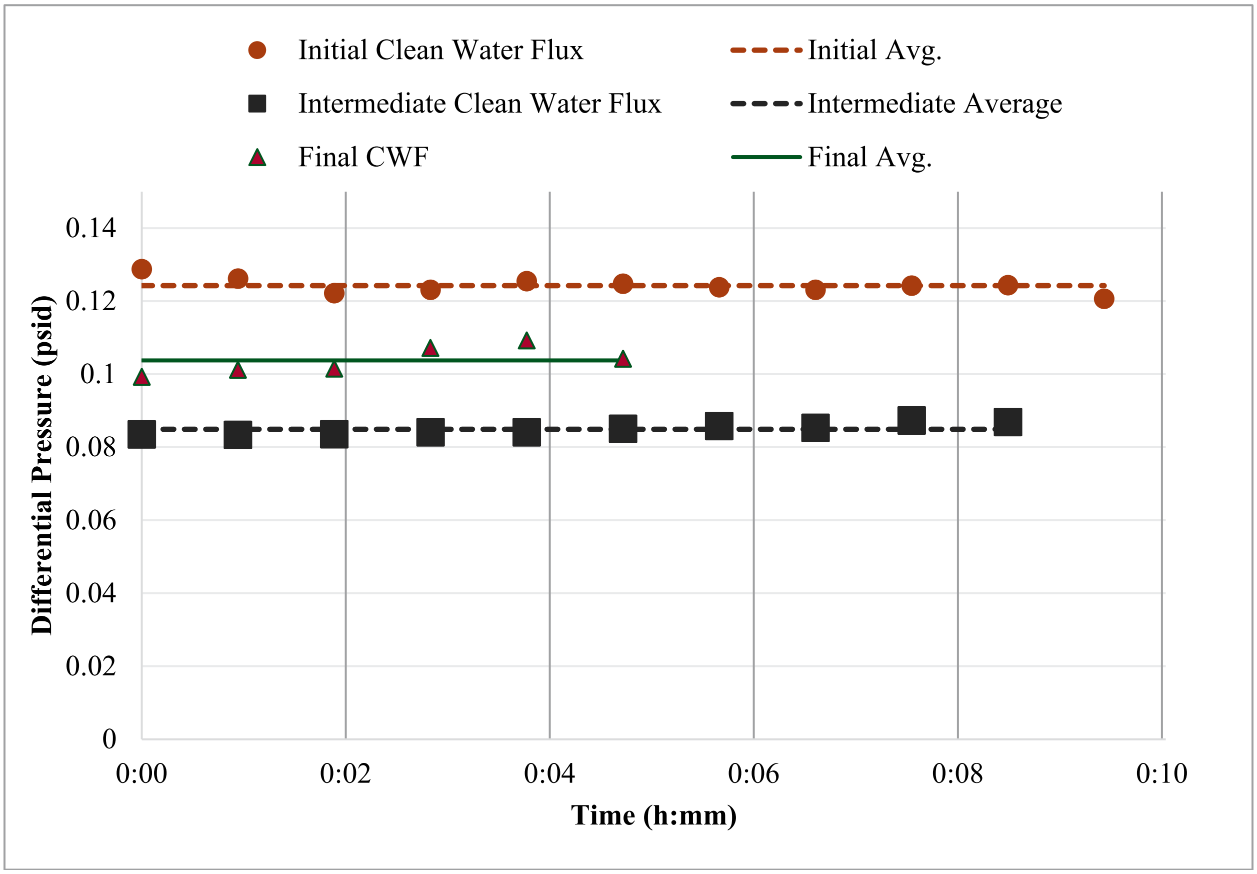

Figure 4.8. Initial and final clean water flux.

4.5 Analytical Results

4.5.1 As-Received AP-105 Supernate Tank Waste Analysis

Inductively Coupled Plasma Optical Emission spectroscopy (ICP-OES) analysis was conducted on the as-received AP-105 supernate tank waste on a mass-per-unit-mass basis (µg/g) as presented in Table 4.9. Subsequently, the molarity of the as-received waste was calculated using a density of 1.4091 g/mL, which was determined upon receipt of the AP-105 tank waste. The detailed ICP-OES report is found in Appendix C.

The molarity was calculated using the following equation:

$$M = \frac{(m * \rho)}{MW}$$

where M is the molarity, m is the mass, ρ is the density, and MW is the molecular weight of the component.

Table 4.9. ICP-OES and ICP-MS results of as-received AP-105 supernate tank waste.

Analysis Method	Analyte	As-Received AP-105 (µg/g)	As-Received AP-105 Molarity (mol/L)
ICP-OES	Na	149,564	9.17E+00
	Al	15,489	8.09E-01
	K	4104	1.48E-01
	S	1316	4.12E-02
	Cr	370	1.00E-02

4.5.2 Total Alpha Energy Analysis

Total alpha analysis (alpha energy analysis, AEA) was conducted to determine the transuranic waste (TRU) content of the filtered permeate. The analysis results are given in Table 4.10 and show no gross breakthrough of TRU components that aren't already soluble. Additional detail is provided in Appendix B. All samples remained below the 0.1 µCi/g threshold defining TRU waste per DOE M 435.1-1, *Radioactive Waste Management Manual*. The third permeate sample did show a higher alpha concentration, likely due to the consolidation of the product feed bottoms throughout filtration, as discussed in Section 4.3.

Table 4.10. AEA for permeate samples.

Analysis Method	Sample ID	(µCi/mL)	(µCi/g)
Total alpha analysis	TI-136-P1	1.75E-4	2.21E-4
	TI-136-P2	8.83E-5	1.12E-4
	TI-136-P3	3.87E-4	4.89E-4
	TI-136-P4	2.07E-4	2.73E-4
	TI-136-P5	1.97E-4	2.59E-4
	TI-136-P6	7.19E-4	9.47E-4

4.5.3 Rheology Analysis of Filtered and Cesium Decontaminated AP-105 Supernate Tank Waste

The viscosity of the filtered and cesium exchanged AP-105 supernatant was measured with a Haake M5-RV20 (equipped with an M5 measuring head and RC20 controller) and an MV1 rotor and cup measuring system. Temperature was controlled using a combination of the standard measuring system temperature jacket and a NESLAB Temperature-Controlled Circulator, Model Number RTE 111. This circulator allows heating and cooling of recirculation fluid to the rheometer over a range of -25 to 150 °C with a stability of ± 0.01° C. Performance checks using a Cannon-certified viscosity reference standard (Cannon Instrument Company) were carried out prior to and after measurements to verify that the system was functioning as expected. Viscosity was measured using a standard flow curve protocol comprising an up-ramp from 0 to 1000 s^{-1} for 5 minutes, a hold of 60 seconds at 1000 s^{-1}, and a finally down-ramp from 1000 to 0 s^{-1} over 5 minutes. Flow curves were measured at four temperatures: 10, 16, 25, and 35 °C. For each temperature, the Newtonian viscosity[1] of the liquid was determined by linear regression of the down-ramp data. The range of fit shear rates was limited to the fit ranges given in Table 4.11 excluding data impacted by onset of secondary flows (i.e., Taylor vortices). The results of linear regression analysis and the resulting best fit Newtonian viscosities are reported in Table 4.11.

Table 4.11. Viscosity results of filtered and Cs decontaminated samples.

		Fit Range	Viscosity	Viscosity
Sample ID	Temperature, °C	Down-Ramp, s^{-1}	mPa s	Uncertainty 3-Sigma
AP-105-7M	10	50-1000	8.24	0.06
	16	50-1000	6.05	0.04
	25	50-800	4.82	0.06
	35	50-650	3.7	0.1
AP-105-5.5M	10	50-900	4.76	0.06
	16	50-700	3.86	0.06
	25	50-600	2.7	0.1
	35	50-400	2.2	0.2

4.6 Microscopy Solids Analysis

Material collected from the concentrated backpulse solution was submitted for examination by scanning transmission electron microscopy (STEM). A full report of the particle analysis can be found in Appendix D. The samples analyzed were received as a liquid with suspended solids that had been centrifuged to concentrate the solids. Samples for microscopy analyses were prepared using a filtering method to avoid as much as possible the formation of evaporative salts. The solutions were wicked through a holey carbon support grid made of copper. Any large particles were manually removed from the transmission electron microscopy (TEM) grid. Several samples were prepared from each condition; however, some TEM grids possessed to high an activity to be further analyzed.

Large particles, more than 100 µm across, were observed frequently; however, it was not possible to allow these to be analyzed in the STEM. With SEM, very large particles can be easily accommodated but the STEM/TEM analysis is limited to particles <50 µm in diameter. The large particles had to be physically removed from the TEM grid prior to introduction in the TEM chamber.

4.6.1 5.5 M Na Batch Solids

The material shown in Figure 4.9 was commonly found throughout the sample. The phase was found to consist mainly of Na, O, and C.

---

[1] While the AP-105 supernatant is expected to be Newtonian, linear regression analysis allowed for non-zero intercept to accommodate a non-zero torque offset introduced by the operator to accommodate negative torques resulting from operating the M5 viscometer outside its standard operating range (in this case, for viscosities below 5.5 mPa s).

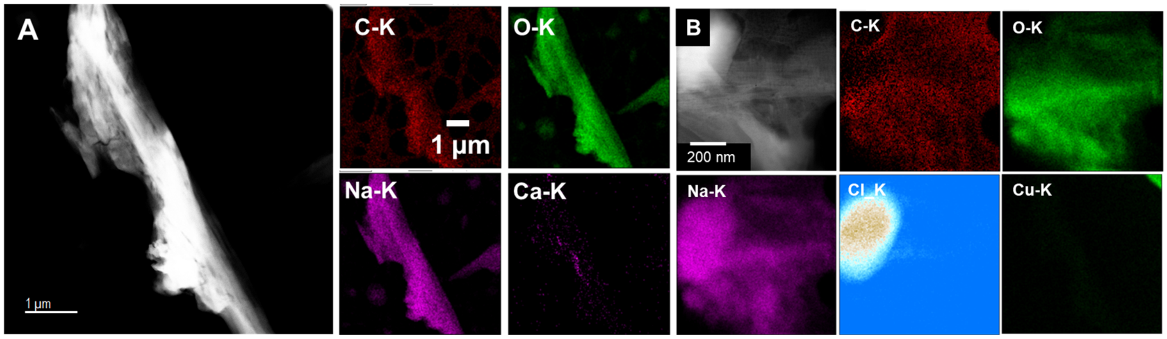

Figure 4.9. STEM images and STEM-EDS maps of (A) a large sodium-rich particle and (B) a NaCl salt particle found in the concentrate

Figure 4.10 shows two sets of STEM-HAADF (high-angle annular dark-field) and STEM EDS (X-ray energy dispersive spectroscopy) maps of commonly observed particles in the 5.5 M solids sample collection. In the Figure 4.10A, the material appeared fibrous and in Figure 4.10B, the material was euhedral. The fibrous material was examined in more detail with TEM and electron diffraction. Not all electron diffraction patterns could be indexed as they either did not show enough reflections or were composed of too many other crystals, where it was not clear if more than one phase was present.

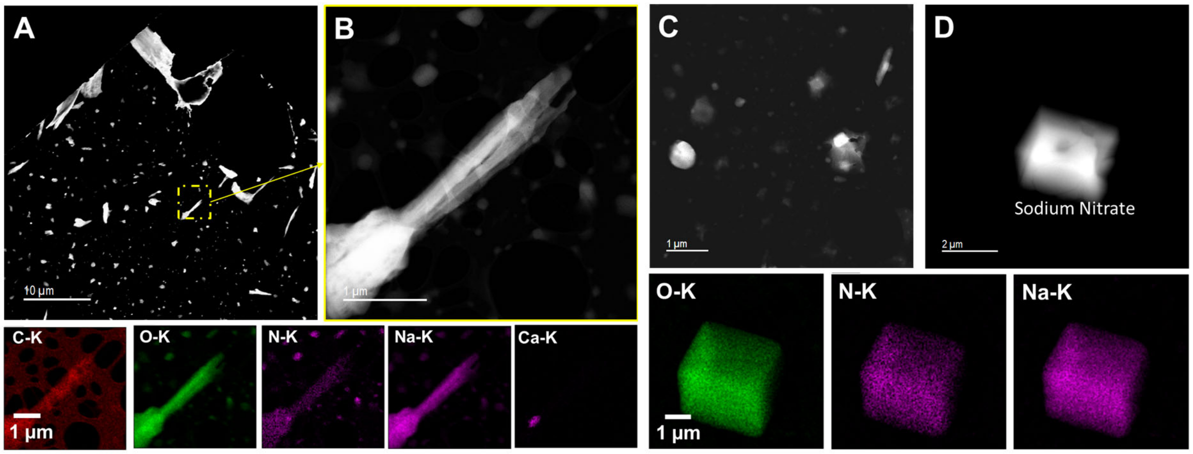

Figure 4.10. Further SEM images of sodium-rich particles found in the concentrate with some composed of precipitated salt material.

The diffraction patterns shown in Figure 4.11A, which had the characteristic pattern indicative of a layered structure, were analyzed with CrysTBox software (Klinger 2017) using potential matches from the American Mineralogist Crystallographic Database (http://rruff.geo.arizona.edu/AMS/amcsd.php) for natrite and dawsonite. Note that there is a small calcium particle in Figure 4.10A. It is thought that calcium originated from the process water and was nucleated from reaction with ligands that were present in the supernate.

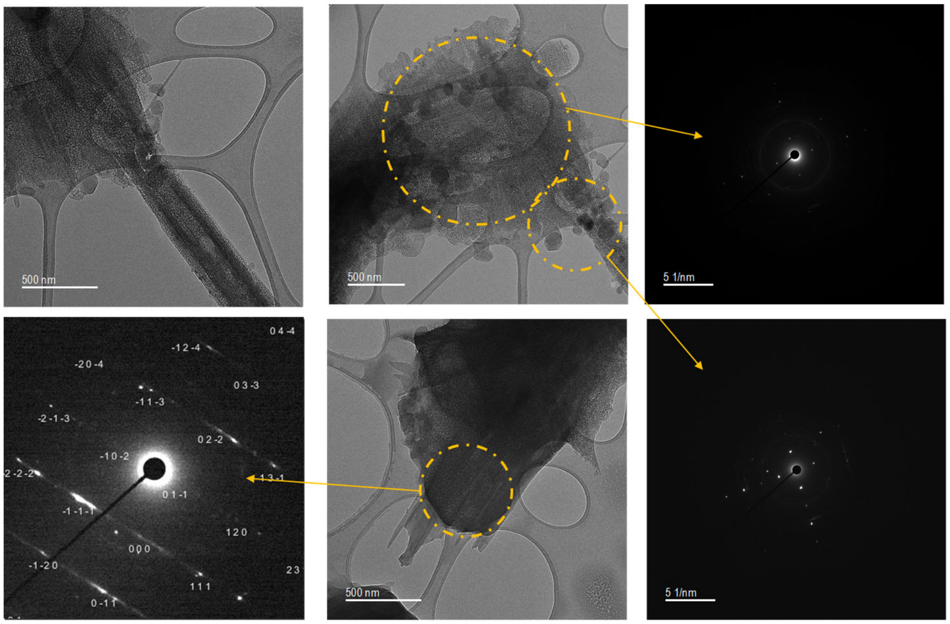

Figure 4.11. TEM analysis of the sodium-rich particles showing a layered structure identified as natrite (Na_2CO_3).

Figure 4.12 shows the varied types of particles imaged with TEM that were found in the 5.5 M solids sample. Many of the particles were irregularly shaped. Their ability to be trapped by the holey carbon film used in the analysis would probably be similar to their ability to be trapped on the dead-end filter.

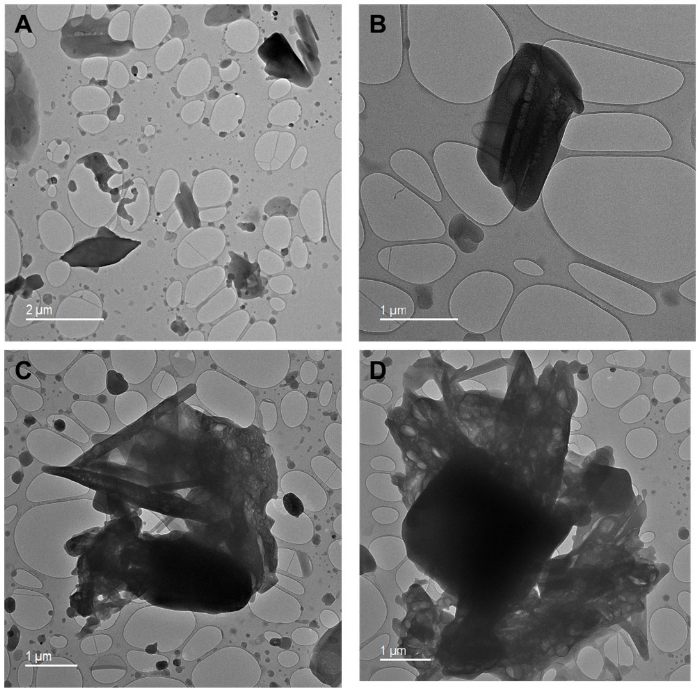

Figure 4.12. Different morphologies of particles from the 5.5M sample.

A subsample of the concentrated backpulse solution was prepared for analysis via scanning electron microscope (SEM). The solution was passed through a TEM grid to prevent evaporative salt formation during sample mounting. Particle size distribution is described in Figure 4.13 where most particles were under 3 µm.

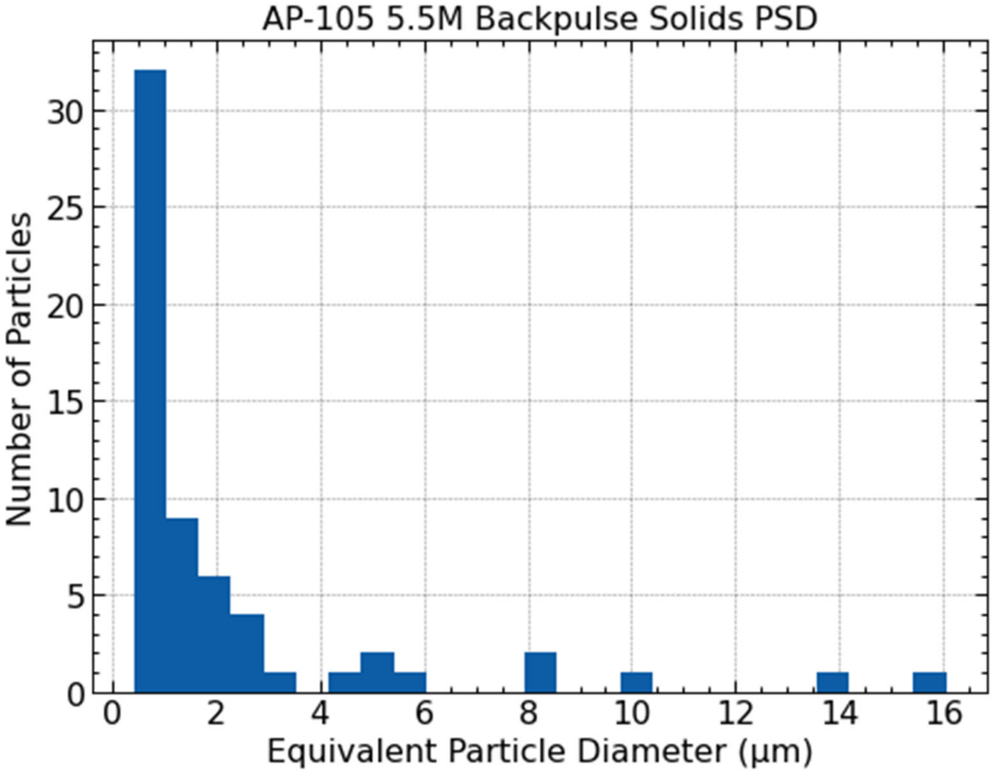

Figure 4.13. SEM particle size distribution analysis of particles observed in the 5.5M solids sample.

4.6.2 7.0 M Na Batch Solids

A sodium carbonate phase, possibly natrite, dominates in Figure 4.14; however, a nanometer-sized aluminosilicate and a calcium-rich phase can also be seen attached to this larger particle. The STEM-HAADF images in Figure 4.14 show several nanoparticle precipitates attached to the larger phase.

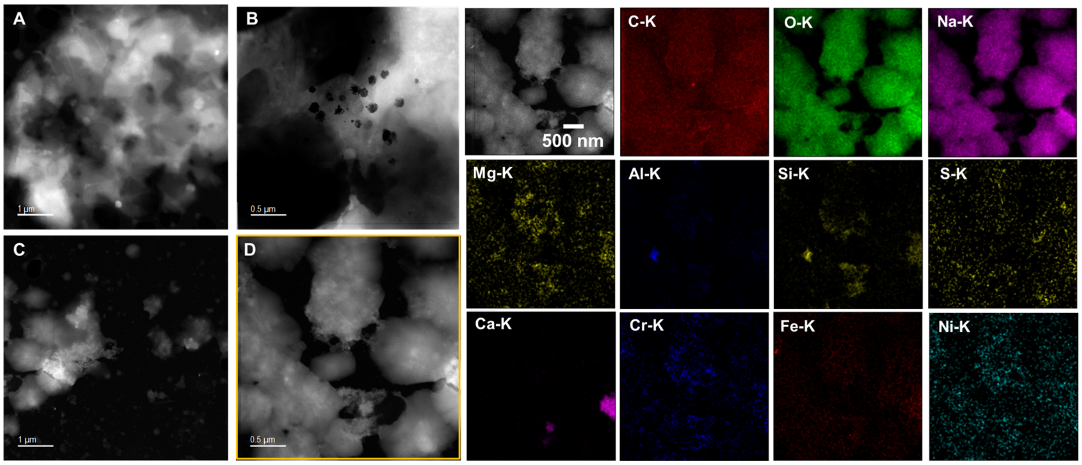

Figure 4.14. HAADF images of particle agglomerates from the 7.0 M sample. Mainly sodium-rich particles, possibly natrite.

Figure 4.15 shows a similar distribution of different phases in the 7.0 M solids sample with Mg-silicate (possibly also containing Ca), Ti-oxide, Fe-oxide, as well as Na-containing phases. Electron diffraction was obtained from regions around these samples, but in this case it was not possible to clearly connect the selected area electron diffraction (SAED) pattern to a known composition (see Figure 4.16).

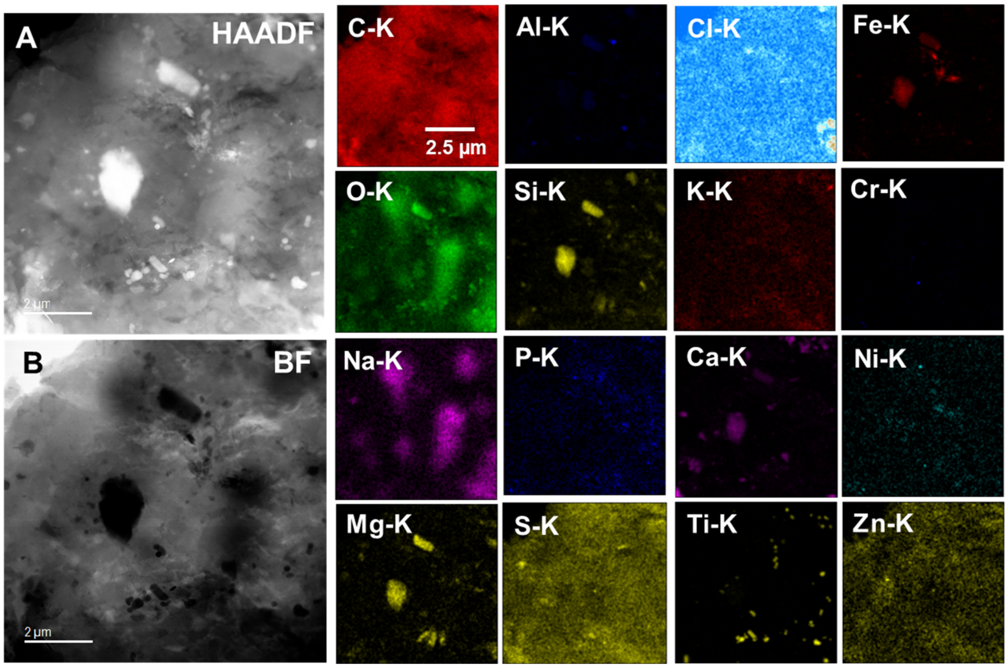

Figure 4.15. HAADF image and STEM-EDS analysis of a particle agglomerate showing an Si-Al phase attached to salt-like phases.

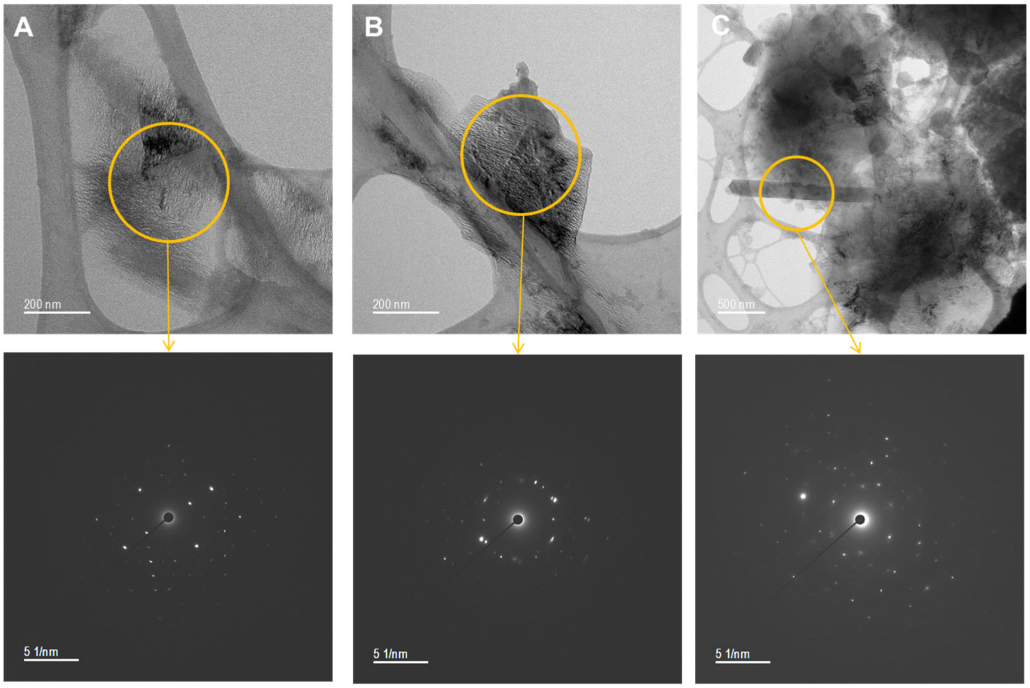

Figure 4.16. TEM analysis of particles observed in the 7.0 M solids sample.

Inspection of a group of particles between the two larger ones is shown in Figure 4.17. In this figure, the phase appears to consist of C, O, F, Mg, and Al. There were also distinct Ti oxide and Fe-oxide particles. The Cu-particle also appears to be genuine. Cu fluorescence can lead to problems measuring Cu, but the brightness of the signal and the location suggest that it is real. These analyses demonstrate that even down to the nanometer level (the scale bar on the images is 100 nm), the particles remain highly heterogenous.

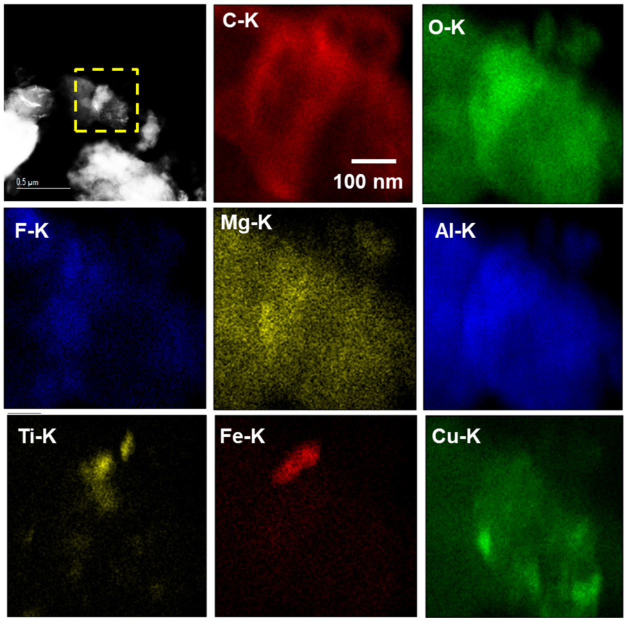

Figure 4.17. Lower magnification STEM EDS analysis of a Ti- and Fe- particles within an Al-phase.

The SEM subsample of the 7.0 M concentrated backpulse solution solids showed a higher density of sub 3 µm particles when compared to the 5.5 M sample as shown in Figure 4.18.

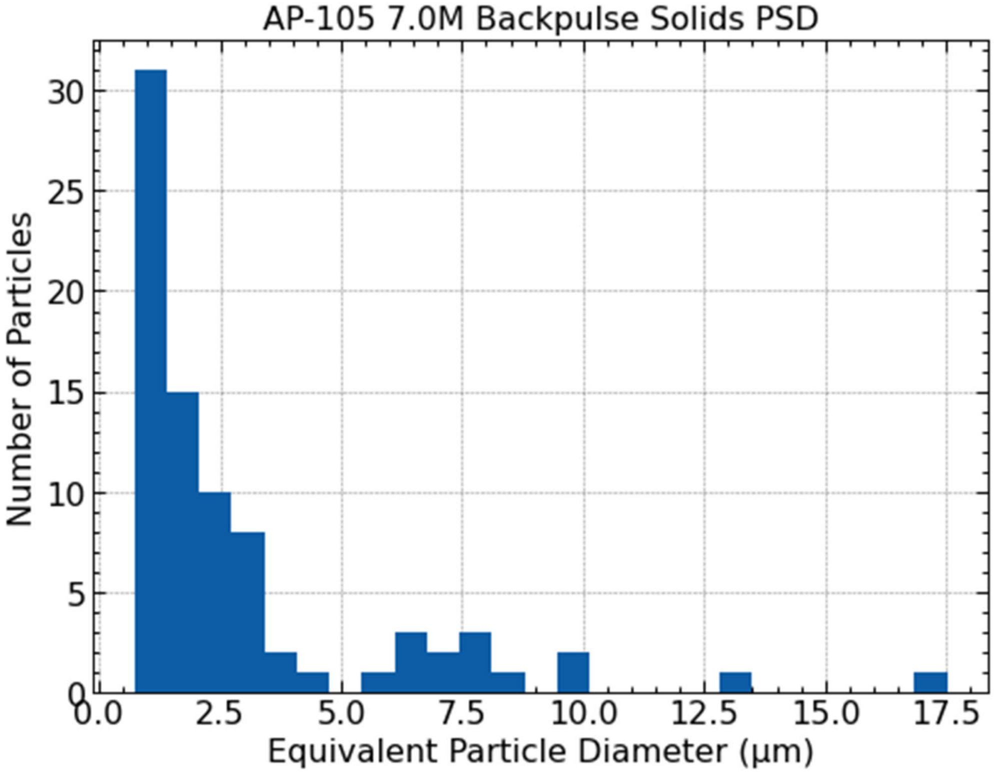

Figure 4.18. SEM particle size distribution analysis of particles observed in the 7.0M solids sample.

5.0 Conclusions

Based on the results of the filtration experiments on supernatant waste from tank 241-AP-105 at 16 °C, the following observations and conclusions were made:

- The Media Grade 5 BDEF filter was run at the TSCR targeted flux of 0.065 gpm/ft^2 with two sodium concentration batches.
- The higher dilution of the feed to 5.5 M Na resulted in greater solids precipitating, but these solids do settle over time. These solids fouled the filter at an increased rate when compared to the settled feed bottoms, resulting in two backpulses being required while filtering 3.97 m^3/m^2 volume of feed.
- The prototypic filter cleaning process effectively restored filter performance.
- Filtration of the 7 M sodium batch did not require a backpulse over 7.29 m^3/m^2 volume of feed. Fouling did begin when the settled bottoms were added to the system.
- Solids concentrated from the backpulse solutions were composed of sodium nitrate, sodium carbonate, calcium sulfate, iron oxide, steel particles, titanium oxide particles, and aluminum oxides. Most of the phases found were only weakly crystalline, possibly owing to their rapid precipitation during the process water treatment.

6.0 References

Allred JR, EC Buck, CC Burns, RC Daniel, JGH Geeting, ZB Webb, AM Westesen, and RA Peterson. 2022. *Fiscal Year 2022 Filtration of Hanford Tank 241-AP-101 Supernatant at 16 °C*. PNNL-32851, Rev. 0 (RPT-DFTP-032, Rev. 0). Pacific Northwest National Laboratory, Richland, Washington.

Allred JR, JGH Geeting, AM Westesen, EC Buck, and RA Peterson. 2021. *Fiscal Year 2021 Filtration of Hanford Tank 241-AP-107 Supernatant Samples Obtained at Prototypic Tank Level and Filtered at 16 °C*. PNNL-31557, Rev. 0 (RPT-DFTP-028, Rev. 0). Pacific Northwest National Laboratory, Richland, Washington.

Allred JR, JGH Geeting, AM Westesen, EC Buck, and RA Peterson. 2020. *Fiscal Year 2020 Filtration of Hanford Tank Waste 241-AP-105*. PNNL-30485, Rev. 0 (RPT-DFTP-021, Rev. 0). Pacific Northwest National Laboratory, Richland, Washington.

ASME. 2000. *Quality Assurance Requirements for Nuclear Facility Applications*. NQA-1-2000. The American Society of Mechanical Engineers, New York, New York.

ASME. 2008. *Quality Assurance Requirements for Nuclear Facility Applications*. NQA-1-2008. The American Society of Mechanical Engineers, New York, New York.

ASME. 2009. *Addenda to ASME NQA-1-2008*. NQA-1a-2009. The American Society of Mechanical Engineers, New York, New York.

Geeting JGH, JR Allred, AM Rovira, and RA Peterson. 2019. *Fiscal Year 2019 Filtration of Hanford Tank AP-107 Supernatant*. PNNL-28780, Rev. 0 (RPT-DFTP-015, Rev. 0). Pacific Northwest National Laboratory, Richland, Washington.

Geeting JGH, AM Rovira, JR Allred, RW Shimskey, CA Burns, and RA Peterson. 2018a. *Filtration of Hanford Tank AP-107 Supernatant*. PNNL-27638 (RPT-DFTP-009, Rev. 0). Pacific Northwest National Laboratory, Richland, Washington.

Geeting JGH, JR Allred, AM Rovira, RW Shimskey, CA Burns, and RA Peterson. 2018b. *Crossflow Filtration of Hanford Tank AP-105 Supernatant*. PNNL-27085 (RPT-DFTP-005, Rev. 0). Pacific Northwest National Laboratory, Richland, Washington.

Gerber MS. 1992. *Legend and Legacy: Fifty Years of Defense Production at the Hanford Site*. WHC-MR-0293, Rev. 2. Westinghouse Hanford Company, Richland, Washington. doi:10.2172/10144167

Hermia J. 1982. "Constant Pressure Blocking Filtration Laws – Application to Power-Law Non-Newtonian Fluids." *Transactions of the Institution of Chemical Engineers* 60(3):183-187.

Klinger M. 2017. "More features, more tools, more CrysTBox." *Journal of Applied Crystallography* 50(4):1226-1234. https://doi.org/doi:10.1107/S1600576717006793

Appendix A – BDEF Piping and Instrumentation Diagram

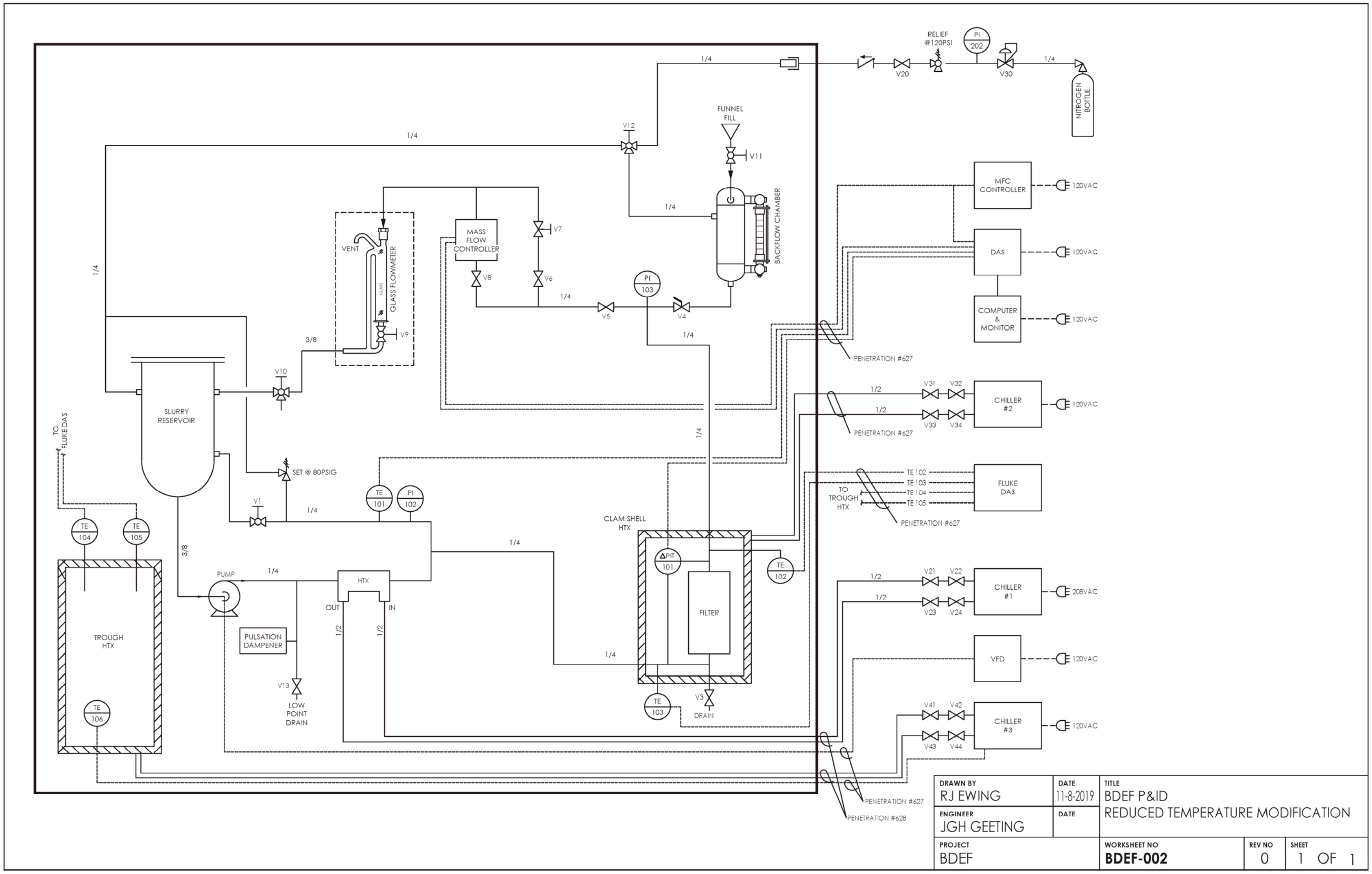

Figure A.1. BDEF piping and instrumentation diagram.

Appendix B – Total Alpha Analysis for Filtration Permeate Samples

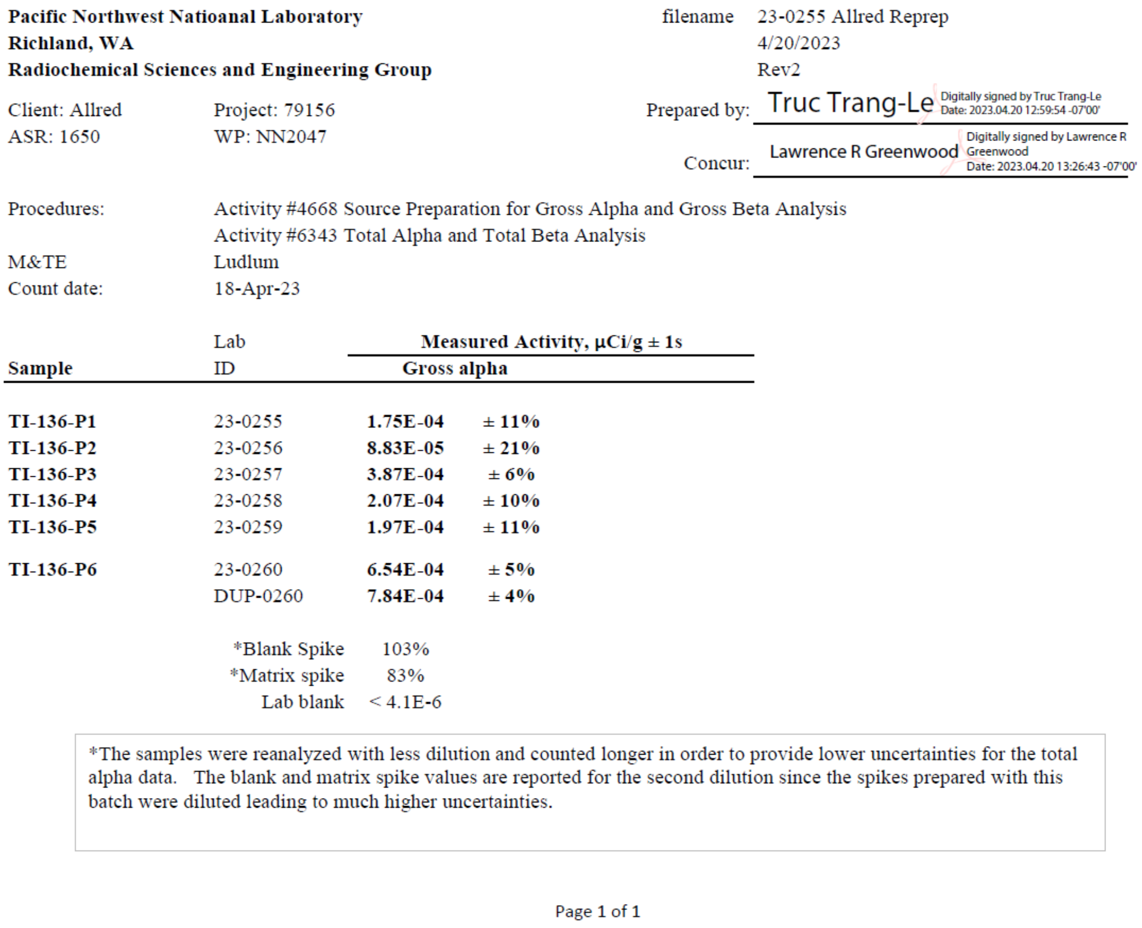

Pacific Northwest Natioanal Laboratory
Richland, WA
Radiochemical Sciences and Engineering Group

filename 23-0255 Allred Reprep
4/20/2023
Rev2

Client: Allred Project: 79156
ASR: 1650 WP: NN2047

Prepared by: Truc Trang-Le Digitally signed by Truc Trang-Le Date: 2023.04.20 12:59:54 -07'00'

Concur: Lawrence R Greenwood Digitally signed by Lawrence R Greenwood Date: 2023.04.20 13:26:43 -07'00'

Procedures: Activity #4668 Source Preparation for Gross Alpha and Gross Beta Analysis
Activity #6343 Total Alpha and Total Beta Analysis
M&TE Ludlum
Count date: 18-Apr-23

	Lab	Measured Activity, µCi/g ± 1s	
Sample	ID	**Gross alpha**	
TI-136-P1	23-0255	**1.75E-04**	**± 11%**
TI-136-P2	23-0256	**8.83E-05**	**± 21%**
TI-136-P3	23-0257	**3.87E-04**	**± 6%**
TI-136-P4	23-0258	**2.07E-04**	**± 10%**
TI-136-P5	23-0259	**1.97E-04**	**± 11%**
TI-136-P6	23-0260	**6.54E-04**	**± 5%**
	DUP-0260	**7.84E-04**	**± 4%**

*Blank Spike	103%
*Matrix spike	83%
Lab blank	< 4.1E-6

*The samples were reanalyzed with less dilution and counted longer in order to provide lower uncertainties for the total alpha data. The blank and matrix spike values are reported for the second dilution since the spikes prepared with this batch were diluted leading to much higher uncertainties.

Page 1 of 1

Appendix C – ICP-OES Analysis for As-Received 241-AP-105 Supernatant

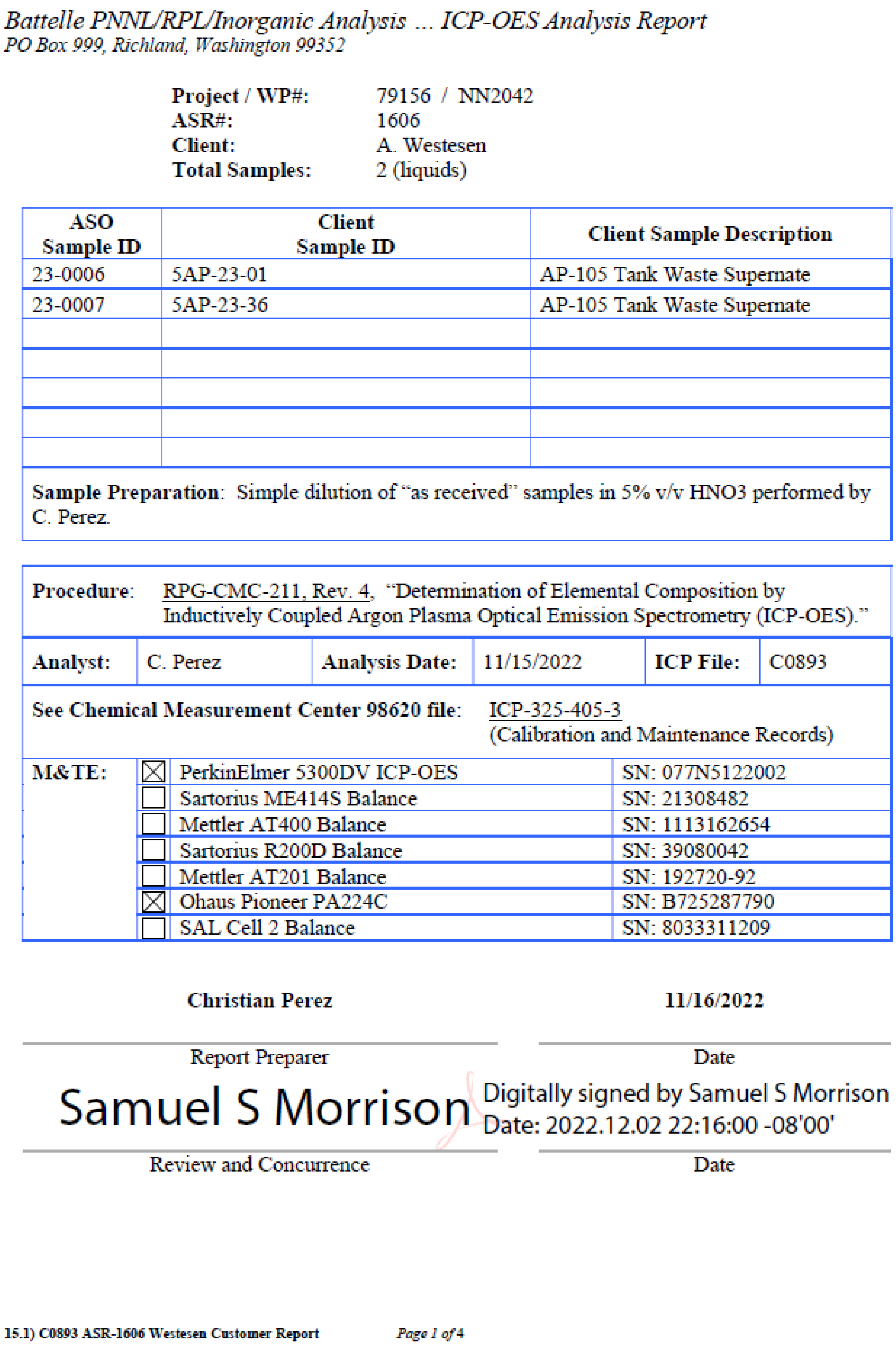

Battelle PNNL/RPL/Inorganic Analysis ... ICP-OES Analysis Report
PO Box 999, Richland, Washington 99352

Project / WP#: 79156 / NN2042
ASR#: 1606
Client: A. Westesen
Total Samples: 2 (liquids)

ASO Sample ID	Client Sample ID	Client Sample Description
23-0006	5AP-23-01	AP-105 Tank Waste Supernate
23-0007	5AP-23-36	AP-105 Tank Waste Supernate

Sample Preparation: Simple dilution of "as received" samples in 5% v/v HNO3 performed by C. Perez.

Procedure: RPG-CMC-211, Rev. 4, "Determination of Elemental Composition by Inductively Coupled Argon Plasma Optical Emission Spectrometry (ICP-OES)."

Analyst:	C. Perez	**Analysis Date:**	11/15/2022	**ICP File:**	C0893

See Chemical Measurement Center 98620 file: ICP-325-405-3 (Calibration and Maintenance Records)

M&TE:	☒	PerkinElmer 5300DV ICP-OES	SN: 077N5122002
	☐	Sartorius ME414S Balance	SN: 21308482
	☐	Mettler AT400 Balance	SN: 1113162654
	☐	Sartorius R200D Balance	SN: 39080042
	☐	Mettler AT201 Balance	SN: 192720-92
	☒	Ohaus Pioneer PA224C	SN: B725287790
	☐	SAL Cell 2 Balance	SN: 8033311209

Christian Perez **11/16/2022**

Report Preparer Date

Samuel S Morrison Digitally signed by Samuel S Morrison
Date: 2022.12.02 22:16:00 -08'00'

Review and Concurrence Date

15.1) C0893 ASR-1606 Westesen Customer Report *Page 1 of 4*

Two aqueous sample(s) submitted under Analytical Service Request (ASR) 1606 were analyzed by ICP-OES. Both samples were diluted to 25x. The samples were not filtered.

All sample results are reported on a mass per unit volume basis (µg/mL) for each detected analyte. The data have been adjusted for instrument dilutions.

Analytes of interest (AOI) were specified in the ASR and are listed in the upper section of the attached ICP-OES Data Report. The quality control (QC) results for the AOI have been evaluated and are presented below. Analytes other than the AOI are reported in the bottom section of the report but have not been fully evaluated for QC performance.

Calibration of the ICP-OES was done following the manufacturer's recommended calibration procedure using multi-analyte custom standard solutions traceable to the National Institute of Standards and Technology (NIST). Midrange calibration verification standards (MCVA and MCVB) were used to verify acceptance of the two-point calibration curves obtained for each analyte and for continuing calibration verification.

The controlling documents were procedures RPG-CMC-211, Rev 4, *Determination of Elemental Composition by Inductively Coupled Argon Plasma Optical Emission Spectrometry (ICP-OES)*, and ASO-QAP-001, Rev. 11, *Analytical Support Operations (ASO) Quality Assurance Plan*. Instrument calibrations, QC checks and blanks (e.g., ICV/ICB, CCV/CCB, LLS, ICS), post-digestion spikes, duplicate, blank spike, and serial dilution were conducted during the analysis run.

Preparation Blank (PB):

A preparation blank was supplied with the samples. All AOI were within the acceptance criteria of <EQL (estimated quantitation level), <50% regulatory decision level, or less than ≤10% of the concentration in the sample.

Blank Spike (BS)/Laboratory Control Sample (LCS):

A 50:50 mixture of the MCVA and MCVB solutions was analyzed as the blank spike. Recovery values are listed for all analytes included in the BS that were measured at or above the EQL. All AOI meeting this requirement were within the acceptance criterion of 80% to 120%.

Duplicate/Replicate Relative Percent Difference (RPD):

A Replicate of each sample was prepared and analyzed. RPD are listed for all analytes that were measured at or above the EQL. All AOI were within the acceptance criterion of ≤20% for liquid samples.

Triplicate Relative Standard Deviation (RSD):

No triplicate sample was analyzed.

Matrix-Spike (MS) Sample:

The samples were analyzed "as received" and diluted as appropriate for analyses of the target analytes. A matrix spike sample was generated due to the sample preparation beforehand. A post spike sample was analyzed, and recovery results reported. Aluminum (Al) and Potassium (K) both passed the percent recovery. Sodium (Na) shows as "nr" on the percentage recovered. The analyzed concentration for Sodium (Na) was above the upper calibration limit (125 µg/mL), but below the upper linearity standard (1000 µg/mL). Therefore, the Matrix Spike returned an "nr" for the recovery percentage. Hand calculation indicates the recovery is 101%.

Initial/Continuing Calibration Verification (ICV/CCV):

MCVA and MCVB solutions were analyzed immediately after calibration, after each group of not more than ten samples, and at the end of the analytical run. All AOI were within the acceptance criteria of 90% to 110%. Strontium (Sr) failed out of range on the QC-MCVA-3 for being at 111%.

Initial/Continuing Calibration Blank (ICB/CCB):

The ICB/CCB solution (5% v/v HNO_3) was analyzed immediately after the ICV solutions and after the CCV solutions (after each group of not more than ten samples and at the end of the analytical run). All AOI were within the acceptance criteria of <EQL.

Low-Level Standard (LLS):

The LLS solution was analyzed immediately after the first CCB solution. All AOI were within the acceptance criteria of 70% to 130%.

Interference Check Standard (ICS/SST):

The ICS solution was analyzed immediately after the first LLS solution and immediately prior to analyzing the final CCV solutions. Recovery values are listed for all analytes included in the SST that were measured at or above the EQL. All AOI were within the acceptance criteria of 80% to 120%.

Serial Dilution (SD):

Five-fold serial dilution was conducted on sample 23-0006. The percent difference (%D) for all AOI were withing the acceptance criteria of ≤ 10%.

Post-Digestion Spike (PS-A) - Sample (A Component):

A post-digestion spike (A Component) was conducted on sample 23-0006. All AOI were within the acceptance criterion of 80% to 120%.

Post-Digestion Spike (PS-B) - Sample (B Component):

A post-digestion spike (B Component) was not conducted. There were no AOI included in the spike B component, so a PS-B was not performed.

Post-Digestion Spike (PS-Q3A) - Sample (A Tormont Component):

A post-digestion spike (A Tormont Component) was not conducted.

Post-Digestion Spike (PS-Q3B) - Sample (B Tormont Component):

A post-digestion spike (B Tormont Component) was not conducted.

Other QC:

All other instrument-related QC tests for the AOI passed within their respective acceptance criteria.

Comments:

1) The "Final Results" have been corrected for all laboratory dilutions performed on the samples during processing and analysis, unless specifically noted.
2) Instrument detection limits (IDL) and estimated quantitation limits (EQL) shown are for acidified water and/or fusion flux matrices as applicable. Method detection limits (MDL) for individual samples can be estimated by multiplying the IDL by the "Process Factor" for that individual sample. The estimated quantitation limit (EQL) for each concentration value can be obtained by multiplying the EQL by the "Process Factor".
3) Routine precision and bias is typically ±15% or better for samples in dilute, acidified water (e.g. 5% v/v HNO_3 or less) at analyte concentrations > EQL up to the upper calibration level. This also presumes that the total dissolved solids concentration in the sample is less than 5000 μg/mL (0.5 per cent by weight). Note that bracketed values listed in the data report are within the MDL and the EQL, and have potential uncertainties greater than 15%. Concentration values < MDL are listed as "- -". Note, that calibration and QC standard samples are validated to a precision of ±10%.
4) Analytes included in the spike A component (for the AS/PS) are; Ag, Al, As, B, Ba, Be, Bi, Ca, Cd, Co, Cr, Cu, Eu, Fe, K, Li, Mg, Mn, Mo, Na, Ni, P, Pb, Sb, Se, Si, Sm, Sn, Sr, Ta, Ti, Tl, V, W, Y, Zn, and Zr. Analytes included in the spike B component are; Ce, Dy, Eu, La, Nd, Pd, Rh, Ru, S, Te, Th, and U.

Battelle PNNL/RPG/Inorganic Analysis ... ICPOES Data Report

Page 1 of 2

		Run Date >	11/15/2022	11/15/2022	11/15/2022	11/15/2022	11/15/2022			
		Process Factor >	1.0	25.0	1250.0	1250.0	1250.0			
			405 Diluent rerun	BLK-0006 @1x	23-0006 @25x	DUP-0006 @25x	23-0007 @25x			
Instr. Det. Limit (IDL)	Est. Quant. Limit (EQL)	Client ID >		Reagents only	5AP-23-01		5AP-23-36			
(µg/mL)	(µg/mL)	(Analyte)	(µg/mL)	(µg/mL)	(µg/mL)	(µg/mL)	(µg/mL)			
0.0101	0.101	Al	0.0250	[.47]	21,800	22,300	21,600			
0.0312	0.312	K	0.0380	2.10	5,790	5,900	5720.00			
0.0073	0.073	Na	--	4.67	211,000	216,000	208000.00			
Other Analytes										
0.0019	0.019	Ag	--	--	--	--	--			
0.0619	0.619	As	--	--	88.00	--	--			
0.0060	0.060	B	0.0110	[3.6]	--	[16.00]	13.00			
0.0001	0.001	Ba	--	[0.0412]	0.770	0.770	0.680			
0.0001	0.001	Be	--	--	--	--	0.170			
0.0245	0.245	Bi	--	--	--	--	--			
0.0056	0.056	Ca	--	1.70	66.00	54.00	51.00			
0.0014	0.014	Cd	--	--	[3.70]	[2.9]	--			
0.0103	0.103	Ce	--	--	--	--	--			
0.0043	0.043	Co	--	--	--	--	--			
0.0020	0.020	Cr	--	--	[518]	532.00	517.00			
0.0023	0.023	Cu	--	--	9.60	9.30	9.40			
0.0023	0.023	Dy	--	--	--	--	--			
0.0006	0.006	Eu	--	--	--	--	--			
0.0014	0.014	Fe	[0.00230]	0.0820	6.40	4.20	3.40			
0.0019	0.019	La	--	--	--	--	--			
0.0007	0.007	Li	--	0.0390	--	1.30	1.00			
0.0018	0.018	Mg	--	[.085]	--	--	--			
0.0002	0.002	Mn	--	--	1.50	1.60	[1.50]			
0.0044	0.044	Mo	--	--	70.20	[74.0]	72.50			
0.0088	0.088	Nd	--	0.270	18.00	[19.00]	--			
0.0022	0.022	Ni	--	0.120	[44.40]	41.90	44.90			
0.0905	0.905	P	--	--	[640.00]	610.00	[600.00]			
0.0269	0.269	Pb	--	--	--	35.00	--			
0.0054	0.054	Pd	--	--	7.30	8.10	[8.70]			
0.0211	0.211	Rh	--	--	--	--	--			
0.0063	0.063	Ru	--	--	19.00	18.00	17.00			
0.1262	1.262	S	--	3.80	1950.00	1770.00	1850.00			
0.0598	0.598	Sb	--	--	--	--	--			
0.1656	1.656	Se	--	--	--	--	--			
0.0086	0.086	Si	0.0680	[1.20]	[139.00]	138.00	[133.00]			
0.0291	0.291	Sn	--	--	--	--	--			
0.0001	0.001	Sr	--	[0.0110]	0.160	0.260	0.180			
0.0246	0.246	Ta	--	--	--	--	--			
0.0197	0.197	Te	--	--	--	--	--			
0.0071	0.071	Th	--	--	--	--	--			
0.0006	0.006	Ti	--	--	1.10	--	--			
0.0814	0.814	Tl	--	--	--	--	--			
0.0410	0.410	U	--	--	--	--	--			
0.0013	0.013	V	--	0.0820	--	--	--			
0.0161	0.161	W	--	--	140.00	150.00	150.00			
0.0006	0.006	Y	--	--	--	--	--			
0.0027	0.027	Zn	--	0.981	[3.90]	--	--			
0.0014	0.014	Zr	--	--	--	--	--			

ASR Staging Template FINAL from C0893 ASR-1606 Westesen Data Reporting FINAL

QC Performance 11/15/2022

Criteria >	≤ 20%	80%-120%	75%-125%	80%-120%	≤ 10%
QC ID >	DUP-0006	LCS/BS	MS-0006	PSA-0006	SRD-0006
Analytes	RPD (%)	%Rec	%Rec	%Rec	%Diff
Al	2.5	99	94	102	5.2
K	1.9	98	92	100	6.7
Na	2.1	101	nr	102	5.4
Other Analytes					
Ag		109		98	
As		95		95	
B		98		99	
Ba		100	91	100	
Be		96	90	96	
Bi		93		98	
Ca		100	91	99	
Cd		96	91	100	
Ce		92	87		
Co		99		101	
Cr	2.5	95	nr	99	8.2
Cu		107	98	104	
Dy		95			
Eu		94			
Fe		102	93	103	
La		93	86		
Li		104	96	104	
Mg		102	93	102	
Mn		101	93	100	
Mo	5.3	97		99	
Nd		93	85		
Ni	5.8	100	97	103	
P		96		98	
Pb		99	96	102	
Pd		91			
Rh		94			
Ru		90			
S	9.6	94			
Sb		95		98	
Se		97		99	
Si	0.8	96		97	
Sn		99		102	
Sr		102	100	109	
Ta		99		101	
Te		95			
Th		94			
Ti		100		100	
Tl		90		92	
U		99			
V		96	90	95	
W		101		103	
Y		96		97	
Zn		96	91	101	
Zr		100		101	

Appendix D – Backpulsed Solids from AP-105 Characterization with Scanning Transmission Electron Microscopy

Materials from a concentrate from Hanford tank waste material representing Hanford waste tank 241-AP-105 (herein AP-105) that had been run through the backpulse dead-end filter (BDEF) system in two batches with differing sodium molarity at 16°C. The first was at 5.5 M and the other at 7 M. These concentrates were examined with scanning transmission electron microscopy (STEM) in the Radiochemical Processing Laboratory (RPL) at Pacific Northwest National Laboratory. The sample was received as a liquid with suspended solids that had been centrifuged to concentrate the solids. Samples for microscopy analyses were prepared using a filtering method to avoid the formation of evaporative salts to the extent possible. The solutions were wicked through a holey carbon support grid made of copper. Any large particles were manually removed from the transmission electron microscopy (TEM) grid. Several samples were prepared from each condition; however, some TEM grids possessed too high of an activity to be further analyzed.

The STEM instrument used was a JEOL (JEOL Inc., Japan) ARM300F (GrandARM) microscope. STEM images were collected using an annular dark field detector and compositional analysis was obtained with X-ray energy dispersive spectroscopy (EDS). Samples were also imaged with TEM, high-resolution TEM (HRTEM), and diffraction. Selected area electron diffraction (SAED) patterns were analyzed with DigitalMicrograph™ 3.0 software and using scripts developed by Mitchell (2008) and CrysTBox (Crystallographic Tool Box) software (Klinger 2017).

D.1 Microscopy Solids Analysis Results

Large particles over 100 µm diameter were observed frequently; however, it was not possible to analyze these in the STEM microscope. With scanning electron microscopy (SEM), very large particles can be easily accommodated, but the STEM/TEM analysis is limited to particles <50 µm in diameter. In fact, unless the particles are <100 nm thick, it is not possible to get good quality TEM analysis. The large particles had to be physically removed from the TEM grid prior to introduction in the TEM chamber. Large particles could also result in damage to the instrument.

D.1.1 5.5M Na Batch Solids

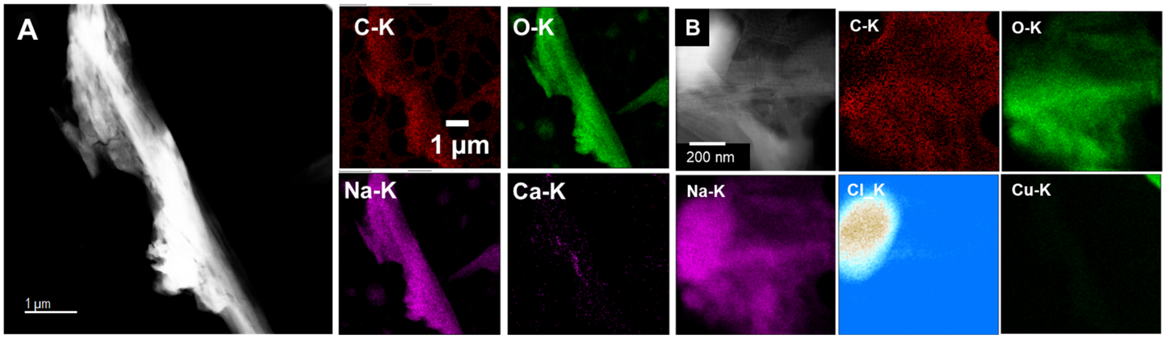

Figure D.1. STEM images and STEM-EDS maps of (A) a large sodium-rich particle and (B) a NaCl salt particle found in the concentrate.

The material shown in Figure D.1 was commonly found throughout the sample. The phase was found to consist mainly of Na, O, and C. Carbon was present in the support film, but it is always possible to distinguish this signal from the carbon in a phase. Copper is more difficult to determine in the phases as the X-ray fluorescence from the grid results in the production of Cu-K lines. However, examples were found that strongly suggested that Cu was present in some particles. This is described in more detail later in the discussion about Figure D.17. Figure D.2 shows two sets of STEM-HAADF and STEM EDS maps of commonly observed particles in the 5.5 M solids sample collection. In Figure D.2A, the material appeared fibrous, and in Figure D.2B, the material was euhedral. The fibrous material was examined in more detail with TEM and electron diffraction. Not all electron diffraction patterns could be indexed as they either did not show enough reflections or were composed of too many other crystals where it was not clear if more than one phase was present.

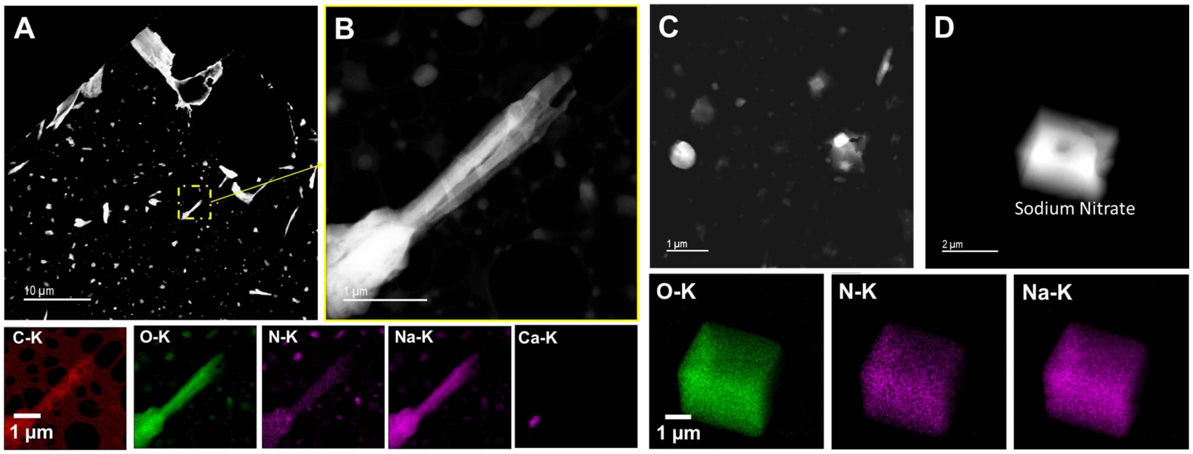

Figure D.2. Further SEM images of sodium-rich particles found in the concentrate with some composed of precipitated salt material.

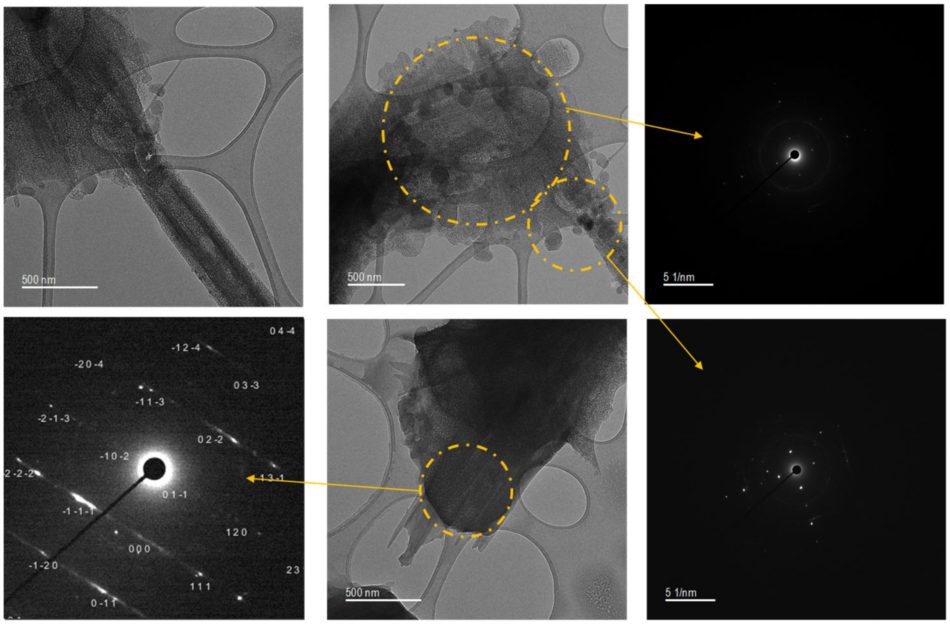

Figure D.3. TEM analysis of the sodium-rich particles showing a layered structure identified as natrite (Na_2CO_3). [1]

Natrite (Na_2CO_3) is a carbonate mineral that is also known as hydrotalcite compounds possessing a layered structure (see Figure D.3). These phases can incorporate Mg^{2+} and Al^{3+}, although in this instance there was no evidence for significant Al or Mg. Carbonate occupies the interlayer spaces to balance the cations. An alternative phase that may be present in the Hanford tanks is dawsonite ($NaAlCO_3(OH_2)$), which was first discussed by Reynolds et al. (2012) as a possible phase that could be present in the Hanford tank wastes. However, STEM-EDS did not indicate the presence of Al in this phase. The diffraction pattern shown in Figure D.3A, which had a characteristic pattern indicative of a layered structure, were analyzed with CrysTBox software (Klinger 2017) using potential matches from the American Mineralogist Crystallographic Database (http://rruff.geo.arizona.edu/AMS/amcsd.php) for natrite and dawsonite. Note that there is a small calcium particle in Figure D.2A. It is thought that calcium originates from the process water and is nucleated from reaction with ligands that were present in the supernate. $NaNO_3$ type phase were also observed in the sample (see Figure D.4 and Figure D.5). These particles were extremely large for TEM/STEM analysis.

---

[1] Ref: (D) Diff 80cm OneView 5-5M Solids 0037.dm4, (E) Diff 80cm OneView 5-5M Solids 0038.dm4, (C) Diff 80cm OneView 5-5M Solids 0039.dm4

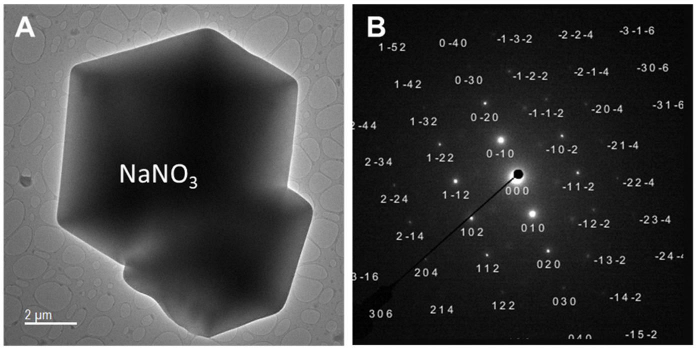

Figure D.4. TEM and electron diffraction analysis of a sodium nitrate particle and the identification of the diffraction spots from natrite ($NaNO_3$) using CrysTBox. [1]

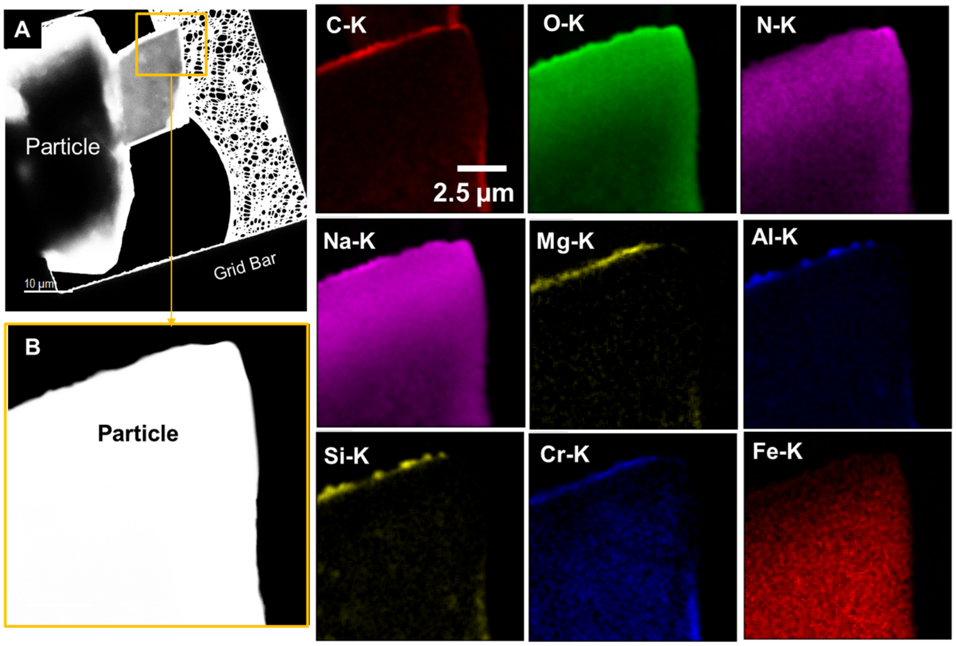

Figure D.5. Large sodium nitrate particle in sample 5.5 M with an apparent coating of an Mg, Al-silicate. It is unclear if the Fe signal is significant.

Silicate particles were also identified in the 5.5 M solids sample. Figure D.6 and Figure D.7 show examples of these particles. The particles were generally too thick for SAED analysis; however, a few patterns were obtained and analyzed with CrysTBox (see Figure D.7C).

---

[1] Ref file: 4000X OneView 5-5M Solids 0041.dm4, Diff 80cm OneView 5-5M Solids 0044.dm4

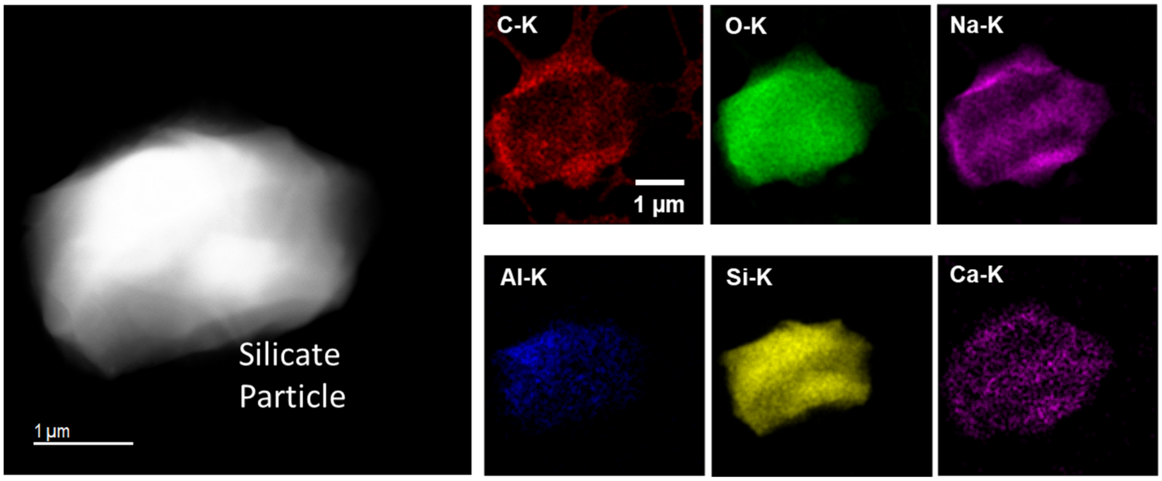

Figure D.6. SEM-EDS elemental maps of the large particle of silicon oxide with a coating of sodium carbonate.

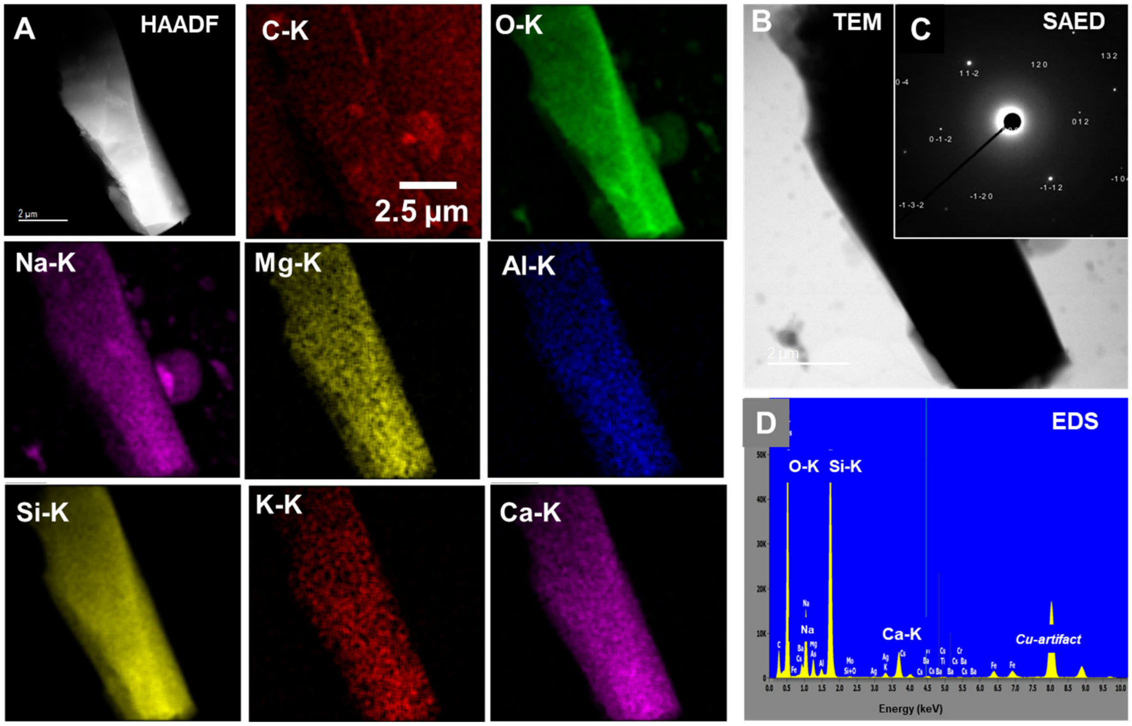

Figure D.7. SEM-EDS elemental maps of a large sodium silicon-rich particle found in the concentrate identified as nitrate-cancrinite through application of CrysTBox software on the SAED patterns.

When trying to match the phases found in these samples, it is important to consider the chemical conditions. Low-temperature, high-pH conditions tend to lead to specific types of silicate phases. Clays and zeolites are some of the most common phases that could form under such conditions. In this case, the materials in Figure D.6 and Figure D.7 contained Na, but Al, Ca, and Mg were also present (see Figure D.7D). Electron diffraction was compared to nitrate-cancrinite as this phase has been observed in Hanford tank waste previously (Buck and McNamara 2004). The phase picks up carbonate and may also incorporate Cs. Light elements such as N and C can be detected with EDS, but because these particles were exceptionally thick, it was not possible to obtain this analysis.

There was a range of particles sizes and morphologies in the 5.5 M solids sample. In previous studies, SEM was used to obtain information on particle sizes; however, with such a heterogeneous sample, that type of analysis would be futile with STEM/TEM. Figure D.8 shows the varied types of particles imaged with TEM that were found in the 5.5 M solids sample. Many of the particles were irregularly shaped. Their ability to be trapped by the holey carbon film used in the analysis would probably be similar to their ability to be trapped on the dead-end filter.

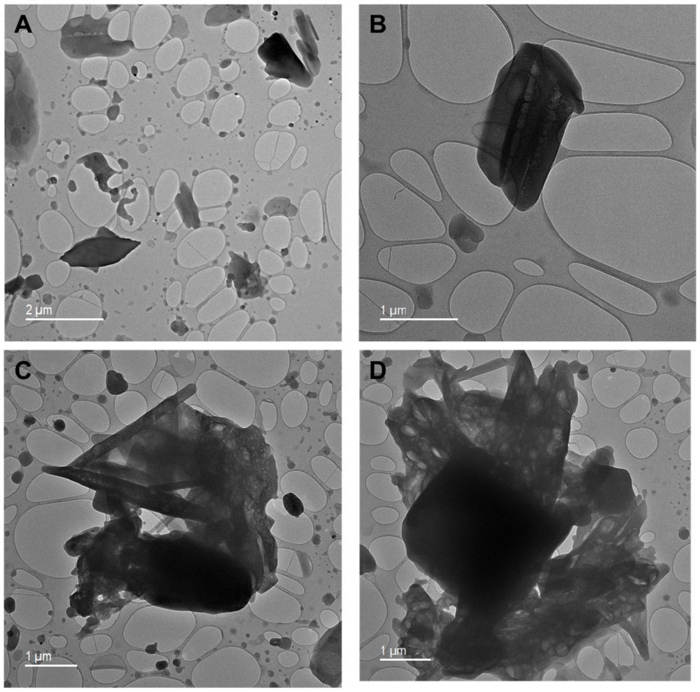

Figure D.8. Different morphologies of particles from the 5.5 M sample.

Several images of different particles taken with TEM HRTEM are shown in Figure D.9. STEM-EDS from the same region is shown in Figure D.10. Most of the material was an aluminum oxide with moderate levels of Fe and Mg also present in the same particles. Separate Ti-oxide particles were also present. Well-known aluminum oxide phases present in the Hanford tanks include boehmite and gibbsite (Chatterjee et al. 2016; Reynolds et al. 2016); however, these particles appeared to be compositionally different from those phases. Within these phases, Mg, Fe, and Ca were also found. These compositions are consistent with the types of compositions found in tank waste of insoluble phases, such as cancrinite and chromium oxides.

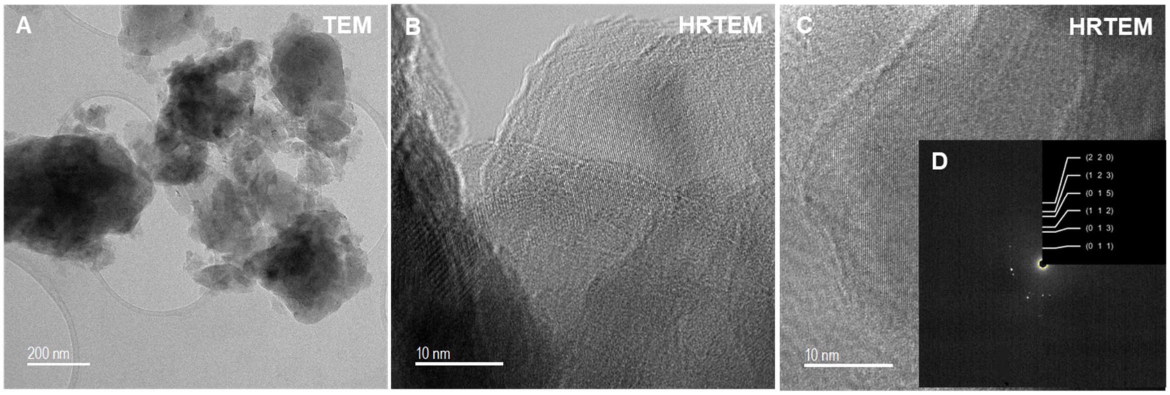

Figure D.9. (A) Low magnification TEM image and (B and C) HRTEM images of particles showing lattice fringes, and (D) SAED with possible match to gibbsite (Al(OH$_3$)).

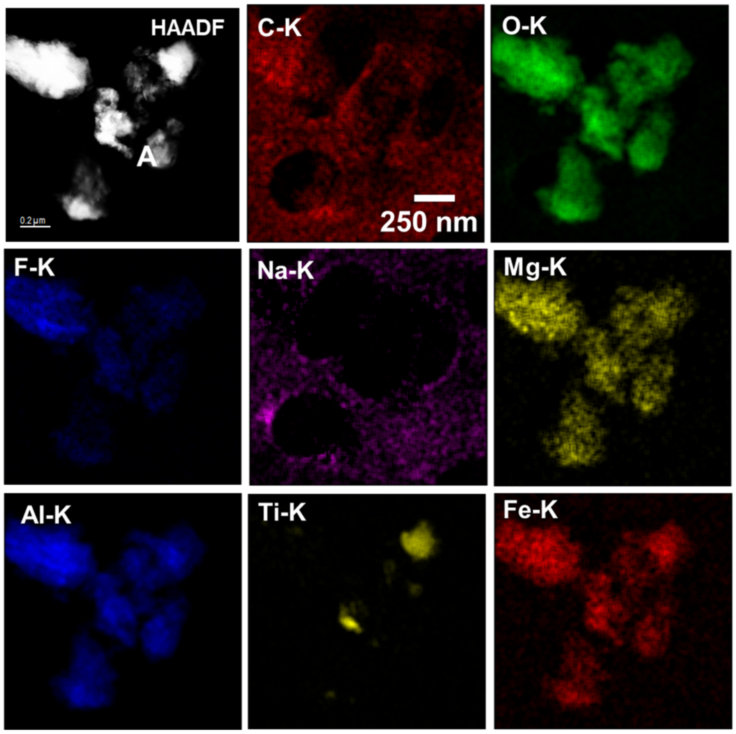

Figure D.10. STEM-EDS and HAADF image of a titanium- and iron-containing region of particles related to Figure D.9.

Table D.1. Electron diffraction from Figure D.9D with possible match to gibbsite.[1]

hkl	theor.	measured
(-1 0 1)	0.678	1.260
(0 0 2)	0.489	0.523
(1 1 3)	0.257	0.258
(2 1 3)	0.226	0.224
(-5 0 1)	0.174	0.174
(1 3 2)	0.157	0.157

A subsample of the concentrated backpulse solution was prepared for analysis via scanning electron microscope (SEM). The solution was passed through a TEM grid to prevent evaporative salt formation during sample mounting. A multi-otsu segmentation method on backscattered SEM images was used to develop a particle size distribution of the solids. An example of one of these images is shown in Figure D.11. Five of these multi-otsu images were combined into a single histogram shown in Figure D.13 where most of the particles were found to be under 3 µm. Figure D.12 highlights the large particles that ended up lying on the copper grid bars from the TEM specimen.

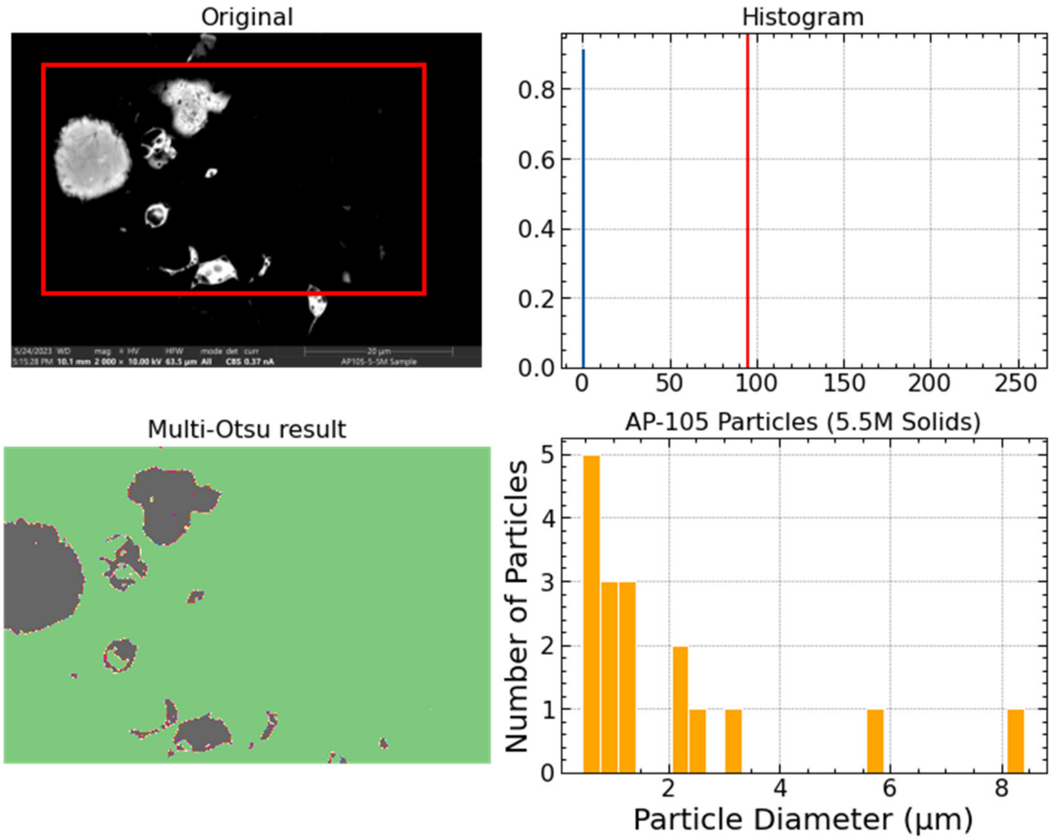

Figure D.11. Multi-otsu segmentation method on backscattered SEM images

---

[1] Ref: Diff003_80cm OneView 5-5M_Solids2-B 0044.dm4

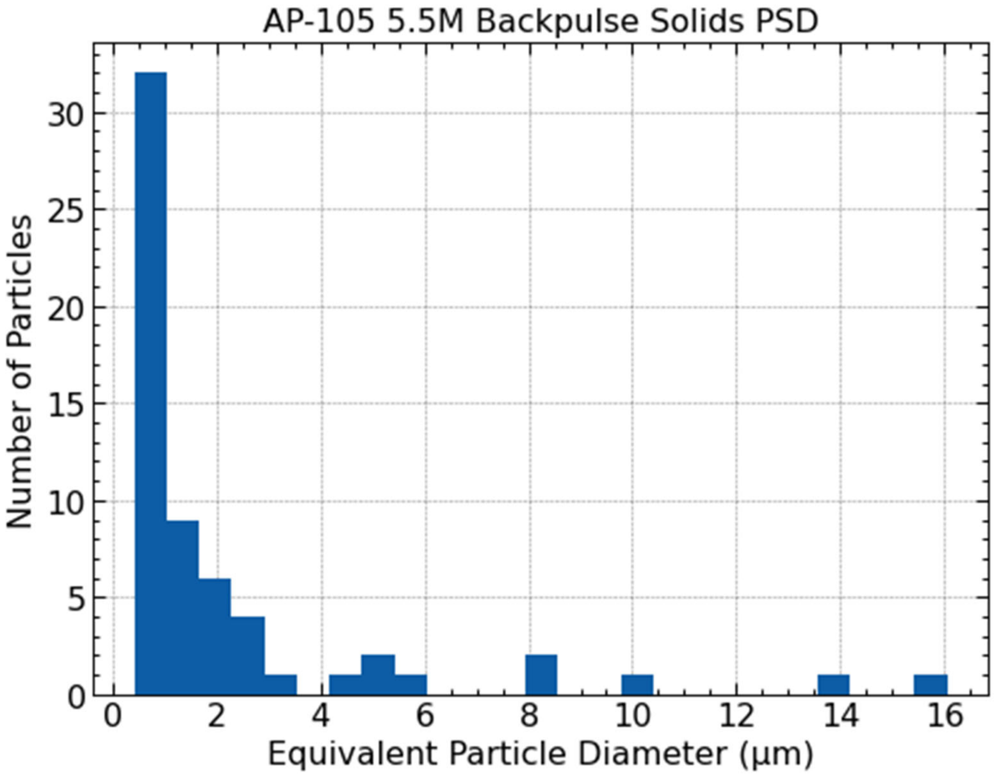

Figure D.12. SEM particle size distribution analysis of particles observed in the 5.5M solids sample.

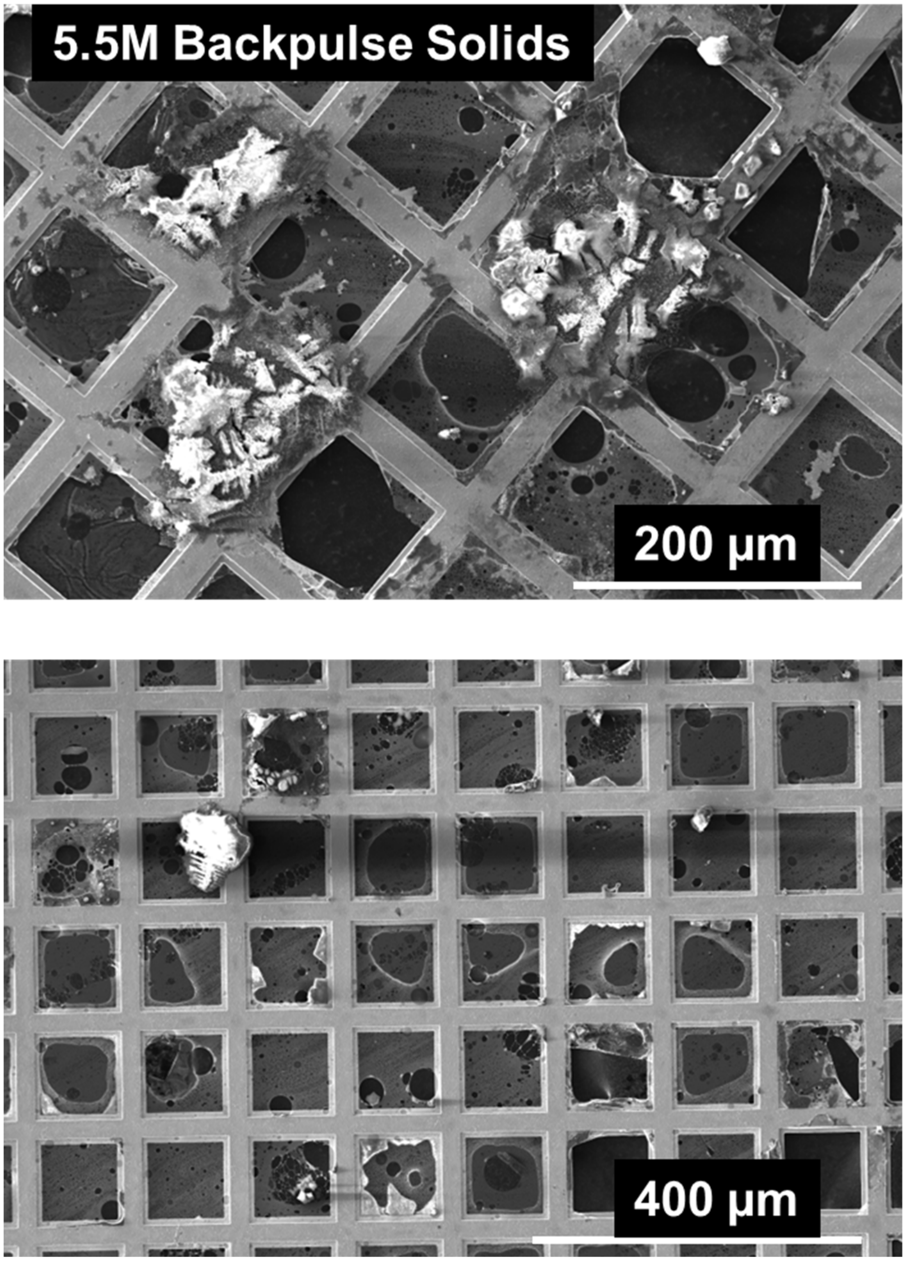

Figure D.13. Large particles lying on the Cu-grid bars of the TEM specimen

D.1.2 7.0 M Na Batch Solids

The second sample examined was run through the BDEF at the higher sodium molarity of 7.0 M. Figure D.14 and Figure D.15 show STEM-HAADF images and STEM-EDS elemental maps of a collection of different particles found in the 7.0 M solids sample. A sodium carbonate phase, possibly natrite, dominates in Figure D.14; however, a nanometer-sized aluminosilicate and a calcium-rich phase can also be seen attached to this larger particle.

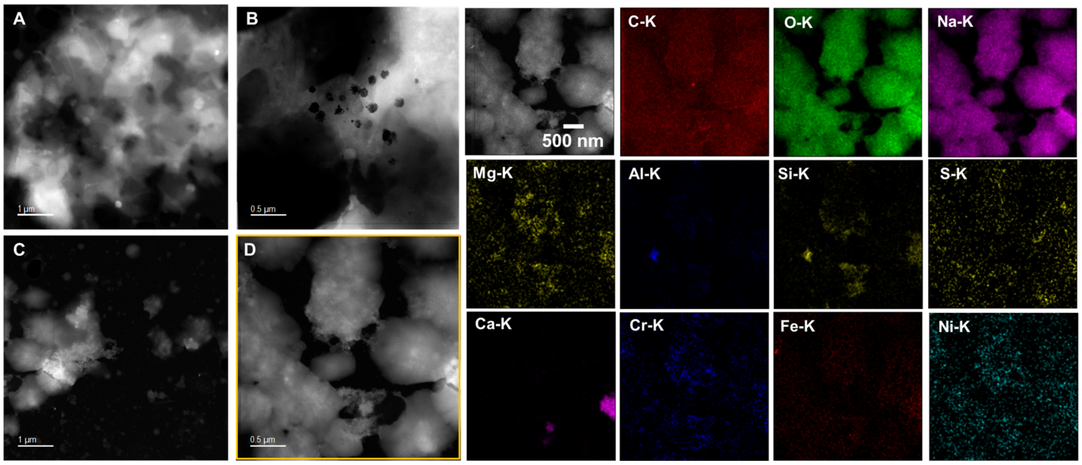

Figure D.14. HAADF images of particle agglomerates from the 7.0 M sample. Mainly sodium-rich particles, possibly natrite.

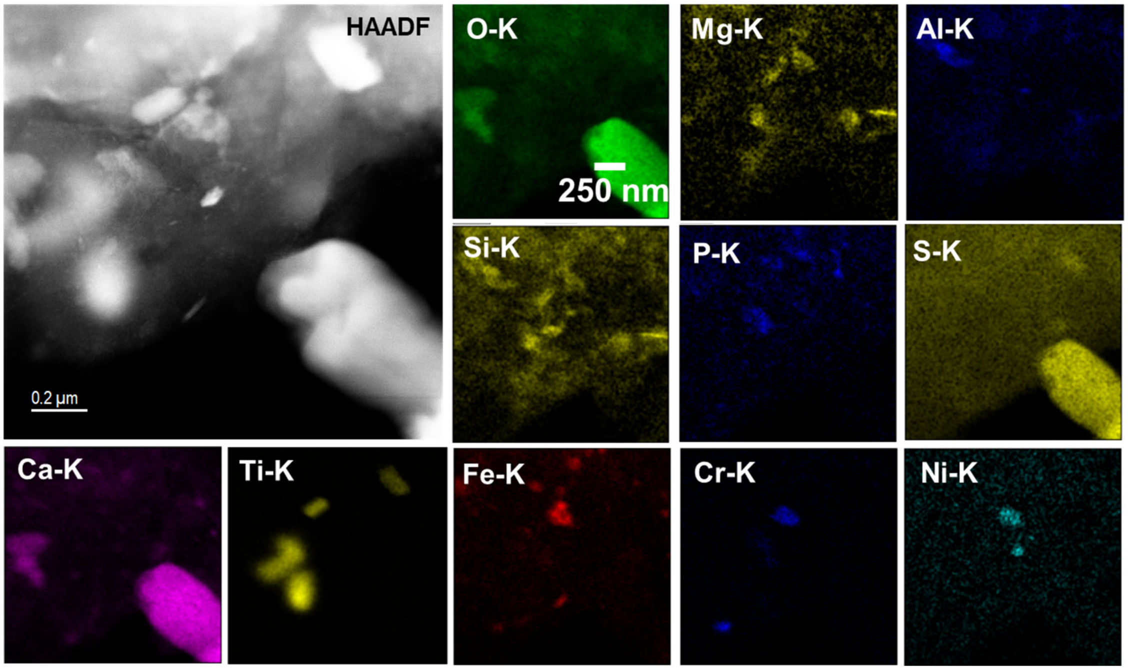

Figure D.15. HAADF image and STEM-EDS analysis of a particle agglomerate consisting of possibly gypsum ($CaSO_4$), titanium oxide, steel, aluminum oxide, and a magnesium silicate.

The STEM-HAADF images in Figure D.14 show several nanoparticle precipitates attached to the larger phase. In Figure D.15, a large gypsum-like composition particle can be observed as well as small particles of Ti-rich phases and a steel-like phase (based on the detection of Fe, Cr, and Ni and the absence of O). A Mg-silicate composition was also detected. Despite the high magnification used in these STEM analyses, certainly when compared to typical SEM analyses that have been conducted previously, the particles were remarkably heterogeneous. For instance, Figure D.16 shows an elongated Mg-silicate in the lower right-hand corner and a series of P-rich elongated phases. The Ti-rich particles were all round or oval and were the brightest (highest average Z-contrast) component visible. The iron and nickel signals do not completely overlap, indicating that there is also an iron oxide phase within the agglomerate. Calcium-rich particles were also scattered throughout the area analyzed.

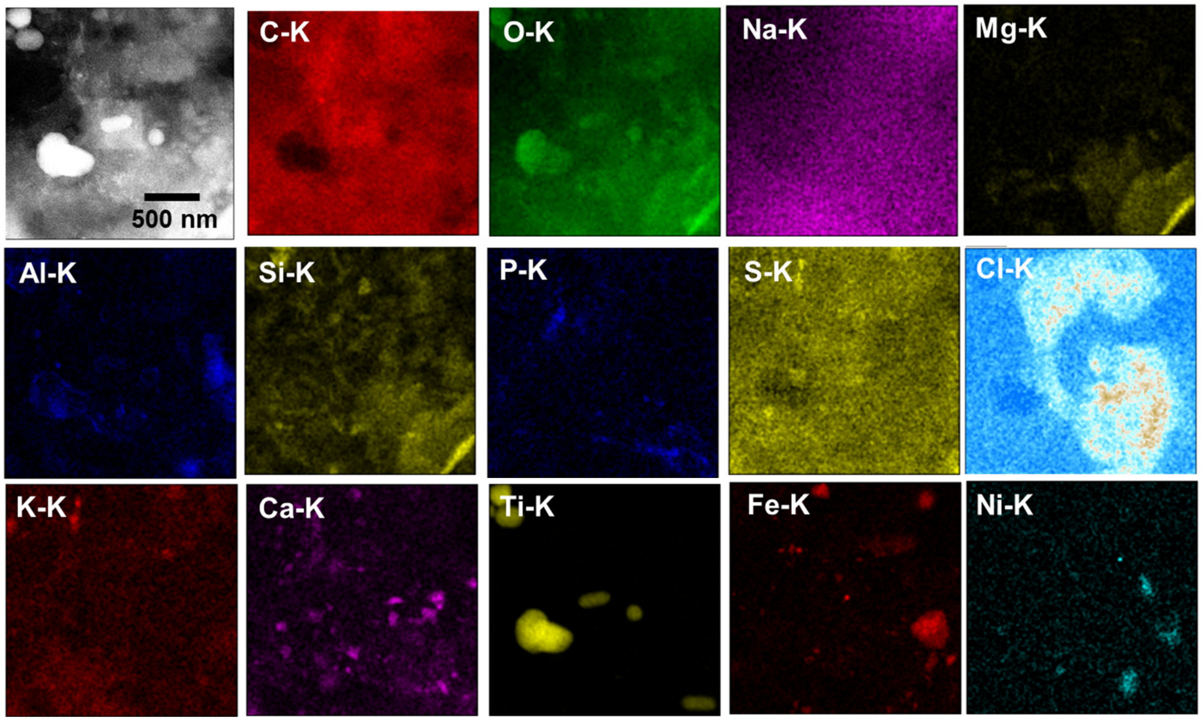

Figure D.16. HAADF image and STEM-EDS analysis of a particle agglomerate showing an Mg-silicate phase as well as Ti-oxide phases and Fe-oxide.

Figure D.17 shows a similar distribution of different phases in the 7.0 M solids sample with an Mg-silicate (possibly also containing Ca), Ti-oxide, Fe-oxide, as well as Na-containing phases. Electron diffraction was obtained from regions around these samples, but in this case, it was not possible to clearly connect the SAED pattern to a known composition (see Figure D.18).

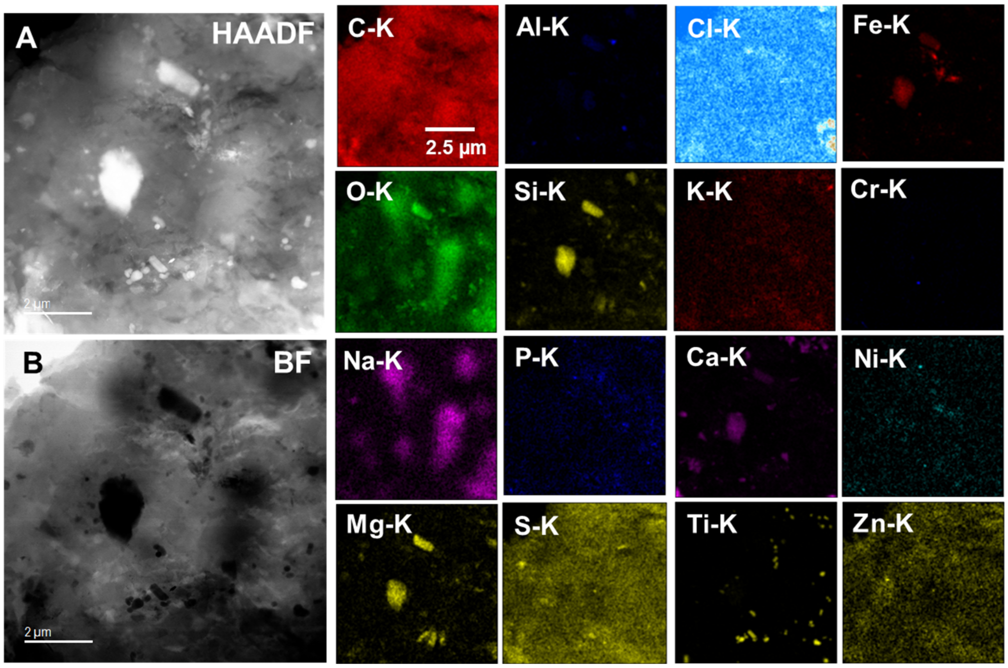

Figure D.17. HAADF image and STEM-EDS analysis of a particle agglomerate showing an Si-Al phase attached to salt-like phases.

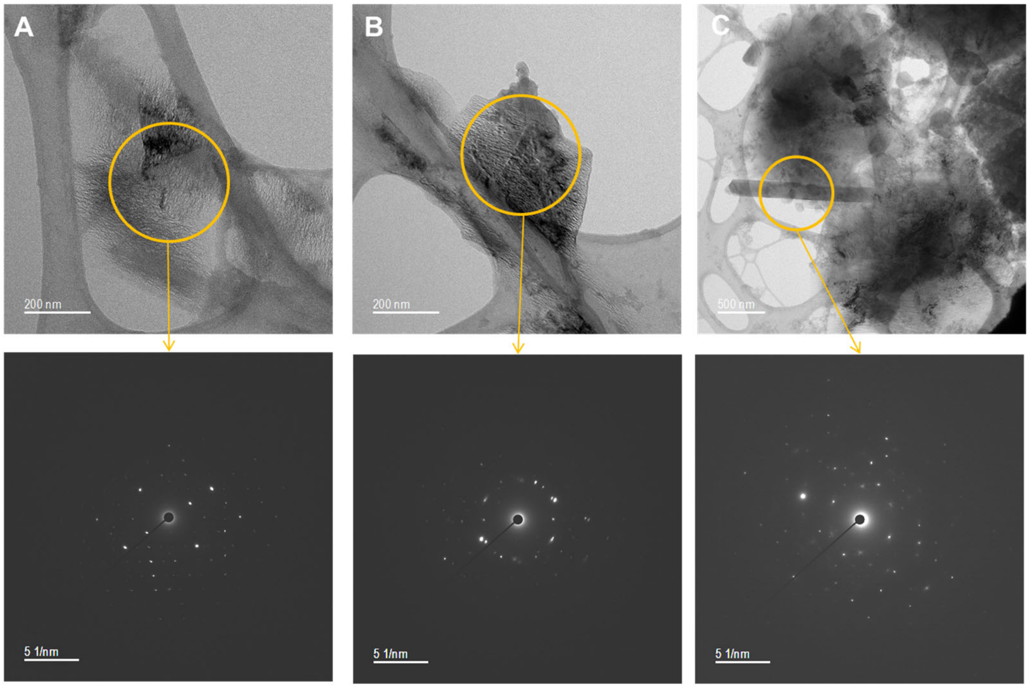

Figure D.18. TEM analysis of particles observed in the 7.0 M solids sample.

From Figure D.19 to Figure D.22, the same series of particles were analyzed with STEM-HAADF, STEM-EDS, TEM, and SAED. The group of particles consisted of two dominant particles, one was a titanium oxide and the other was an aluminum oxide. Figure D.19 displays the STEM-EDS elemental mapping of the Al particle. Within this particle, a ribbon of titanium oxide nanoparticles was attached. The Al-oxide phase also contained Mg.

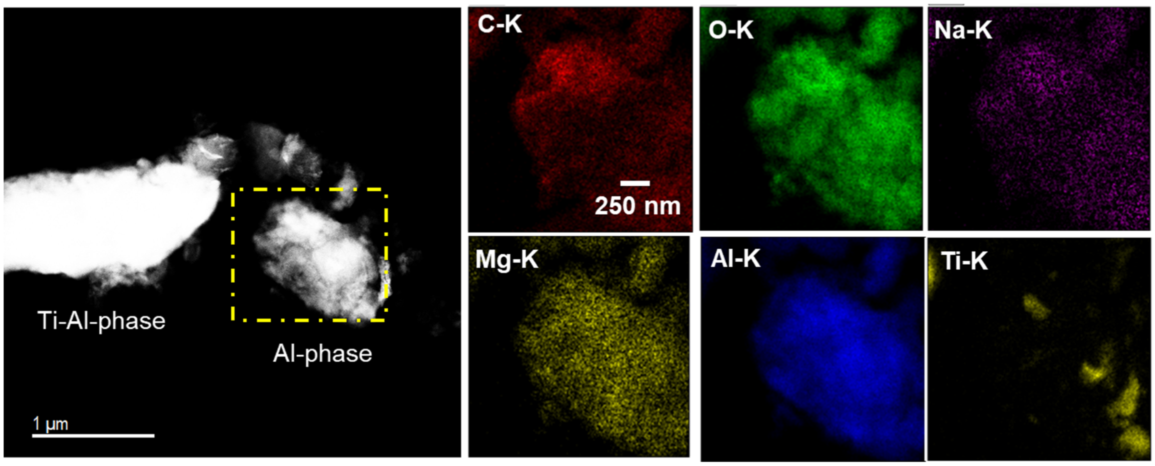

Figure D.19. STEM EDS analysis of a Mg-Al-particle (yellow-dotted highlighted region) with interspersed Ti-oxide nanoparticles in the 7.0 M solids sample.

Inspection of a group of particles between the two larger ones is shown in Figure D.20. In this figure, the phase appears to consist of C, O, F, Mg, and Al. There were also distinct Ti oxide and Fe-oxide particles. The Cu-particle also appears to be genuine. Cu fluorescence can lead to problems measuring Cu, but the brightness of the signal and the location suggests that it is real. These analyses demonstrate that even down to the nanometer level (the scale bar on the images is 100 nm), the particles remain highly heterogenous.

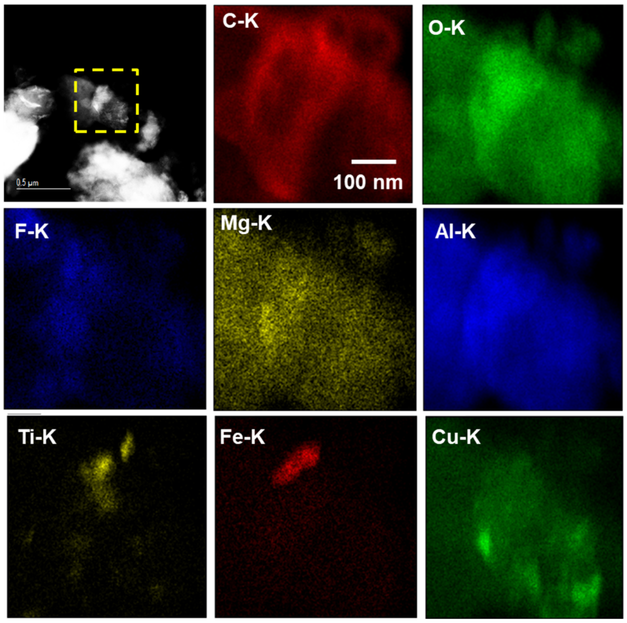

Figure D.20. Lower magnification STEM EDS analysis of a Ti- and Fe- particles within an Al-phase.

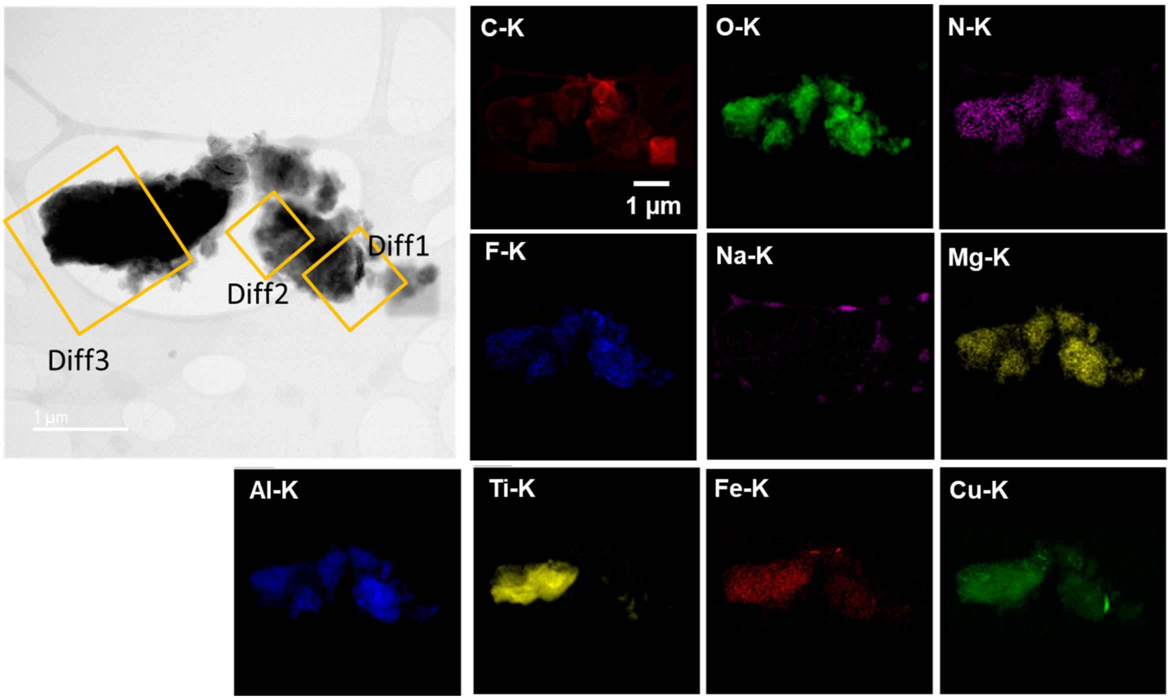

Figure D.21. Lower magnification STEM EDS analysis showing highlighted regions that were analyzed with TEM and diffraction. (SAED-03: Ti-bearing; SAED-02 and SAED-01: Al-bearing)

Three regions were targeted for electron diffraction analysis as shown in Figure D.21. The STEM-EDS elemental maps clearly show the dominant phases in the agglomerate. However, the diffraction patterns obtained in TEM mode (see Figure D.22) were poorly defined. They were analyzed with CrysTBox to two possible phases: gibbsite and anatase. The matches were poor but these but these would be phases that could occur under the chemical conditions.

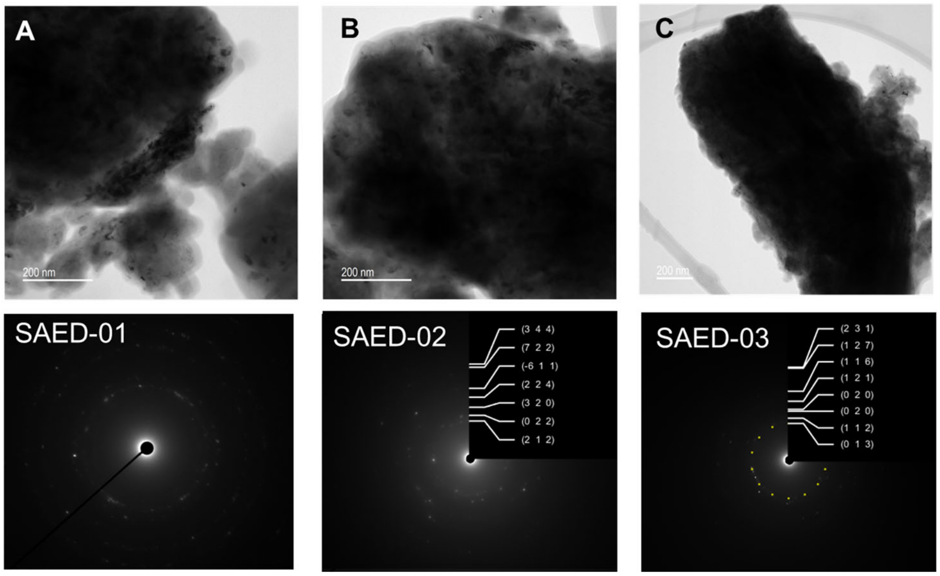

Figure D.22. TEM images and SAED of the particles (A) Al-oxide, (B) Al-oxide, (C) Ti-oxide. The particles were too thick for good quality electron diffraction.

Table D.2. Electron diffraction from Figure D.19 with possible matches to gibbsite and anatase.[(a)]

Gibbsite			Anatase		
hkl	theor.	measured	hkl	theor.	measured
(2 1 2)	0.267	0.264	(0 1 3)	0.243	0.262
(0 2 2)	0.226	0.228	(1 1 2)	0.233	0.230
(3 2 0)	0.192	0.192	(0 2 0)	0.189	0.198
(2 2 4)	0.160	0.160	(0 2 0)	0.189	0.190
(-6 1 1)	0.140	0.140	(1 2 1)	0.167	0.164
(7 2 2)	0.107	0.108	(1 1 6)	0.136	0.141
(3 4 4)	0.104	0.104	(1 2 7)	0.106	0.106
			(2 3 1)	0.104	0.105

(a) Ref: SAED-02_Diff02_80cm OneView 7M Solids2 0027.dm4 (gibbsite), SAED-03_Diff003_80cm OneView 7M Solids2 0029.dm4 (anatase)

Another heterogenous agglomerate is shown in Figure D.23 and Figure D.24. The STEM-EDS elemental maps are consistent with earlier results. A large amount of STEM data is being presented in this report owing to inoperability of the SEM systems and the need to build some consistency in the data. The common features were again an Mg-Al oxide and nanoparticles of Ti-oxide. No major Ca-bearing phases were observed in this agglomerate.

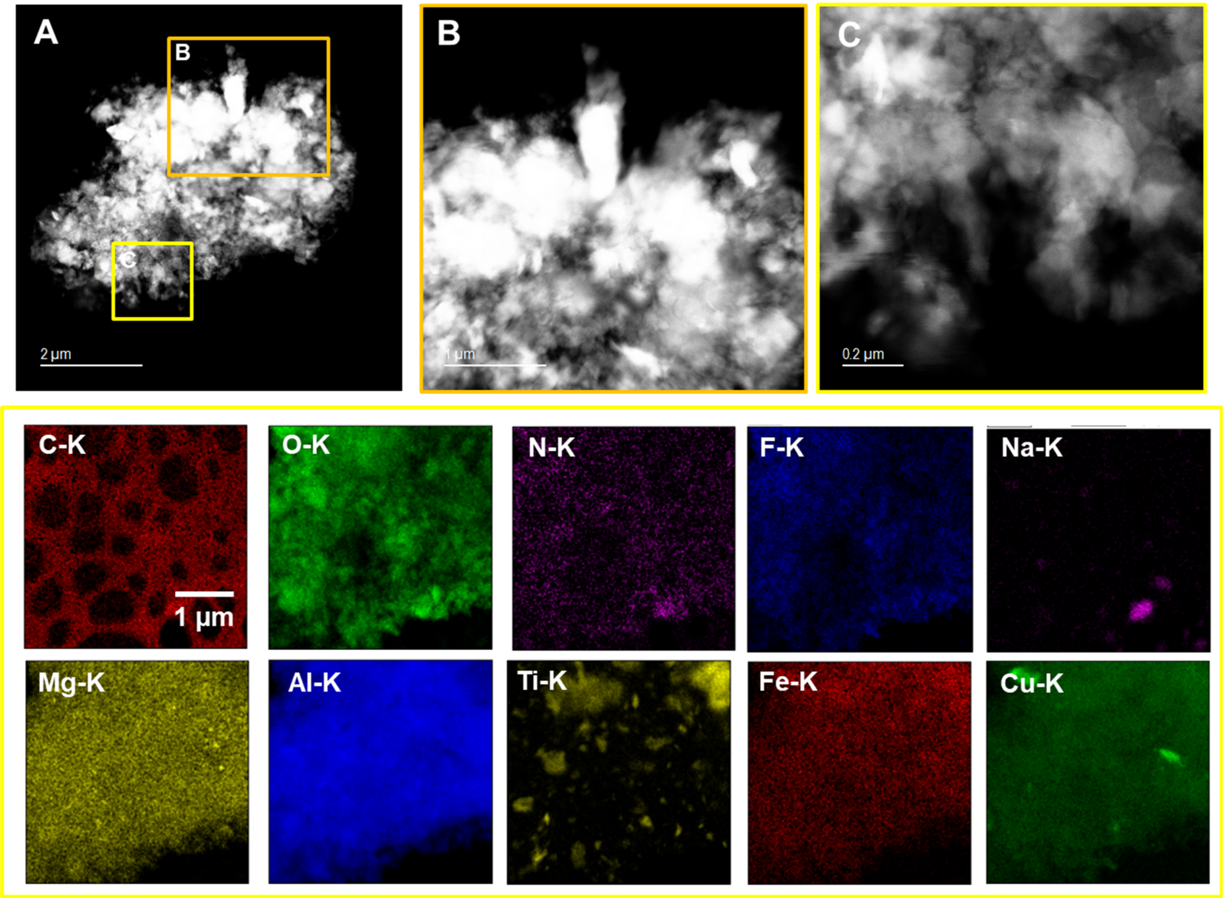

Figure D.23. Lower magnification STEM EDS analysis showing two regions where elemental maps were obtained. The maps show an agglomerate of Ti, Cu particles on a larger Al particle.

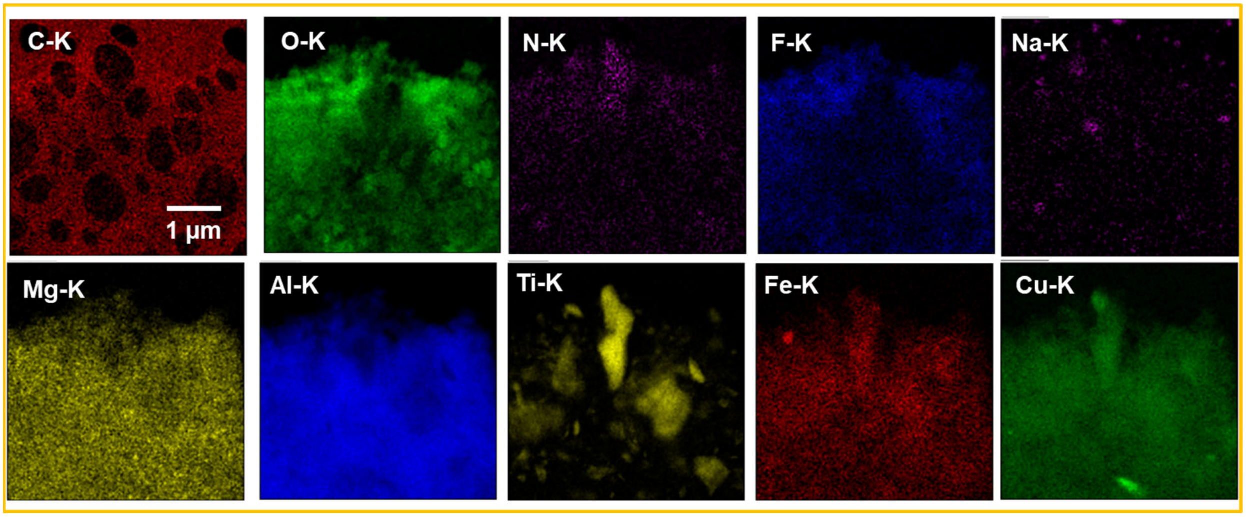

Figure D.24. Lower magnification STEM EDS analysis – from the orange highlighted region showing the same distribution of Ti particles on an Al-matrix.

Note that in Figure D.23 and Figure D.24 the carbon maps clearly show the TEM holey carbon film pattern. This is not the case in Figure D.25, where the carbon appears to be a component in the phase. The only other elements present in the phase were O and Na. This indicates that the phase is a sodium carbonate. Electron diffraction from this phase (see Figure D.26) was extremely weak and the material tended to be easily destroyed in the beam under TEM imaging. There was also a small amount of Si, which seems to be interspersed within the Na_2CO_3. The SAED pattern was matched with CrysTBox software to natrite. The figure shows a match to the B[001] zone axis. The identification of this phase is supported by historical analyses of the Hanford tank phases and is reasonable based on the chemistry of the system under investigation. However, the weakness of the patterns means that the analysis remains tentative.

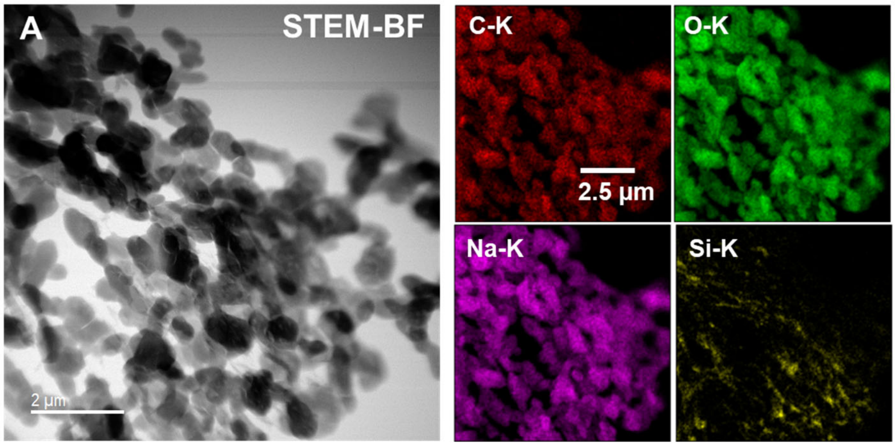

Figure D.25. Lower magnification of unusual morphology found in sample 7.0 M showing STEM EDS Analysis indicating a sodium carbonate with nanoparticles of Si.

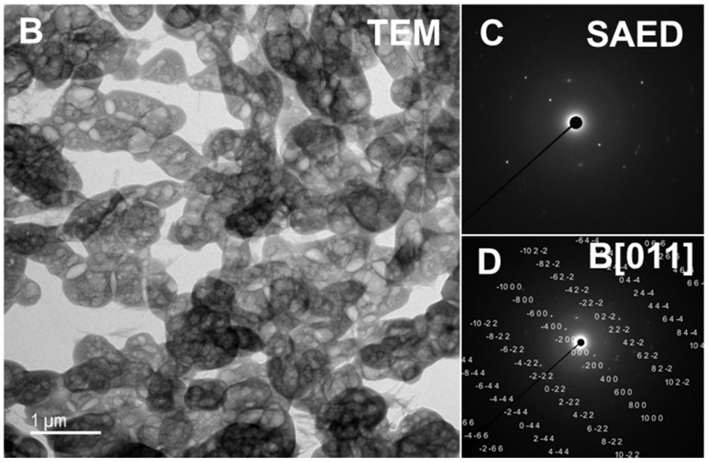

Figure D.26. TEM images and diffraction of sodium carbonate (Na_2CO_3) particles.[1]

Figure D.27 and Figure D.28 show the analysis of an aluminum-rich phase. HRTEM analysis reveals lattice fringes in the material. Fast Fourier transform (FFT) of the lattice images enables us to obtain some structural information on the materials. The STEM-EDS analysis indicated most of the particle was Al and O, but there was an indication of Ti nanoparticles, possibly TiO_2, interspersed in the particle. The EDS spectra (see Figure D.28) clearly shows that Al and O were the major elements present in the particle.

---

[1] Ref: Diff09_80cm_Amorphous round particles OneView 7M Solids2 0061.dm4

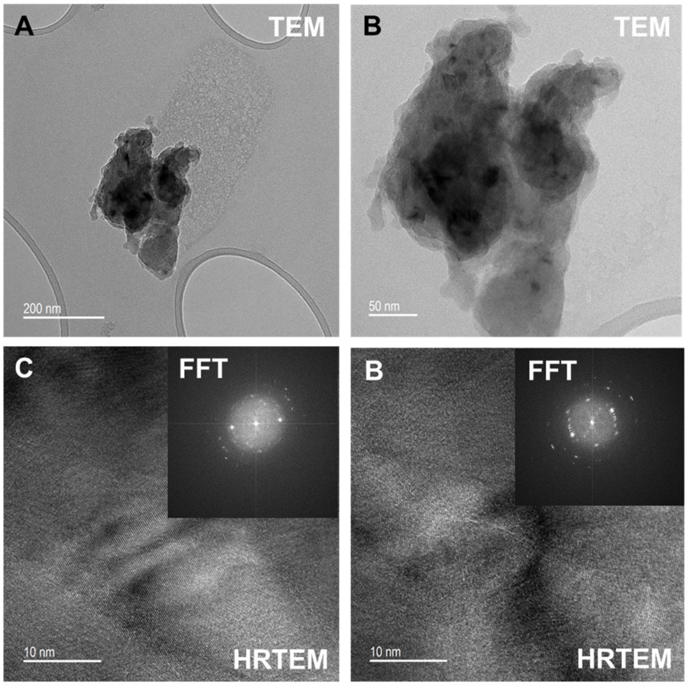

Figure D.27. Low magnification images and HRTEM images and diffraction (FFT) of Al-rich particles in the 7.0 M solids sample.

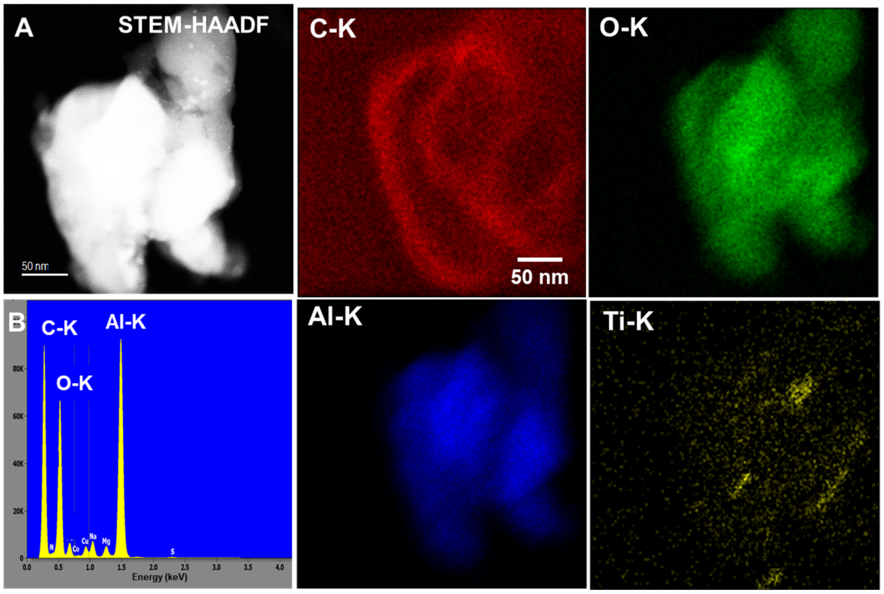

Figure D.28. Lower magnification STEM EDS analysis of an aluminum oxide shown in Figure D.27.

The FFT from Figure D.27 yielded d-spacings at 0.341, 0.2353, 0.144, and 0.120 nm. A possible match is the mineral allophane ($Al_2O_3(SiO_2)$•1.2-$2H_2O$), with reported major d-spacings at 0.331, 0.225, 0.140, 0.123, and 0.186 nm. Allophane also tends to contain Si. Allophane can form from the rapid precipitation of soluble Al and Si.

As with the 5.5M sample the 7.0M concentrated backpulse solution subsampled and prepared for analysis via scanning electron microscope (SEM). Five multi-otsu segmentation method images (see Figure D.29) were combined into a single histogram shown in Figure D.30. When compared to the 5.5M sample a greater concentration of sub 3 µm particles were observed. Figure D.31 highlights the smaller particles found on the TEM specimen.

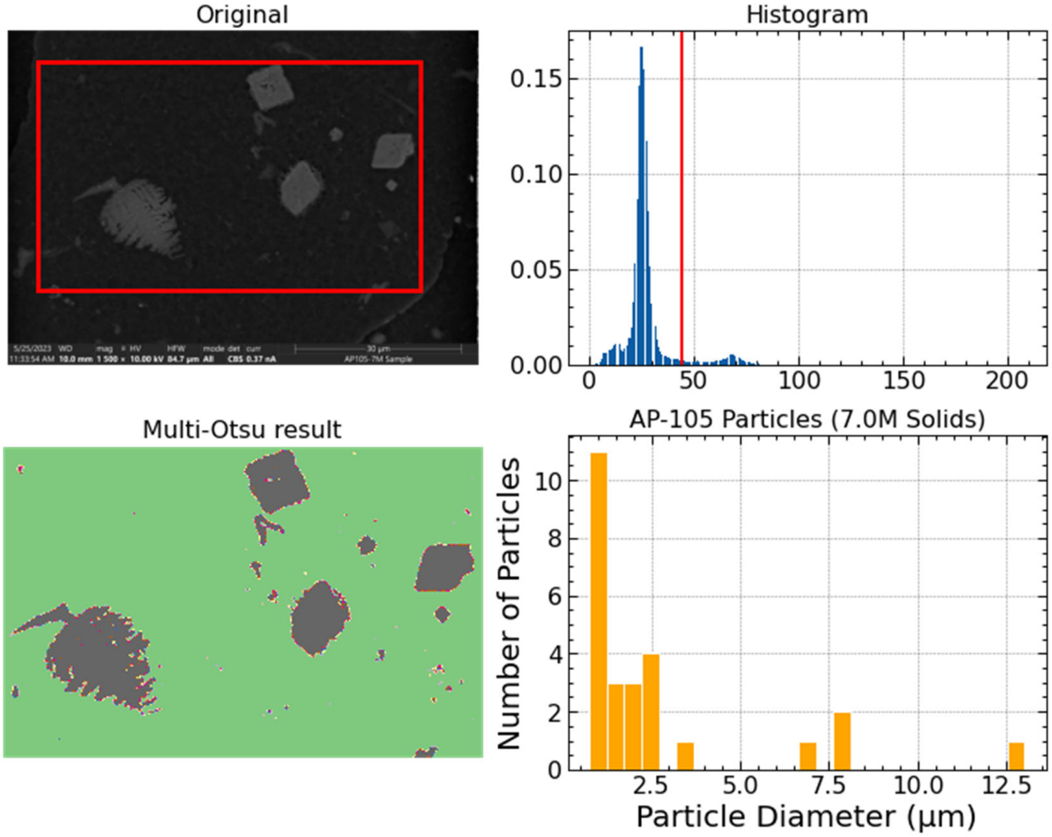

Figure D.29. Multi-otsu segmentation method on backscattered SEM images

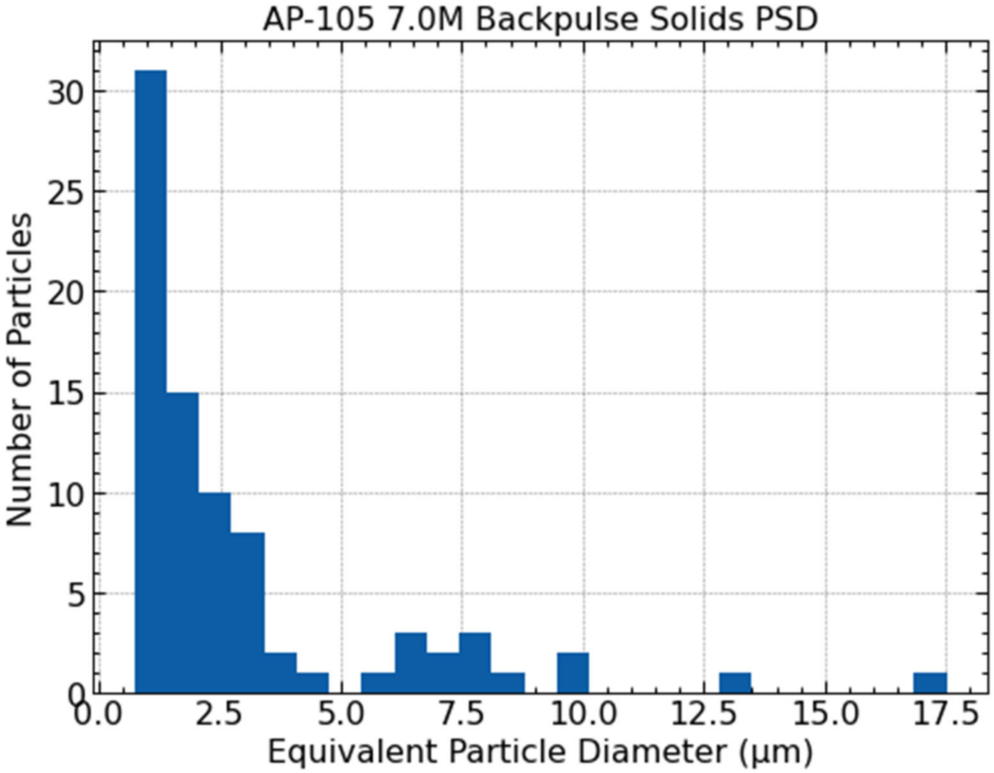

Figure D.30. SEM particle size distribution analysis of particles observed in the 7.0M solids sample.

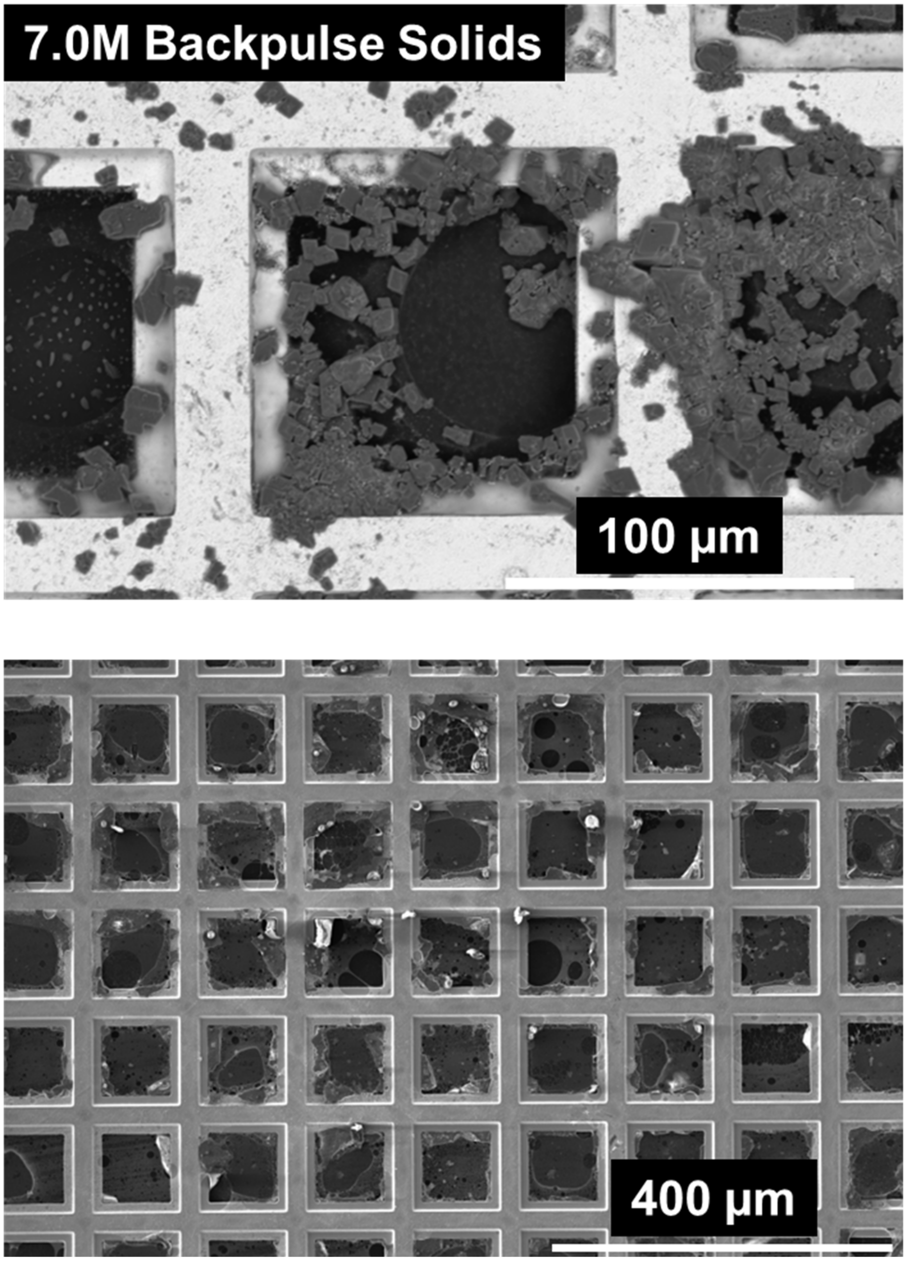

Figure D.31. Large particles lying on the Cu-grid bars of the TEM specimen

D.2 Conclusions of Microscopy Study

The objective of this set of tests was to assess the impact of raw water dilution on the formation of solids. The results from this work are consistent with prior work that indicated the addition of process water results in solids formation. The overall number of solids was small. In this study, we were unable to use SEM as the primary tool for analysis. This significantly reduces the ability for the microscopy analysis to provide any information regarding the relative amounts of the different types of solids. The study only used STEM and TEM methods to analyze collected solids. A few different compositions were found, including sodium nitrate, sodium carbonate, calcium sulfate, iron oxide, steel particles, titanium oxide particles, and aluminum oxides. Electron diffraction was used to determine the types of phases that were present in the solids. The possible identification of gibbsite, natrite, nitrite, gypsum, anatase, allophane, and cancrinite was made during this investigation. Most of the phases found were only weakly crystalline, possibly owing to their rapid precipitation during the process water treatment. The identifications of the phases therefore are tentative.

D.3 References

Buck EC and BK McNamara. 2004. "Precipitation of nitrate-cancrinite in Hanford tank sludge." *Environmental Science & Technology* 38(16):4432-4438.

Chatterjee S, M Conroy, F Smith, H-J Jung, Z Wang, RA Peterson, A Huq, DG Burtt, ES Ilton, and EC Buck. 2016. "Can Cr(III) substitute for Al(III) in the structure of boehmite?" *RSC Advances*. https://doi.org/10.1039/C6RA20234A

Klinger M. 2017. "More features, more tools, more CrysTBox." *Journal of Applied Crystallography* 50(4):1226-1234. https://doi.org/doi:10.1107/S1600576717006793

Mitchell DRG. 2008. "DiffTools: Electron diffraction software tools for DigitalMicrograph™." *Microscopy Research and Technique* 71(8):588-593.

Reynolds JG, GA Cooke, DL Herting, and RW Warrant. 2012. "Evidence for dawsonite in Hanford high-level nuclear waste tanks." *Journal of Hazardous Materials* 209–210:186-192. https://doi.org/http://dx.doi.org/10.1016/j.jhazmat.2012.01.018

Reynolds JG, JK McCoskey, and DL Herting. 2016. "Gibbsite Solubility in Hanford Nuclear Waste Approached from above and below Saturation." *Industrial & Engineering Chemistry Research* 55(19):5465-5473. https://doi.org/10.1021/acs.iecr.6b00743

Pacific Northwest
National Laboratory

902 Battelle Boulevard
P.O. Box 999
Richland, WA 99354
1-888-375-PNNL (7665)

www.pnnl.gov